UNIVERSITAT POLITÈCNICA DE CATALUNYA
BARCELONATECH
Electronic Engineering Department

ASSESSMENT OF TRENDS IN THE CARDIOVASCULAR SYSTEM FROM TIME INTERVAL MEASUREMENTS USING PHYSIOLOGICAL SIGNALS OBTAINED AT THE LIMBS

Thesis submitted in partial fulfillment of the requirements for the PhD Degree issued by the Universitat Politècnica de Catalunya, in its Electronic Engineering Program.

Author: **Joan Gómez Clapers**
Directors: **Dr. Ramon Pallàs Areny**
Dr. Ramon Casanella Alonso

November 2015

To my family,

Osvald, Montserrat, Caterina, and Lara,

with great appreciation for their abundant support, patience, and love.

Abstract

CARDIOVASCULAR diseases are an increasing source of concern in modern societies due to their increasing prevalence and high impact on the lives of many people. Monitoring cardiovascular parameters in ambulatory scenarios is an emerging approach that can provide better medical access to patients while decreasing the costs associated to the treatment of these diseases.

This work analyzes systems and methods to measure time intervals between the electrocardiogram (ECG), impedance plethysmogram (IPG), and the ballistocardiogram (BCG), which can be noninvasively obtained at the limbs in ambulatory scenarios using simple and cost-effective systems, to assess cardiovascular intervals of interest in research and clinical practice, such as the pulse arrival time (PAT), pulse transit time (PTT), or the pre-ejection period (PEP).

The first section of this thesis analyzes the impact of the signal acquisition system on the uncertainty in timing measurements in order to establish the design specifications for systems intended for that purpose. The minimal requirements found are not very demanding yet some common signal acquisition systems do not fulfill all of them. On the other hand, some capabilities typically found in signal acquisition systems could be downgraded without worsening the uncertainty of timing measurements hence resulting in more cost-effective designs. This section is also devoted to the design of systems intended for timing measurements in ambulatory scenarios according to the specifications previously established. The systems presented have evolved from the current state-of-the-art and are designed for adequate performance in timing measurements with a minimal number of active components, which results in a lower cost and longer battery life.

The second section is focused on the measurement of time intervals from the IPG measured from limb to limb, which is a signal that until now has only been used to monitor heart rate and whose detailed physiological origin was unknown. A model to estimate the contributions to the time events in the measured waveform of the different body segments along the current path from geometrical properties of the large arteries is proposed, and the simulation under blood pressure changes suggests that the signal is sensitive to changes in proximal sites of the current path rather than in distal sites. Experimental results show that the PAT from the R wave of the ECG to the hand-to-hand IPG, which is obtained from a novel four-electrode handheld system, is strongly correlated to changes in the PEP whereas the PAT from the R wave of the ECG to the foot-to-foot IPG shows good performance in assessing changes in the femoral PAT. Therefore, limb-to-limb IPG measurements significantly increase the number of time intervals of interest that can be measured at the limbs since the signals deliver information from proximal sites complementary to that of other measurements typically performed at distal sites.

The next section is devoted to the measurement of time intervals that involve different waves of the BCG obtained in a standing platform and whose origin is still under discussion. From the relative timing of other physiological signals, it is hypothesized that the IJ interval of the BCG is sensitive to variations in the PTT. Experimental results show that the BCG I wave is a better

surrogate of the cardiac ejection time than the widely-used J wave despite of the lower signal-to-noise ratio (SNR) of the I wave, which is also supported by the good correlation found between the IJ interval and the aortic PTT. Finally, the novel time interval from the BCG I wave to the foot of the IPG measured between feet, which can be obtained from the same weighing scale than the BCG, shows good performance in assessing the aortic PTT. The results presented reinforce the possible role of the BCG as a tool for ambulatory monitoring since the main time intervals targeted in this thesis can be obtained from the timing of its waves.

Even though the methods described were tested in small groups of subjects, not larger than 14, the results presented in this work show the feasibility and potential of several time interval measurements between the proposed signals that can be performed in ambulatory scenarios, provided the systems intended for that purpose fulfill some minimal design requirements.

Keywords: Ambulatory measurements, electrocardiogram (ECG), impedance plethysmogram (IPG), ballistocardiogram (BCG), physiological instrumentation, pulse arrival time (PAT), pulse transit time (PTT), pre-ejection period (PEP), RJ interval, RI interval, IJ interval.

Acknowledgements

THIS work could never have been completed without the contribution of many people, but I am especially thankful to my advisors, Dr. Ramon Pallàs and Dr. Ramon Casanella, for their constant and indefatigable support during this long journey. From Dr. Pallàs I not only admire his rigor as a scientist and the tremendous amount of knowledge that he amasses, but the sincere care that he takes about the well-being of his students, for which I am very grateful. From Dr. Casanella I admire his criticism and the strong foundations of his beliefs, which always pushed me to give the best of myself. I am also very thankful for the countless hours that they have spent on discussing and refining the results presented on this work.

I would like to thank everyone on the ISI Group and the EETAC campus for making it such a nice place to work and to collaborate but particularly to the students whom I shared most of my good and bad experiences here: Pablo, Delia, Joan, Maliha, Carles, Alberto, Oleguer, Martí, Miquela, Adam, Hagan, Parth, Vicky, and Maria. I would like to thank them for making my experience here so fulfilling, with the hope that our paths will cross many times in the future. I would also thank to the members of our group that happily volunteered for the experiments performed along this work.

I am also grateful to everyone on the Biomedical Signal Processing Group at Lund University, and especially to its director Dr. Leif Sörnmo, for receiving me during my research stay and for the warm welcome I had. Some of the nicest memories that I will keep of this period of my life are, without a doubt, from the time that I spent there.

The funding of this project was made possible by the State Office of Research, Development, and Innovation of the Spanish Ministry of Economy and Competitiveness, under the project TEC2009-13022 and the grants BES-2010-032893 and EEBB-I-13-06744, and by the ISI Group.

Finally and most importantly, I would like to thank my parents Osvald and Montserrat. I would not be where I am today without their support, sacrifice, and unconditional love. There are no words to describe my gratitude to them.

List of acronyms and symbols

A	Cross-sectional area
ADC	Analog-to-digital converter
AWGN	Additive white Gaussian noise
BCG	Ballistocardiogram
BP	Blood pressure
C	Compliance
CMRR	Common-mode rejection ratio
D	Distensibility
DRL	Driven-right-leg circuit
E	Elastic modulus
ECG	Electrocardiogram
EEG	Electroencephalogram
EMG	Electromyogram
h	Arterial wall thickness
ICG	Impedance cardiogram
IPG	Impedance plethysmogram
l	Length
P	Mean blood pressure
PAT	Pulse arrival time
PCG	Phonocardiogram
PEP	Pre-ejection period
PPG	Photoplethysmogram
PPT	Pressure pulse transducer
PTT	Pulse transit time
PWV	Pulse wave velocity
ϱ	Resistivity
ϱ_b	Blood density
ϱ_e	Blood resistivity
R	Resistance
r	Arterial radius
rms	Root mean square
SCG	Seismocardiogram
SNR	Signal-to-noise ratio
WHO	World Health Organization

Table of contents

Index of figures

Index of tables

Chapter 1

Motivation and objectives

CARDIOVASCULAR diseases are the leading cause of death in the world. According to the most recent report of the World Health Organization (WHO) [1], 17.3 million people died from it in 2008, which represents 1 in every 3 total deaths, and this number is expected to raise up to 23.3 million in 2030. However, a large proportion of patients still remain undiagnosed until the last stages of disease, when they become symptomatic and require admission into hospitals and costly aggressive treatments such as surgery or transplantation. In this scenario, healthcare systems are shifting its focus to preventive therapies, which have the greatest potential to inverse the progression of the disease, reduce the number of hospitalizations, and decrease healthcare costs [2]. Besides, early detected diseases can be treated with softer therapies, such as pharmacotherapy and habit changes, that have a lesser impact on the patient lifestyle.

Nevertheless, the cost-effectiveness of preventive therapies has long been debated because whereas some of them save more money than they cost, others do not [3]. Screenings can help in reducing costs by identifying individuals that can benefit from preventive therapies but most of the current methods to evaluate the performance of the cardiovascular system rely on the availability of limited resources such as expensive equipment or highly-specialized staff. For this reason, regular screenings in large population groups are unsustainable by healthcare systems, and these are currently being limited to simple and affordable regular controls of blood pressure (BP), cholesterol and triglycerides, body weight, blood glucose, and lifestyle habits in individuals with a high number of risk factors.

If this rising trend is expected to be reversed, traditional approaches must be revised and discussed. The development of new cost-effective screening approaches, which has been recently

included in the top-five research priorities in cardiovascular diseases [4] by the WHO, is the key to a more effective and accessible medical treatment of cardiovascular diseases while reducing the always significant medical costs.

1.1. Measurement of cardiovascular parameters in ambulatory scenarios

The measurement of physiological parameters in ambulatory scenarios from cost-effective devices has become popular in the last decades and fits the requirements for effective screenings. The aim of this approach is to provide patients with affordable tools to perform regular fast checks, looking for physiological changes indicating deterioration or early signs of a disease, in the same way that millions of people regularly keep track of their body weight with home weighing scales. In addition, the regular measurement of physiological parameters in ambulatory scenarios has also potential interest for monitoring chronically ill patients, recovery after surgery, or fitness.

Compared to traditional measurements performed in hospitals, this new approach has the following advantages:

- **Scalability**: The cost of the measurement device, including its operation and maintenance, is lower and can even be assumed by the patient.
- **Effectiveness**: Screenings can be performed more frequently, which leads to early detections.
- **Optimization**: Some critical and expensive resources such as devices, personal, and accommodation are released for other uses.
- **Comfort**: The total amount of displacements to medical facilities is reduced and most of the measurements are performed in a more comfortable environment.

On the other hand, these measurements are subjected to some additional requirements:

- **Noninvasiveness**: Any excessive discomfort or embarrassment to the patient should be avoided in order to ease frequent use.
- **Simplicity**: The procedure should be simple enough to be understood and reproduced without any error by users without any specific training.
- **Cost-effectiveness**: The cost should be affordable for healthcare systems or even particulars in order to reach a broad population group.

Focusing on cardiovascular parameters, the existing technologies can be classified according to the schema shown in Fig. 1.1.

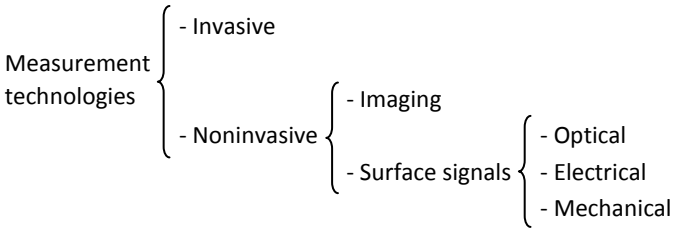

Fig. 1.1. Classification of technologies to obtain cardiovascular parameters.

Invasive measurements are performed with sensors placed inside the body of the patient, via catheterization, endoscopy, or subdermal implants. The cost of these measurements is high due to the requirement of specialized operators and sanitized environments. The discomfort of the patient is also often high, as the placement of some sensors may require surgical procedures, anesthesia, or both.

Imaging measurements, such as ultrasound echography, magnetic resonance, or *x*-ray, are noninvasive but still require costly devices operated by specialized staff.

The most common surface optical measurement is the photoplethysmogram (PPG) [5], which is the recording of changes in transmitted or absorbed light in superficial tissues as a result of changes in blood perfusion. The sensor must to be preferably placed above a superficial artery and some typical measurement sites are the fingers and the earlobe, although the signal can also be obtained from other places, such as the carotid artery, femoral artery, or the forehead, with an accurate placement of the sensor performed by a specialist.

Two surface electrical measurements that can deliver information about cardiovascular function are the electrocardiogram (ECG) [6] and the impedance plethysmogram (IPG) [7]. The ECG is the recording of the electrical activity of the heart and it can be measured differentially from several standardized points on the body surface. Further, the signal can be obtained from other non-standard sites, such as between feet, although these may pose some challenges such as a very small amplitude and higher electromyogram (EMG) level. The IPG is the recording of volumetric-related changes in tissue conductivity due to cardiovascular activity. Unlike the ECG, which is passively recorded, the IPG requires the injection of a high-frequency current and it can theoretically be measured from any pair of points on the body surface.

Mechanical surface measurements are for example the ballistocardiogram (BCG) [8], phonocardiogram (PCG) [9], signals from pressure pulse transducers (PPT) [10] and the seismocardiogram (SCG) [8]. The BCG is the recording of forces related to cardiac ejection of blood and some modern systems are usually built to record its longitudinal component from the strain gauges of a weighing scale. The PCG is the recording of cardiac vibrations in the audible band (40-440 Hz) from a noninvasive and cost-effective microphone fixed on the chest, whose placement requires some skill. PPT record changes of pressure due to vascular activity on superficial arteries and can be noninvasively acquired from cost-effective sensors although its placement, above a superficial artery with a solid tissue such as bone below to assure mechanical stability, requires a skilled operator and limits the number of available measurement sites. Finally, the SCG is the recording of chest vibrations in the infrasonic band (0-30 Hz) due to cardiac activity with an accelerometer attached to the chest.

Table 1.1 summarizes these technologies and its fit to the requirements for the measurement of cardiovascular parameters in ambulatory scenarios previously stated.

Table 1.1. Technologies for the measurement of cardiovascular parameters and its fit to ambulatory scenarios.

	Technology examples	Noninvasive	Simple	Cost-effective
Invasive	Catheterization, endoscopy	✗	✗	✗
Imaging	Echography, MRI, *x*-ray	✓	✗	✗
Surface optical	PPG	✓	✓	✓
Surface electrical	ECG	✓	✓	✓
	IPG	✓	✓	✓
Surface mechanical	BCG	✓	✓	✓
	PCG	✓	✗	✓
	PPT	✓	✗	✓
	SCG	✓	✓	✓

The PPG, ECG, IPG, BCG, and the SCG are the most suitable technologies for the measurement of cardiovascular parameters in ambulatory scenarios. However, four additional points that limit the range of suitable technologies have been considered in this thesis.

First, the measurement sites have been limited to the limbs, *i.e* hands and feet. Measurements on such areas do not require removing excessive amounts of clothing, as hands are usually exposed and feet are easily accessible by removing shoes and socks, hence these are less invasive for the subject and can be faster performed. Further, some signals such as the BCG or the IPG can be measured without removing socks or even shoes in the case of the BCG. While the ECG, PPG, IPG, and the BCG can be obtained at the limbs, SCG recordings require a sensor placed on the chest, preferably without clothing and strapped with an elastic band or attached with an adhesive, which is uncomfortable and time-consuming, and makes the measurement less fitted to the previously stated requirements.

Second, the PPG and the IPG reflect volumetric changes in blood vessels due to cardiovascular activity hence it could be assumed that the signals are to some extent interchangeable. However, there is evidence that the contact pressure of the PPG sensor can affect the obtained waveform [11] and introduce shifts on the measured features [12]. Since the underlying mechanisms of both signals are not fully understood yet, the performance of the IPG as surrogate of the PPG, which has received most of the attention in research and clinical practice [5], has scientific interest by itself. Further, IPG systems are more cost-effective since the photo emitter and receiver pair is replaced by inexpensive dry electrodes. These can be easily embedded in any surface, thus providing better integration with existing objects such as portable devices or furniture, and can be easily integrated with other electrode-based systems, such as ECG or other IPG systems, to reduce the overall number of electrodes required. Therefore, the IPG constitutes a better option for systems intended to operate in ambulatory scenarios.

Third, the IPG measured from limb to limb [13] instead of along a single blood vessel is better suited to ambulatory scenarios since two electrodes on each hand or feet are easier to contact with than four in a single hand or feet. However, to the best of our knowledge, the physiological basis of

the limb-to-limb IPG has not yet been discussed although it is plausible that the signal can deliver complementary information to the PPG or the local IPG since it is sensitive to changes along the whole current path besides of local ones.

Finally, the high levels of EMG compared to the amplitude of the ECG typically found on ECG recordings obtained at the feet [14] makes the measurement of beat-to-beat features very challenging even in the best scenarios. The ECG is easier to obtain at the hands and can be integrated into a weighing scale through a handle bar or similar [15].

In consequence, the technologies for the measurement of cardiovascular parameters better suited to the previously stated requisites are the ECG, local IPG, limb-to-limb IPG, and the longitudinal BCG. Fig. 1.2 shows the signals and the sites where these will be obtained in this thesis.

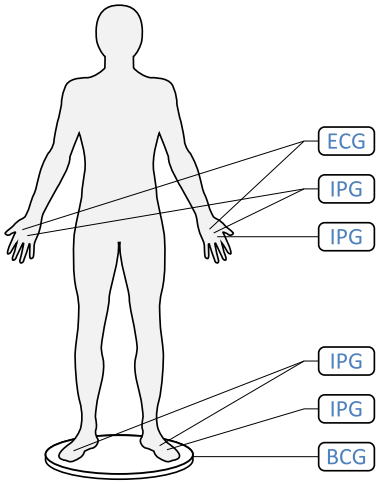

Fig. 1.2. Selected signals and sites of interest for ambulatory measurement of cardiovascular parameters.

The targeted signals can be obtained at the limbs with simple, noninvasive, and cost-effective devices hence they are especially fitted to the measurement of cardiovascular parameters in ambulatory scenarios.

1.2. Time intervals to assess trends in the cardiovascular system

A biomedical signal can be defined as a time-varying quantity that carries information about a biomedical process. Although some useful information can be extracted from the waveform amplitude or morphology, time-domain measurements are typically better suited to the particularities of ambulatory scenarios, which are usually performed in less controlled environments where the recorded signals include more noise and artifacts than in clinical measurements. Then, events in the time domain are easier to analyze than amplitude or morphology features, and the measurements can be performed with higher accuracy. Besides, time-domain measurements do not require normalization, which is a critical problem for several biomedical signals and especially in

ambulatory scenarios, where a wrong sensor placement or an excessive electrode unbalance can lead to an unpredictable signal distortion. Further, measurements on the time domain can be performed not only in a given signal but also between different signals that reflect different physiological processes, to exponentially increase the potential of measuring cardiovascular parameters of interest.

The measurement of time intervals between electrical and mechanical signals to assess the performance of the cardiovascular system has been explored since long ago. The measurement of the pressure pulse propagation through the arterial tree is nowadays the most simple, noninvasive, robust, and reproducible method to evaluate the status of the arterial walls [16]. On each heartbeat, the blood ejected by the heart causes an increase of arterial pressure that propagates through the arterial tree from proximal to distal sites. The velocity of this pulse, the so-called pulse wave velocity (PWV), is related to the stiffness of the arterial walls and can be measured by dividing the estimated distance between these points by the difference of time arrival at two sites, the so-called pulse transit time (PTT) [17]. As volume and flow are in phase on early waveform features such as the foot or the upstroke, the arrival of the pressure pulse can be measured from any device able to measure these quantities, although PPG is the most widely used signal for that purpose due to its simplicity.

In order to get accurate PTT values, the measurement sites should be separated as much as possible but proximal arteries are not easily accessible. For this reason, the proximal pressure pulse is sometimes replaced by the R wave of the ECG, which means that the measured interval, named pulse arrival time (PAT) to differentiate it from the PTT, partially includes the time between the electrical onset of the heart and the aperture of the aortic valve, which marks the beginning of cardiac ejection and propagation of the pressure pulse. This electromechanical delay, named the pre-ejection period (PEP), starts by definition from the beginning of the QRS complex, the Q wave, and has also great interest by itself as it can be used to evaluate the health status of the heart [18]. Fig. 1.3 shows the PTT, PAT, and the PEP measured from the ECG, aortic BP, and the finger BP.

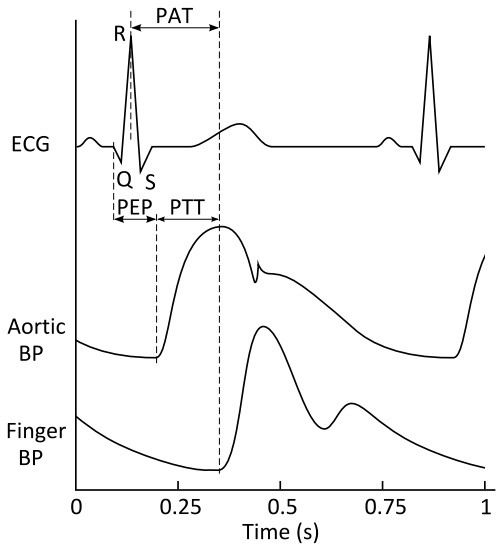

Fig. 1.3. PTT, PAT, and PEP measured from representations of the ECG, aortic BP, and the finger BP.

These three time intervals, the PTT, PAT, and the PEP, are widely used in research and clinical practice since several cardiovascular parameters of interest can be obtained from them. The PTT is a direct indicator of arterial stiffness, which is related to several factors such as ageing or hypertension [15] and associated to many cardiovascular diseases including stroke and myocardial infarction [16]. The carotid-to-femoral PTT measurement, the so-called aortic PTT, is currently the gold standard for the assessment of regional arterial stiffness [17] and it has been included in the "2013 ESC/ESH guidelines for the management of arterial hypertension" [18], although similar information can be delivered from PTT measurements obtained at other sites such as the ankle-wrist segment [19]. The PTT can also be used to monitor peripheral arterial diseases in distal sites caused by pathologies such as diabetes [20], and BP in ambulatory scenarios [19].

The PAT is easier to measure than the PTT as the proximal pressure pulse waveform, which can be difficult to obtain, is replaced by the easily-obtained ECG. Even though in certain situations the influence of the PEP must be considered [20], the PAT has proved to be useful for the detection of sleep disorders [21] and autonomic nervous system activation [22], and for the tracking of fast beat-to-beat changes in BP using intermittent [23] or one-point [24] calibration. Further, the PTT can be derived from two PAT measurements sequentially obtained at different sites [25].

The PEP can be used to monitor left ventricular contractility [26], which provides valuable information about myocardial performance, and sympathetic activity under stable conditions of preload and afterload [27]. Besides, abnormal interval durations can be used to diagnose various diseases such as left ventricular muscular failure, left bundle branch block, or aortic valve disease [28].

These three time intervals, the PAT, PTT, and the PEP, are excellent indicators of cardiovascular performance and can potentially be obtained from the signals here proposed hence

these are especially fitted to be measured in ambulatory scenarios for the assessment of trends in the cardiovascular system.

1.3. Overview of current technologies to obtain the ECG, IPG, and the BCG

Nowadays, several systems able to acquire the ECG, IPG, and the BCG are being used to assess cardiovascular parameters in research and clinical practice from time intervals between their waves. However, many of those systems have been designed for general purposes since it is commonly assumed that systems suitable for medical diagnose do not limit the accuracy of time-interval measurements and that the uncertainty in cardiovascular parameters assessed from time intervals is often limited by other factors, *e.g.* the uncertainty of the aortic length in PWV measurements [29]. For this reason, the uncertainty of cardiovascular parameters assessed from timing measurements is generally reported in comparison to a reference method [29][30][31][32] whereas the uncertainty of the individual timing measurements, which can be affected by the signal acquisition system, is omitted.

While the effect of the sampling frequency of ECG systems in heart rate variability indexes has been briefly analyzed [33], the effect of several parameters such as the phase response of analog filters, noise level, sampling frequency, or the resolution of the analog-to-digital converter (ADC) that have been studied for magnitude-domain measurements has not been quantified for the measurement of time intervals in the proposed signals despite of its scientific interest. A detailed analysis of these uncertainties is fundamental for a better understanding of the reported uncertainties in time interval measurements and could be helpful in the design of cost-effective acquisition systems intended to be used in broad population groups.

Further, many of the measurement systems being used nowadays are legated from old designs intended for purposes other than time interval measurement. Even though these designs can still perform well, the inclusion of parts unsuited to current measurement scenarios results in an unjustified increase of cost and power consumption with a null impact on improving the measurement uncertainty. Therefore, it is mandatory to review the current state-of-the-art of instrumentation to identify the designs that provide the best performance in ambulatory scenarios.

1.3.1. The ECG in ambulatory scenarios

The measurement of the ECG in ambulatory scenarios has been widely explored in the last decades up to the point that several technologies that include Holter monitors, loop recorders, and event recorders are commercially available nowadays [34]. These systems follow a specific standard for ambulatory ECG devices [35], which allows some minor waveform distortions as compared to diagnostic ECG devices [36] as tradeoff for better performance against noise, interference, and artifacts commonly found in ambulatory recordings.

Whereas Holter monitors and loop recorders are designed to be worn for long time periods, event recorders are intended to perform fast short measurements when the patient is symptomatic

hence these are better suited to screenings or regular checks. Event recorders are typically designed to obtain the ECG at the hands by avoiding the use of electrolytic gel, which is commonly used in clinic ECG systems to increase skin conductivity, reduce contact losses due to movements, and absorb surface irregularities such as hair. Instead, the ECG is obtained from metallic surfaces contacted with the palms or the fingers, as in the example device shown in Fig. 1.4.

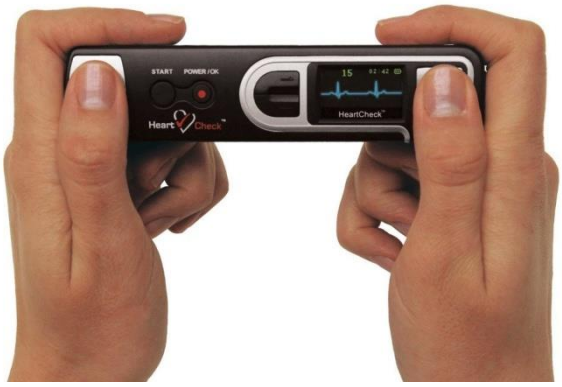

Fig. 1.4. ECG event recorder HeartCheck™ Pen, from CardioComm Solutions Inc.

Further, the ECG can be measured through clothing [37] and even insulating layers such as plastic, which increases the number of design options. Although wet electrodes are preferred in clinical practice, properly designed systems using dry or insulated electrodes can show similar or even better performance [38]. However, systems that use insulated electrodes usually suffer from long settling time after saturation [39], which is common in ambulatory scenarios as a result of motion artifacts, and the recordings can be affected by microphonics [40].

Several systems are similarly designed to obtain the ECG from the hands and only differ in the measurement sites, which can be the indexes [41], thumbs [42], palms [43], fingertips [44], or a combination of the palm and the index of the opposite hand [45]. Another option is to measure the ECG from a system embedded in a wristwatch [46], with an electrode in the wrist and another electrode contacted with a finger of the opposite hand. Finally, some alternative designs use electrodes embedded in common objects or furniture frequently contacted by hands such as a steering wheel or the armrests of a chair [47].

1.3.2. The IPG in ambulatory scenarios

As a result of the popularity of the PPG, the IPG has been relegated to a second plane as tool to obtain pressure-pulse waveforms in research and clinical practice. However, impedance measurements are still common practice for the diagnosis of deep vein thrombosis from blood flow measurements in limbs [48] and for the evaluation of cardiac function by impedance cardiography (ICG) [49], which is routinely used in intensive care units.

The PPG is the most used technology to record pressure-pulse waveforms from limbs in clinical settings and its utility as a cardiovascular monitoring tool has been widely proved [5]. In consequence, the surrogate use of the IPG should show similar performance, as both signals reflect

plethysmographic changes in arteries. However, although the PPG correlates well with blood volume changes because these increase blood density and the path of the light through the tissues, other factors such as the flow-dependent orientation of the erythrocytes have influence on the waveform and can hardly be differentiated [50]. On the other hand, flow-related changes of blood resistivity in large arteries are estimated to represent about 21.5 % of the measured impedance change in the IPG [51], which is enough to change the morphology of the impedance waveform. Further, the contact pressure of the PPG sensor can distort the obtained waveform [11] and shift the measured features [12]. In such circumstances, the performance of the IPG as a surrogate of the PPG could be questionable hence its evaluation has scientific interest.

In [52] the IPG is obtained at the arm and the forearm to assess the PAT, and the correlation with a simultaneous PAT measurement obtained from a finger PPG is strong. Several systems obtain two IPG waveforms along a limb to measure the PTT [53][54][55][56] by injecting a current from two distanced electrodes and measuring impedance in a proximal and a distal site between the injection electrodes. However, this measurement is unpractical in hands or feet as the measurement uncertainty is high due to the short distance between electrodes. Besides, a simultaneous contact with the six electrodes is difficult and can lead to false contacts and motion artifacts. Finally, in [57] the IPG waveform is obtained at the wrist from a handheld devices to detect heart rate. Some modern wristwatches intended for health monitoring are able to acquire this signal and can potentially measure the PAT as they also obtain the ECG, as in the example device shown in Fig. 1.5.

Fig. 1.5. Multi-sensor wearable platform Simband™, from Samsung Electronics Co.

Other IPG measurements at the limbs are performed between distal sites instead of along a single vessel, which yields better signals in terms of signal-to-noise ratio (SNR). The IPG is used to detect the pressure-pulse waveform at the root of the aorta from a whole-body impedance measurement [58] performed from wrists to ankles that is assumed to have a similar performance than the impedance cardiogram (ICG) [49]. However, the influence of impedance changes in limbs, which affect other whole-body impedance measurements [59], is neglected although the systematic underestimation of PTT reported when using the whole-body impedance measurement as a

proximal signal suggests that the waveform is delayed with respect to the ICG waveform and therefore reflects changes in more distal sites.

Other measurements at the limbs performed in distal sites can potentially reflect changes in proximal sites and be easily integrated in daily-used devices. The IPG is obtained from foot to foot in [13] and [60] to detect heart rate, and in [15] to increase the reliability in heartbeat detection from the BCG. Although the physiological basis of this signal is not reported, the signal could be sensitive to the arrival of the pressure pulse at the abdomen as the current flows from leg to leg through it. Analogously, the measurement of impedance from hand to hand, which is described in [61] although no application is reported, could be sensitive to volume changes in the arteries of the thorax that reflect the earliest volume changes caused by cardiac ejection. Therefore, the physiologic basis of both limb-to-limb IPG measurements is unexplained and has scientific interest as they can deliver complementary information to other signals obtained at distal sites such as the ECG, PPG, or other local IPG measurements.

1.3.3. The BCG in ambulatory scenarios

Even though the first observations of the BCG were performed in 1877 [62] and several measurement systems were developed in the late 1930s [63], the signal never became common in medical practice because it required cumbersome measurement setups, like that shown in Fig. 1.6, and the cardiovascular parameters obtained from it could be alternatively obtained from other methods such as the ICG and, later, Doppler ultrasound.

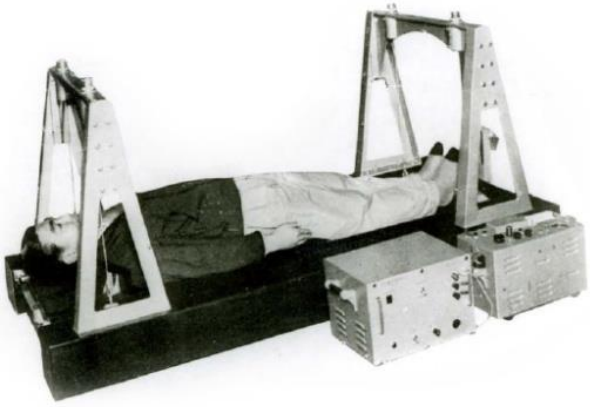

Fig. 1.6. Ballistocardiograph from the 50s, adapted from [64].

Nevertheless, several simple and cost-effective BCG acquisition systems have been developed in the last years, prompting a new interest on this signal. Nowadays, the BCG is obtained from chairs [65], weighing scales [66], beds [67], and accelerometers [68]. Among these, weighing scales and other platforms are the most suitable for short periodic measurements because BCG recordings in chairs are highly influenced by changes in the subject position and systems to record the BCG in beds are cumbersome and most of them do not record the signal along the most interesting longitudinal axis.

The longitudinal BCG acquired from a weighing scale is used to measure heart rate [66] and has been proposed to measure cardiac output [69]. Since the BCG waves are caused by cardiac ejection, most of the research effort is focused on the measurement of the time between the ECG R wave and the BCG J wave, the so-called RJ interval, to assess cardiovascular parameters modulated by the PEP [70] and contractility [71], which is inversely proportional to the PEP under stable conditions of preload and afterload. The RJ interval is also used to monitor changes in systolic BP [14], which has a strong correlation with PEP in short effort tests [72]. However, the J wave is delayed by about 100 ms with respect to the upstroke of the aortic pressure that marks the end of the PEP, as shown in Fig. 1.7.

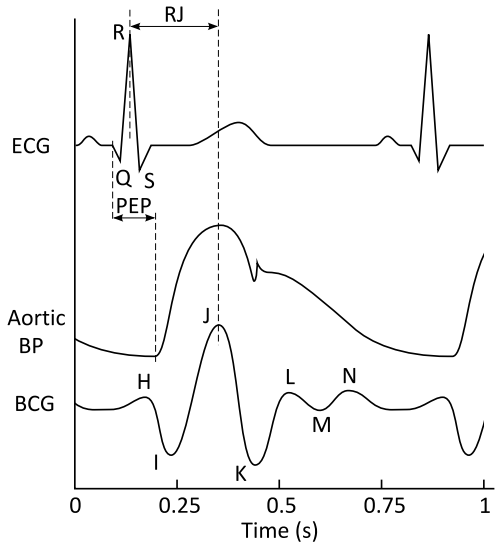

Fig. 1.7. PEP and RJ interval measured from representations of the ECG, aortic BP, and the BCG.

Even though the physiological basis of the BCG was fully described for systems weakly coupled to the environment such as hanging beds [73], which record the ultra-low-frequency BCG [8], it is not possible to elucidate if any of the waves measured from modern systems strongly coupled to the environment such as weighing scales reflect the opening of the aortic valve. For this reason, the J wave is usually taken as a reference for being the greatest feature in the BCG waveform and therefore the wave with the highest SNR. However, the relative timing of the BCG with respect to other physiological waveforms suggests that the J wave is influenced by events caused by the propagation of the pressure pulse along the arterial tree and earlier waves could be more closely related to cardiac ejection. Since the H wave, whose use to assess the PEP was suggested in [74] and is nearly simultaneous with the aortic valve opening, is attributed to ventricular movements due to its absence in recordings without ventricular contraction [75], only the I wave seems to be more closely related to cardiac ejection than the J wave. In consequence, the time interval from the ECG R wave to I wave could show better performance in assessing the PEP than the RJ interval whereas the higher dependency of the J wave on events in distal sites suggests that the IJ interval could be used to assess the PTT from the I wave.

Further, the measurement of time intervals between the BCG and pressure-pulse signals that can be obtained in a weighing scale, such as the IPG, has not been fully explored, even though some systems reported are theoretically capable of performing these measurements [15]. The I wave of the BCG has been very recently used in [76] as a proximal signal to measure the PTT to the finger, which showed a moderately strong correlation to diastolic BP. Since the BCG waveform is caused by cardiac ejection, it is reasonable to assume that the interval from the BCG to a distal pressure-pulse signal obtained at the feet includes the aortic PTT and could be used for its assessment.

1.4. Objectives and their interest

The aim of this thesis is to prove that it is possible to reliably assess changes in the cardiovascular system from time intervals between physiological signals obtained at the limbs. The PEP, PAT, and the PTT have been identified as useful markers of cardiovascular performance that can be noninvasively measured in ambulatory scenarios from the ECG, IPG, and the BCG obtained at the limbs. The main research interests of this endeavor identified from the state of the art are:

1. **To establish the requirements for ECG, IPG, and BCG data acquisition systems intended for the measurement of time intervals.** Most of the systems currently used to acquire signals for time interval measurements have not been specifically designed for that purpose. The effect of several parameters of data acquisition systems such as the phase response of analog filters, noise level, sampling frequency, or the resolution of the ADC that can limit the uncertainty of timing measurements should be studied and quantified. The results will help in identifying the sources of uncertainty in timing measurements and help in the design of cost-effective systems intended for timing measurements.
2. **To design and characterize systems intended to obtain the ECG, local IPG, limb-to-limb IPG, and BCG for the measurement of time intervals in ambulatory scenarios.** Several systems currently used to measure the ECG, local IPG, limb-to-limb IPG, and the BCG have evolved from legacy designs intended for other purposes. The designs should be reviewed and adapted according to the findings of the first objective, to be cost-effective and reliable in ambulatory scenarios. Further, the performance of the systems designed compared to other reference systems for the measurement of time intervals is also relevant. Some examples of particular interest are the performance of ambulatory ECG systems compared to diagnostic ECG systems or the performance of the IPG as a surrogate of the PPG. The systems developed will constitute a reference for further timing measurements.
3. **To evaluate the performance of the IPG measured between hands and between feet for detecting the pressure pulse arrival at proximal sites.** The IPG from limb to limb can potentially reflect changes in proximal sites even though it is measured in distal sites.

However, a model is still required to understand the physiological basis of the signal and predict its behavior. After that, time intervals measured between this signal and other signals measured at the limbs should be able to assess some of the parameters of interest. The results will help in gaining knowledge about this signal to fully explore its potential.

4. **To evaluate the influence of BCG waveform changes in time intervals measured from its waves.** The I wave of the BCG is more likely related to aortic ejection than the J wave hence the RI interval should perform better in assessing the PEP than the RJ interval. In consequence, timings between the I wave and other waves of the BCG that reflect later events of the pressure-pulse propagation through the arterial tree should be correlated to changes in the PTT. Finally, time intervals measured from the I wave to other distal signals obtained from a compact system embeddable in a weighing scale have potential interest as these are also influenced by the PTT. The results will help in increasing the capabilities of weighing scales intended for periodic monitoring of cardiovascular parameters.

1.5. Overview of this document

Chapter 2 is focused on the instrumentation developed to obtain the selected signals in ambulatory scenarios. Section 2.1, 2.2, and 2.3 are devoted to the ECG, IPG, and the BCG, respectively. Each section starts with an introductory background of the physiological basis of the signal followed by a short overview of the instrumentation to obtain it. After that, several factors that limit the uncertainty in timing measurements from the signal are described and characterized. Afterwards, a data acquisition system is proposed and characterized with respect to other reference measurement systems. Finally, section 2.4 describes the data acquisition system and other systems used throughout the experiments to obtain several reference physiological signals.

Chapter 3 is focused on the IPG measured form limb to limb. Section 3.1 gives an introduction to IPG measurements performed from distal sites. Section 3.2 proposes a model to describe the physiological basis of the signal generated from the available physiological data. Section 3.3 evaluates the model for measurements from hand to hand by analyzing the performance of the signal in assessing changes in the PEP from a novel four-electrode handheld system able to obtain the IPG and the ECG. Section 3.4 evaluates the model for foot to foot measurements by analyzing the performance of the signal, combined with the ECG, in assessing changes in the femoral PAT.

Chapter 4 deals on time intervals measured between ECG and BCG waves, inside BCG waves, and between the BCG and the IPG. Section 4.1 describes the possible origin of the BCG waves and the time distances between them to support the hypotheses later tested. Section 4.2 compares the performance of the RI and RJ intervals in assessing cardiac ejection. Section 4.3 analyzes the performance of time intervals measured between the I wave and the J wave in assessing the PTT. Finally, section 4.4 describes and characterizes a novel system to measure the aortic PTT from the BCG and the foot-to-foot IPG embedded in a weighing scale.

Chapter 5 concludes the work with a summary of the contributions, some of their possible implications, and some guidelines for future work.

Chapter 2

Physiological signals and instrumentation

THE ECG, IPG, and the BCG have been previously identified as some of the physiological signals best fitted to the assessment of cardiovascular parameters from time interval measurements in ambulatory scenarios. However, the effect of several factors intrinsic to the signals or the measurement system that can influence the measurement of time intervals, such as the phase response of analog filters, sampling frequency, noise level, or the resolution of the ADC, has not yet been characterized. Further, most of the systems currently being used to obtain them were not originally designed for that purpose and some of their features could be unsuited to modern scenarios. This chapter provides an introductory background of the physiological basis of the signals, analyzes the factors that can influence the measurement uncertainty of time intervals, and describes the instrumentation designed for their measurement in ambulatory scenarios.

2.1. The electrocardiogram (ECG)

The heart is responsible of pumping blood through the vascular tree to transport oxygen, nutrients, and other substances to all the organs and tissues of the body while taking away waste products and regulating the body temperature. The heart is a muscular organ, composed by four chambers separated by valves, which need to be activated in a given order to pump blood continuously to the pulmonary and systemic circuits. The ECG is the recording of the electrical potentials originated during the simultaneous activation of the cardiac cells on different areas of the myocardium, and can be measured either on the heart surface or the body surface. These electrical

potentials were first observed in 1887 by Waller [77] and later recorded by Einthoven in 1902 [78], which named the recording the ECG. Since then, it has become the main tool for heart disease diagnosis as it can be noninvasively acquired from electrodes placed on the body surface and its waveform reflects several pathologies such as myocardial infarction, dysrhythmias, or pulmonary embolism among others.

The electrical activity of the heart is traditionally modeled as a current dipole source, whose position, orientation, and magnitude define a cardiac vector. The measured potentials are the projection of this cardiac vector into a lead vector, defined by the position of the measurement electrodes on the body surface. A standard ECG recording is composed by 12 leads, obtained from 10 electrodes placed on different points of the body surface [36], that measure complementary projections of the cardiac vector. Fig. 2.1 shows a representation of an ECG waveform with its main waves.

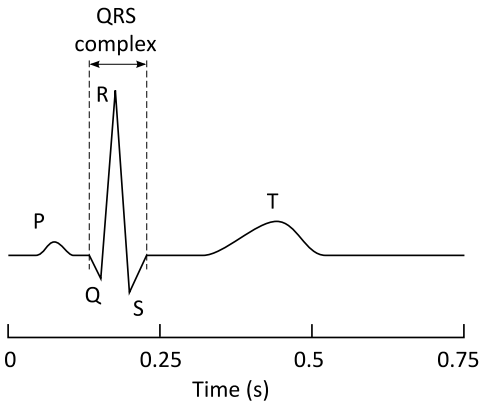

Fig. 2.1. Representation of the ECG waveform and its main waves.

ECG waves are conventionally named by consecutive letters starting by the P wave, which marks the onset of the electrical activity and is caused by atria depolarization. Typical P waves last from 80 ms to 100 ms and their amplitude is less than 300 μV. Afterwards the electrical impulse is delayed from 120 ms to 200 ms in the sinoatrial node before continuing with the depolarization of the ventricles, marked by the QRS complex. In non-pathological hearts, the QRS complex lasts from 60 ms to 100 ms and constitutes the largest amplitude of the ECG waveform, reaching up to 2 mV to 3 mV. Finally, ventricular repolarization causes the T wave, which usually extends about 300 ms after the QRS complex.

In order to avoid waveform distortion caused by analog filters, standard diagnostic ECG systems require a minimal passband from 0.05 Hz to 100 Hz [36], which is designed to have a flat response in phase and amplitude in the whole ECG bandwidth, shown in Fig. 2.2.

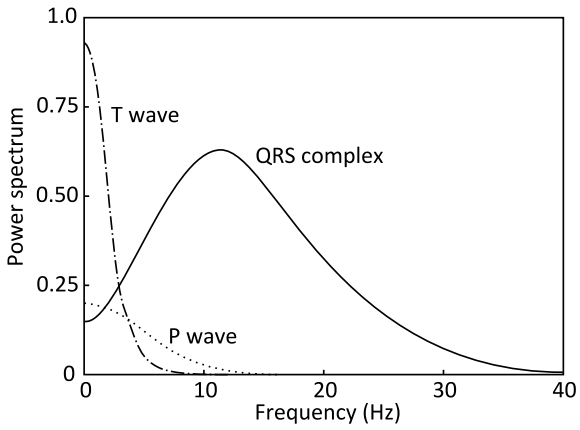

Fig. 2.2. Power spectrum of the ECG and its waves, adapted from [6].

Nevertheless, portable ambulatory devices intended to only analyze rhythm and relevant waveform morphology can have a narrow passband, from 0.5 Hz to 40 Hz [35], which includes most of the spectrum but may introduce some distortions, especially on low-frequency features such as the ST segment.

The most common sources of noise in ECG recordings, identified in [6], are the EMG, power-line interference, baseline wander, and motion artifacts.

The EMG is due to the electrical activity of skeletal muscular cells during contraction [6] and, although it can be avoided in short duration tests if the patient is in resting condition, its presence is usually unavoidable in ambulatory scenarios. Typical amplitudes go from 0.1 mV to 1 mV and its spectrum goes from 5 Hz to 1 kHz, with most of the power overlapped with the QRS spectrum.

50/60 Hz power-line interference can be present in ECG recordings from several mechanisms, identified in [79], although most of it can be avoided if the system is properly designed. Further, the interference in ambulatory ECG devices is outside the signal bandwidth and can be removed by filtering, although it must still be considered as it may cause saturation of intermediate stages.

Baseline wander is due to lung volume changes during respiration, which affect the electrical impedance between the heart and the electrodes. As it is respiration-induced, its spectral content is usually between 0.15 Hz and 0.3 Hz hence it does not significantly overlap with the ECG power spectrum, but it must be considered to avoid amplifier saturation.

Motion artifacts are caused by changes of the skin-electrode impedance as a result of patient movements or poor electrode attachment. They often occur in the band from 1 Hz to 10 Hz and their amplitude can be large enough to cause amplifier saturation.

2.1.1. An overview of ECG instrumentation

ECG leads are acquired from electrodes applied to the skin, usually with some gel to increase skin conductivity, avoid contact loss due to movements, and absorb surface irregularities such as hair. However, the use of wet-gel electrodes is not suited to measurements in ambulatory scenarios: Gel is embarrassing and its application is time-consuming, whereas pre-gelled electrodes must be

replaced after every use. Dry electrodes, where the absence of an electrolyte is rapidly compensated by perspiration [80], are better suited to fast measurements in ambulatory scenarios although these show a higher contact impedance than wet electrodes, about a few megohms at low frequencies, which commonly leads to a higher degree of motion artifacts and power line interference.

The chemical reactions in the metal-electrolyte-skin interface pump electric charges between the electrode and the skin that result in a half-cell potential [81]. In the presence of currents, this half-cell potential can become unbalanced as a result of electrode impedance mismatch, which can be especially high in dry electrodes, and create a differential offset of several tenths of millivolt superposed to the ECG. Further, electrode movements change the contact impedance, which leads to changes in this offset recorded as motion artifacts, especially in dry electrodes due to their higher contact impedance. ECG analog front-ends are usually ac-coupled to reject this offset, with a maximal corner frequency of 0.05 Hz to avoid waveform distortion [36]. However, this cutoff frequency is not high enough to reject motion artifacts and imply long recovery times after saturation.

Systems intended for measuring in ambulatory scenarios are allowed to have a maximal high-pass corner frequency of 0.5 Hz [35] that provides better performance against motion artifacts and causes only minor distortions in low-frequency waveform features, such as the ST segment, that limit the diagnostic capabilities to arrhythmia monitoring and event detection. However, the phase response of filters with this cutoff frequency introduces systematic shifts in the QRS that should be considered when measuring time intervals with respect to other signals.

The ECG is differentially amplified about 1,000 times to obtain a signal in the range of a few volts and afterwards it is low-pass filtered to reduce noise and 50/60 Hz power-line interference, which can reach amplitudes high enough to cause amplifier saturation. Four mechanisms for power-line interference to couple into the ECG analog front-ends identified in [79] are: variable magnetic fields, capacitive coupling to electrode leads, volumetric distribution effects, and capacitive coupling to the body, which results in common-mode and differential mode interference. Fig. 2.3 shows a general model to describe the coupling of some power-line interference to ECG systems.

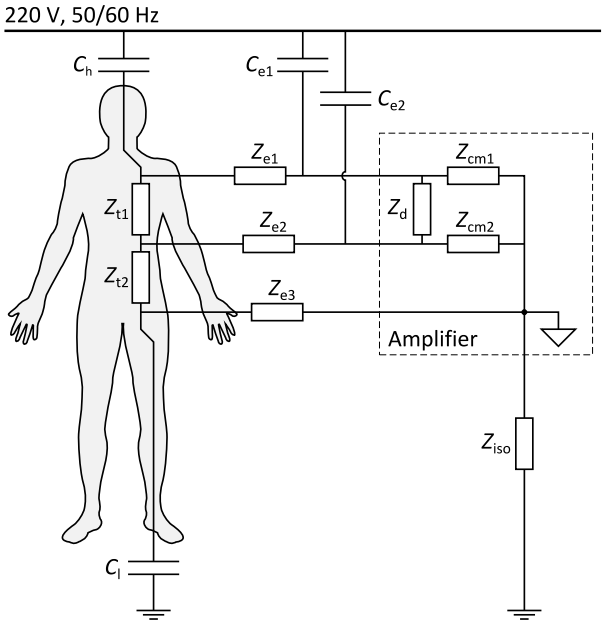

Fig. 2.3. Model for some power-line interference coupling to ECG acquisition systems.

Currents induced by magnetic fields can be reduced by twisting and shortening the lead wires, although these are minimal in handheld devices, which are typically compact and without any external wires. For the same reason, currents directly coupled to the wires are small. Currents coupled to the electrodes can be reduced by shielding them, although the power-line coupling is minimal if the electrodes are covered by the body of the subject leaving no exposed areas. Another option is to decrease electrode impedances Z_{ei}, which in dry electrodes can only be achieved by increasing their area.

The common-mode interference caused by currents coupled to the body is typically rejected by using a third electrode (Z_{e3} in Fig. 2.3) connected to the amplifier reference node, which at the same time is used to provide a return path for the amplifier input bias currents. Although measurements without a reference electrode are feasible, they are not advisable as they are more sensitive to electrostatic charges [82]. The common-mode interference in three-electrode systems depends on the current flowing through the body, which cannot be altered, and the reference electrode Z_{e3}, which motivated the design of the driven-right-leg circuit (DRL) to virtually decrease the impedance of this electrode to zero [83] in ancient grounded ECG systems (where $Z_{iso} = 0$). However, modern ECG systems, and especially battery-operated portable devices, are isolated hence the current through the third electrode is minimal and the common-mode interference is easily rejected by typical values of common-mode rejection ratio (CMRR). Therefore, the impact of this interference on the recorded signals is minimal and the use of a DRL, which implies additional components that increase the cost, may be unjustified. Further, the impact of the DRL on the volumetric distribution of currents into the body Z_{ti} is unknown and can even cause an increase of the overall interference. A more detailed analysis of this issue was reported in [C1].

The differential interference caused by common mode currents coupled to the body is proportional to the common-mode voltage and the imbalance between electrode impedances Z_{ei} compared to the amplifier input impedance Z_{cm}, which turns the common-mode voltage into differential thus reducing the effective CMRR. This interference can only be reduced by decreasing the impedance of the electrodes, which in dry electrodes can only be achieved by increasing their area, or by using an amplifier with $Z_{cm}>>Z_{ei}$.

Finally, volumetric effects, modeled by Z_{ti}, are strongly dependent on the position of the electrodes relative to interference sources hence cannot be predicted. The placement of two symmetrical ground electrodes close to the recording electrodes leads to lower levels of interference in grounded systems [84] but this needs more electrodes and its effectiveness in isolated systems has not been verified.

The remaining ECG interference can be removed by analog filtering although the minimal low-pass cutoff frequency to acquire the ECG without distortion set by the standard for diagnostic ECG devices is 100 Hz [36]. In ambulatory scenarios, where power-line interference is potentially higher, ECG acquisition systems are allowed to have a minimal low-pass corner frequency of 40 Hz [35] that allows filtering of the interference and causes only minor distortions on high-frequency waveform features. However, the same as in the high-pass stage, analog filters introduce systematic shifts in the QRS that should be characterized when measuring time intervals between the ECG and other signals.

Finally, the effect of phase response can be avoided by using digital filters offline, applied in forward and reverse directions, which cause zero-phase response due to phase cancellation in both directions and an amplitude response that equals the squared amplitude response of the original filter. Consequently, these filters have lesser impact on timing measurements although some analog filtering must still be included to avoid amplifier saturation.

2.1.2. Determination of error sources in the ECG R-wave timing

Most of the time intervals measured from the ECG take the R wave as a reference, as it is the most prominent feature of the waveform and can be easily detected with the widely-used Pan-Tompkins algorithm [85]. In handheld devices, the uncertainty of the R-wave timing is tipically limited by the EMG, which is present in higher levels than in clinical recordings and cannot be fully removed by linear filtering as its spectrum is overlapped with the QRS spectrum and constitute a limit for the standard uncertainty [86] in the R-wave timing. However, several parameters of the signal acquisition system, such as the phase response of analog filters, sampling frequency, interpolation and the number of bits of the ADC, can introduce significant errors to the measurement that must be characterized to maintain the uncertainty of the R-wave timing in the level set by the EMG.

The effect of the EMG on the uncertainty of the R-wave timing has been evaluated from the timing shifts Δt of the R wave in a noise-free recording with different levels of added simulated

EMG noise [87]. Typical EMG levels in handheld ECG recordings were estimated from 14 healthy subjects using the system described in section 2.1.3 with the bandwidth set according to the standard for diagnostic ECG devices. In order to induce hemodynamic changes, the subjects were asked to perform a paced respiration maneuver [88] at 0.1 Hz for 50 s. The same maneuver was used to evaluate the performance of a multi-signal system intended for measuring several intervals of interest in [C3]. The signals were acquired and sent to a PC using the system described in section 2.4.1. The EMG was measured in the isoelectric interval between T and P waves of the first 5 heartbeats of each recording. The mean and maximum of the measured EMG root mean square (rms) was 17 mV and 34 mV, respectively, which correspond to 17 μV and 34 μV rms at the input.

Several successive levels of simulated EMG were added to a 100 ms ECG recording, obtained from a single subject by using the standard diagnostic ECG system described in [89] with attachable wet-gel electrodes placed at the shoulders. The EMG was modeled by filtering additive white Gaussian noise (AWGN) with a first-order band-pass filter with cutoff frequencies 35 Hz and 90 Hz, which gives a mean frequency of 90 Hz and a median frequency of 73 Hz according to the characterization of the signal reported in [6]. This method was developed to evaluate the performance of a heart rate algorithm suited to signals with high levels of EMG in [J1]. Fig. 2.4 shows a power spectral density estimation of the simulated EMG.

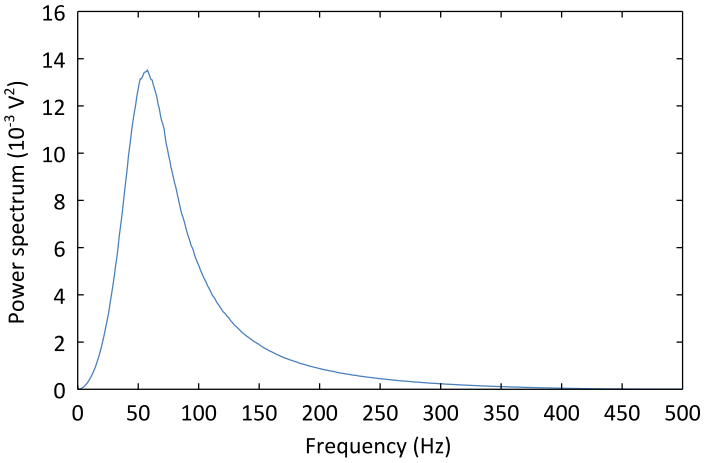

Fig. 2.4. Power spectrum estimation of the simulated EMG.

The uncertainty of the R-wave timing was estimated from the standard deviation of the timing shifts of the R waves on the recordings with added EMG with respect to the original recordings, $\sigma(\Delta t)$. Fig. 2.5 shows the standard uncertainty of the R-wave timing for several levels of EMG in diagnostic and ambulatory ECG systems.

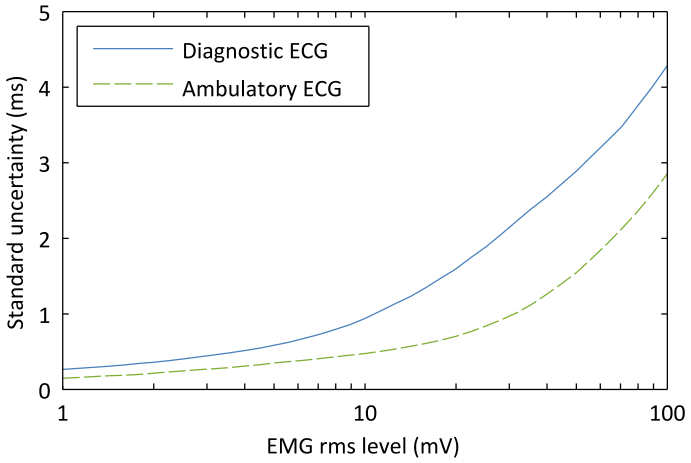

Fig. 2.5. Effect of the EMG noise level on the standard uncertainty of the R-wave timing in diagnostic and ambulatory ECG systems.

For a typical level of EMG below 35 mV rms, the standard uncertainty of the R-wave timing is about 2 ms in diagnostic ECG systems and about 1 ms in ambulatory ECG systems, where most of the EMG power is rejected by the 40 Hz low-pass filter. Therefore, the best option to achieve a minimal uncertainty in ambulatory scenarios is to use the ambulatory ECG bandwidth, since the EMG limits the uncertainty in the measurement, while keeping the other uncertainty sources below the 1 ms level.

Analog filters are also a source of error in timing measurements since their phase response can change the waveform morphology and shift the detected waves. As most of this error is systematic it is mainly reflected on a mean time shift $E(\Delta t)$ and should be estimated and corrected by calibration before estimating the uncertainty of the R-wave timing.

The influence of the cutoff frequency of the ECG high-pass and low-pass filters was estimated from the same 14 recordings previously used to measure the EMG by using three common analog filters: a first order, a second order Butterworth, and a second order Bessel. The systematic shift of the ECG R-wave timing introduced by analog filters is shown in Fig. 2.6.

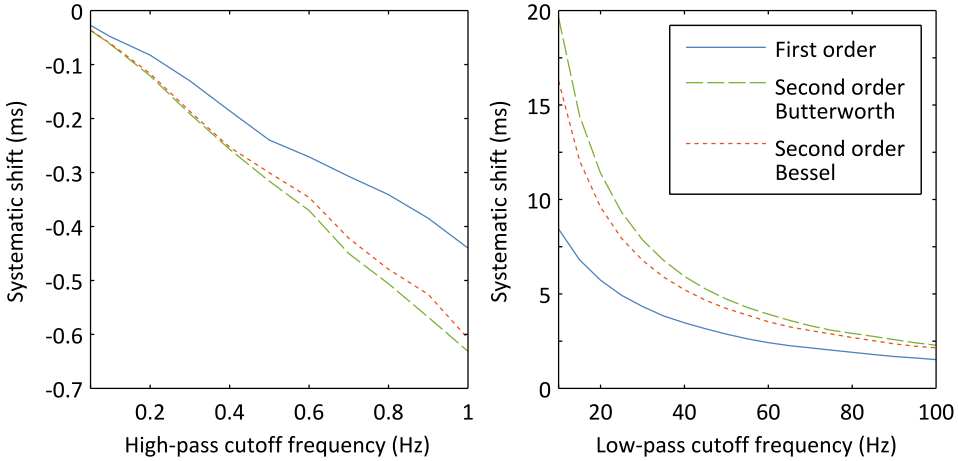

Fig. 2.6. Systematic shift of the R-wave timing introduced by analog filters.

The systematic shift of the R-wave timing introduced by analog high-pass filters in the frequency range studied is below the standard uncertainty introduced by typical EMG noise although the systematic shift introduced by low-pass analog filters is significantly greater. Therefore, measurements using the ambulatory ECG bandwidth will require calibration to achieve a minimal uncertainty when measuring time intervals with respect to other signals.

Finally, the ADC is a source of uncertainty in time interval measurements as time and amplitude quantization cause a shift of the measured points. First, time quantization is an implicit limit of timing measurements although the resolution can be increased by interpolation if the limits set by the Nyquist theorem are respected. However, this requires additional offline processing, which can be limited in low-cost microprocessors, and the uncertainty of the measurement will be determined by the performance of the different interpolators.

The uncertainty introduced by interpolation was estimated from the 100 s recordings previously used to characterize the uncertainty introduced by the EMG (Fig. 2.5). The signal was down-sampled at several factors and then interpolated to the original frequency by using two common interpolators: linear and spline. The standard uncertainty was calculated from the R-wave timing differences between the original and the interpolated recordings. Fig. 2.7 shows the standard uncertainty of the R-wave timing introduced by interpolation.

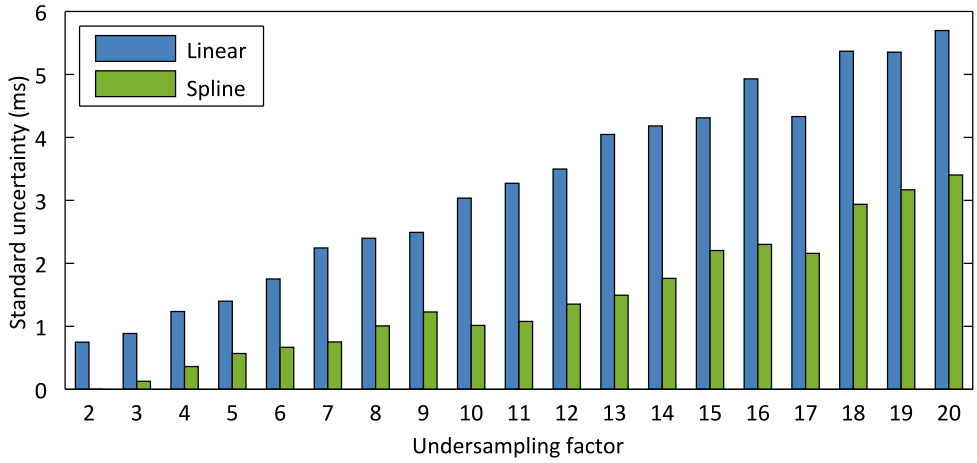

Fig. 2.7. Standard uncertainty of the R-wave timing introduced by interpolation.

In order to achieve an uncertainty in the R-wave timing below the level of 1 ms set by the EMG noise, the sampling frequency can be reduced up to 333 Hz with linear interpolation and up to 125 Hz with a spline interpolation.

Waveform distortions caused by amplitude quantization that can also shift the detected waves. The effect of amplitude quantization was evaluated from the previous recording by decreasing the number of quantization levels. After that, the recordings were band-pass filtered with a first-order filter with cutoff frequencies 0.05 Hz and 100 Hz applied forward and reverse and the standard uncertainty was calculated from the R-wave timing differences between these and the original

recording. Fig. 2.8 shows the standard uncertainty of the R-wave timing with respect to the resolution of the ADC.

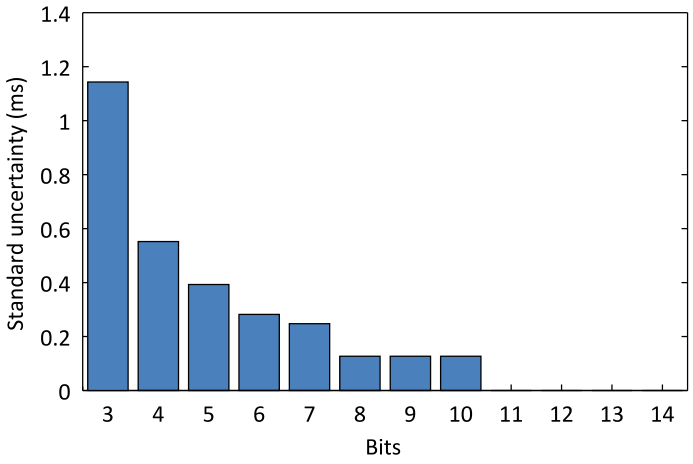

Fig. 2.8. Standard uncertainty of the R-wave timing with respect to the ADC resolution.

A minimal resolution of 4 bits in the ADC is required in order to achieve a standard uncertainty of the R-wave timing below the level of 1 ms set by the EMG noise.

2.1.3.ECG analog front-end design

In addition to the requirements established for a minimal uncertainty in the measurement of the R-wave timing in section 2.1.2, the ECG analog front-end has been designed to operate in ambulatory scenarios while having a minimal number of active components, which results in a lower cost and lower power consumption. The gain and bandwidth was set according to the standard for ambulatory ECG acquisition systems [35], which reject more EMG than diagnostic ECG systems (see Fig. 2.5), and the maximal output noise was set below typical EMG levels (30 mV). The resolution of the ADC was set to 8 bits to match the capabilities of common cost-effective signal acquisition systems, and the sampling frequency was set to 1 kHz, which introduces an uncertainty in the R-wave timing below the level set by the EMG (1 ms) without requiring interpolation.

The design specifications for the ECG analog front-end are summarized in Table 2.1.

Table 2.1. ECG analog front-end specifications.

Parameter	Value
Gain	1,000
Bandwidth	0.5-40 Hz (ambulatory ECG)
Maximal rms output noise	30 mV
Resolution	8 bits
Sampling frequency	1 kHz
Additional considerations	Compatible with dry electrodes. Compatible with an IPG system, which can add up to 1.5 V at 20 kHz.

Although four-electrode dual-ground systems have better performance against volumetric effects of currents coupled to the body, the simultaneous measurement of an IPG requires isolation between system references, which is unpractical since dual grounds interfere with the current injection system. Further, two-electrode systems do not easily drain electrostatic charges hence three-electrode systems perform better.

Dry electrodes contacted by fingers are a practical design that works with different hand morphologies and is suitable for fast short-term measurements. A common option is to connect the dry electrodes to a capacitor in series with each sensing electrode and in parallel with a resistor to block differential voltages caused by mismatches in skin polarization that can saturate the instrumentation amplifier [90]. However, in order to assure an optimal performance these systems require input resistors of several hundreds of megohms, which can cause amplifier saturation due to bias currents, hence the only solution is to directly connect the dry electrodes to a high-impedance amplifier input.

Although dry electrodes can be directly connected to the instrumentation amplifier, this configuration does not reject input offsets or the IPG, which would drastically limit the maximal gain of the instrumentation amplifier and require an additional amplification stage. An alternative solution is to connect the dry electrodes to voltage followers and use a fully-differential band-pass filter to couple them to the instrumentation amplifier. This configuration provides a high-impedance input for the dry electrodes, rejects the offset caused by skin polarization and input bias currents, and at the same time reduces interference and motion artifacts to prevent amplifier saturation. The filter used for that purpose, shown in Fig. 2.9, is a novel design evolved from the topology proposed in [89], designed to allow the flow of bias currents without using any grounded component.

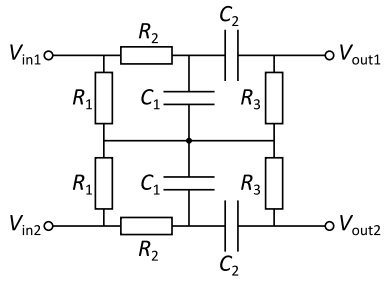

Fig. 2.9. Fully-differential band-pass filter.

The corner frequencies of the band-pass filter shown in Fig. 2.9 are

$$f_l = \frac{1}{2\pi C_2(R_2 + R_3)} \tag{2.1}$$

$$f_h = \frac{R_2 + R_3}{2\pi C_1 (R_2 R_3)} \tag{2.2}$$

and the gain is

$$G = \frac{R_3}{R_2 + R_3}. \tag{2.3}$$

By choosing $R_3 >> R_2$, the gain is about 1, although at frequencies above f_h the input impedance is low due to its dependency on R_2. However, the use of buffered inputs makes this feature irrelevant. The corner frequencies of the filter were set to 0.5 Hz and 40 Hz.

The ECG requires a gain about 1,000 but the instrumentation amplifier should not saturate because of the IPG. At 20 kHz, the band-pass filter provides -54 dB attenuation and any amplifier with a gain-bandwidth product below 5 MHz, which is common in instrumentation amplifiers, would introduce an additional -12 dB (-6 dB/octave) hence 1.5 V, 20 kHz at the input would result in a ripple of approximately 0.75 V at the output of the instrumentation amplifier, which is low enough to avoid amplifier saturation.

Finally, in order to reject the remaining IPG signal and power-line interference, an additional first order low-pass filter with cutoff frequency set to 40 Hz was placed at the output of the amplifier. The equivalent output impedance of the filter is small enough as compared to the input impedance of the following stage.

Fig. 2.10 shows the full analog front-end designed for ECG acquisition.

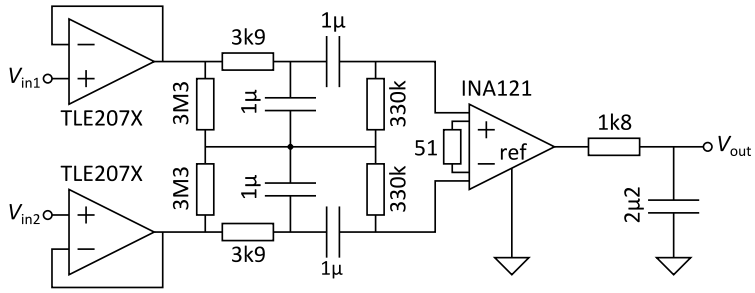

Fig. 2.10. Designed ECG analog front-end.

2.1.4.ECG analog front-end characterization

The designed ECG analog front-end was characterized and evaluated according to the current standards for ECG acquisition systems. Fig. 2.11 shows the measured gain and phase response of the ECG analog front-end in the range from 0.05 Hz to 1 kHz.

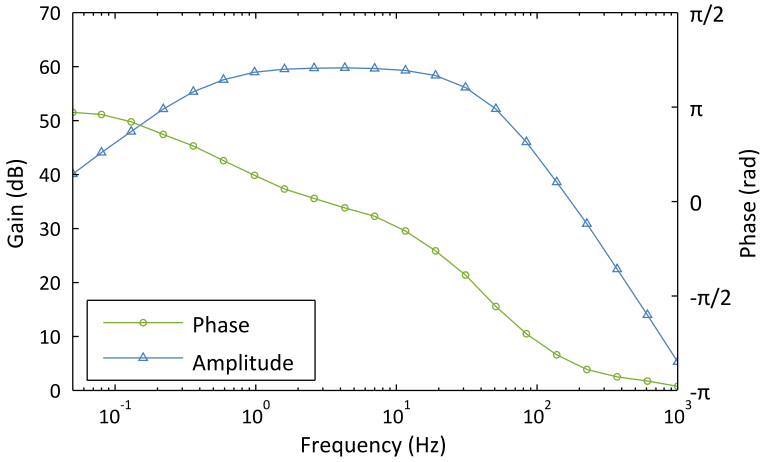

Fig. 2.11. Measured gain and phase response of the ECG analog front-end.

The measured gain at the output of the instrumentation amplifier at 20 kHz was about -4 dB, which is enough to ensure compatibility with the IPG system described in section 2.2.3. The measured CMRR at 50 Hz was 106 dB, which is enough to reject typical values of common-mode interference from power lines in portable battery-operated devices. The rms noise at the output was 1.8 mV, which is much lower than typical EMG noise levels.

In order to estimate the uncertainty introduced by the analog front-end on the R-wave timing, two simultaneous 100 s ECG samples were obtained from a single subject by using the designed system and the standard ECG amplifier for diagnostic described in [89] with pre-gelled electrodes placed at the shoulders. Fig. 2.12 shows a sample of the measured recordings.

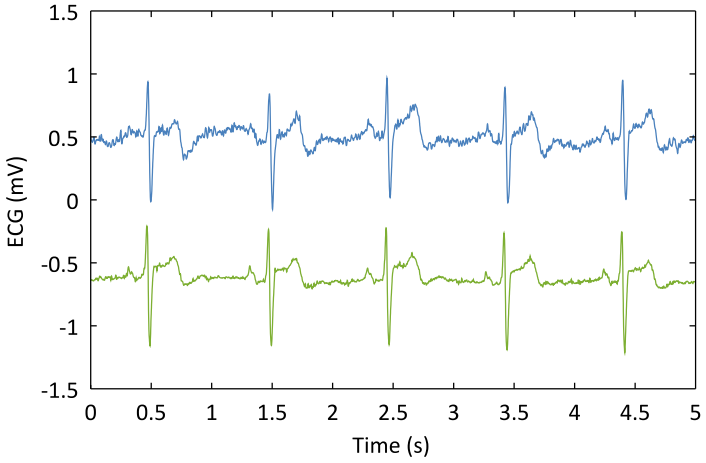

Fig. 2.12. Simultaneous ECG samples from the designed system (top) and a standard diagnostic ECG system [89] (bottom).

Compared to the standard diagnosis ECG, the signal from the designed system shows more artifacts and EMG noise although the main features are still clearly identifiable for diagnosing arrhythmias. The time positions of the R-wave were measured with a modified Pan-Tompkins algorithm and the uncertainty introduced by the designed system was calculated as the difference with respect to the standard system. The mean of the timing shifts was 7.6 ms and the standard

uncertainty was 1.1 ms, which is coherent with the shifts introduced by filters shown in Fig. 2.6 and the uncertainty introduced by EMG noise shown in Fig. 2.4 respectively.

Fig. 2.13 shows the aggregated 122 pairs of RR intervals measured from the standard ECG system, $RR_{standard}$, and the designed ECG system, $RR_{handheld}$, obtained from the subject during the experiment.

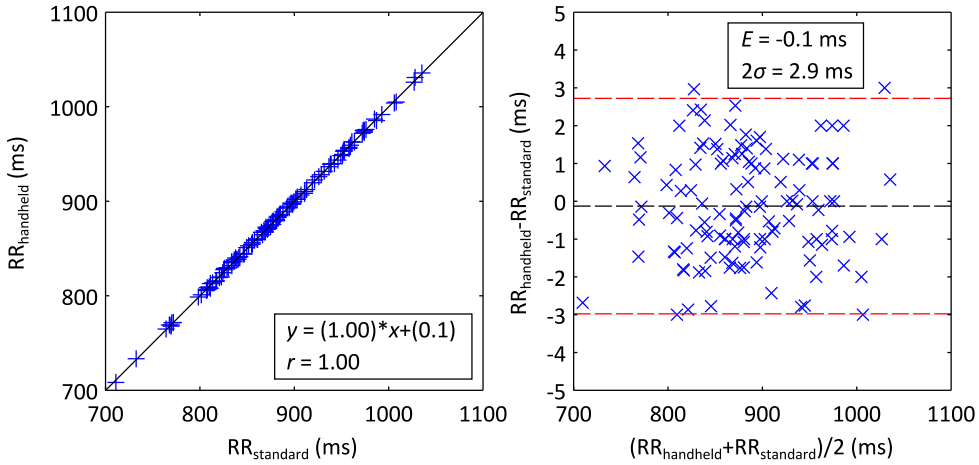

Fig. 2.13. $RR_{handheld}$ vs. $RR_{standard}$, and Bland-Altman analysis of $RR_{handheld}$ vs. $RR_{standard}$ during paced respiration.

The agreement between RR intervals in the correlation analysis is high, and the uncertainty of the $RR_{handheld}$ is coherent with the reported uncertainty of the R-wave timing using the designed ECG system (1.1 ms) and the general equation for the uncertainty of a time difference

$$\sigma(a-b)=\sqrt{\sigma^2(a)+\sigma^2(b)}, \tag{2.4}$$

and is about 35 times larger than the standard deviation of the RR interval during heart rate variability analyses (50 ms) [91].

2.2. The impedance plethysmogram (IPG)

The term IPG was first introduced in the 1950s as a tool for the assessment of blood flow in limbs from changes in blood perfusion [7], although similar techniques had been published under different names since the 1930s. The IPG is the recording of impedance changes on a body segment caused by volume changes related to the pressure-pulse propagation through elastic arteries. For an arterial segment of fixed length l, cross-section A, and resistivity ϱ, the basal resistance R is determined by

$$R=\rho\frac{l}{A}. \tag{2.5}$$

Assuming an increase of volume only in the radial axis, the increase of resistance ΔR is related to the increase of cross-sectional area ΔA according to

$$\Delta R \approx -\frac{\rho l}{A^2}\Delta A. \tag{2.6}$$

IPG waveforms have the same characteristic features observed in other pressure-pulse waveforms such as the PPG or the PPT. Fig. 2.14 shows a representation of an IPG waveform and the main waves that can be identified in it [92].

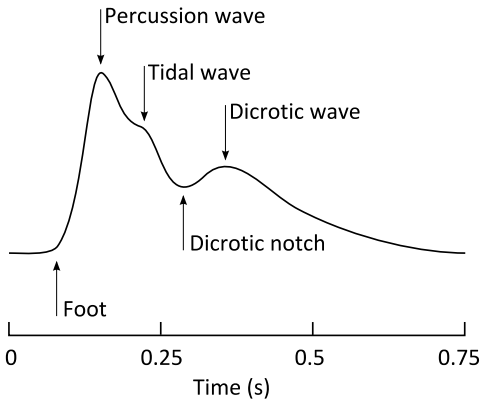

Fig. 2.14. Representation of the IPG waveform and its waves.

IPG waveforms start with the percussion wave, caused by cardiac ejection during systole. After that, there is a second peak named tidal wave that results from the overlapping between the percussion wave and its reflections in arterial branches, mainly at the end of the aorta. The tidal wave amplitude depends on the PTT to the reflection site hence stiffer arteries show higher tidal waves compared to elastic ones [93] whereas distal sites show higher tidal waves than proximal sites. Subsequently, the closure of the aortic valve causes the dicrotic notch, immediately followed by the dicrotic wave caused by reflections of the pressure pulse at distal sites.

Pressure-pulse signals reflect mostly respiration-related changes of venous blood volume in the band from 0.1 Hz to 0.4 Hz and cardiac-related changes of arterial blood volume in the band from 0.8 Hz to 2.5 Hz [94]. However, it is commonly accepted that systems intended for the measurement of pressure-pulse signals must be able to record from the 1st to the 10th harmonic, which typically fall within the band from 0.5 Hz to 20 Hz [95], although the maximal high-pass corner frequency to avoid waveform distortion in the PPG is 0.2 Hz [96]. Some bandwidths reported for IPG devices are 0.5-10 Hz [13], 0.8-4.4 Hz [52][55] and 0.87-12.5 Hz [57].

Motion artifacts, caused by changes in electrode impedance due to movements, are the most relevant source of noise in IPG recordings and typically occur in the band from 1 Hz to 10 Hz.

Further, IPG recordings suffer from higher levels of pink noise than other pressure-pulse signals such as the PPG due to the higher gains that are required for its measurement.

2.2.1. An overview of IPG instrumentation

The IPG is measured at relatively high frequencies, in the range from 1 kHz to 100 kHz, to reduce the influence of basal impedance of tissues and electrodes, and to assure safety conditions for the patient [97]. The IPG can be obtained with only two electrodes, simultaneously used to inject current and measure the voltage drop, but this method also measures electrode impedances that can change due to movements and introduce motion artifacts [98]. Further, two-electrode systems are more sensitive to changes in the areas close to the electrodes than in other areas along the current path due to current constriction near the electrodes [99].

Most IPG systems use four electrodes to separate injection form measurement and to exclude the impedance of injection electrodes from the measurement. However, motion artifacts can still affect recordings due to changes in the contact impedance of the measurement electrodes, which change the offsets caused by input bias currents [98], or due to changes in impedance of the injection electrodes in low-CMRR systems [100].

Typical basal impedances measured at these frequencies are in the range of a few hundreds of ohms hence the currents injected are usually from 0.5 mA to 2 mA in order to get a drop in voltage of a few volts. The differential signal from the measurement electrodes is usually converted to single-ended by using an ac-coupled instrumentation amplifier that rejects electrode drift, low frequency noise and power-line interference, with typical gains between 1 and 100. Afterwards, the signal is downshifted to baseband by synchronous sampling [13], rectification with diodes and low-pass filtering [98], or synchronous demodulation with a switched-gain amplifier and low-pass filtering [60].

Once in the baseband, the signal still requires filtering the dc component, which belongs to the basal impedance, and amplification of the pulsatile signal from 10 to 1,000 times. Some systems include a low-pass filter to provide additional high-frequency noise rejection at this point.

2.2.2. Determination of error sources in the IPG pressure-pulse timing

The IPG pressure-pulse timing is typically measured from the foot of the wave, as this feature is less affected by waveform changes due to pulse propagation and by the overlap of reflected waves, with the intersecting tangents method due to its superior performance [32]. Unlike the ECG, which is measured in the base band, the IPG modulates a high-frequency carrier hence the signal acquired is narrowband and the EMG has little effect on it. However, the uncertainty in the pressure-pulse timing is still limited by motion artifacts, which can be avoided with a proper measurement setup and data acquisition system. As a result of the low gain of the instrumentation amplifier stage and the high total gain of the system, IPG recordings usually show higher levels of pink noise than other pressure-pulse signals such as the PPG that constitute a limit for the uncertainty in the pressure-pulse timing. However, unlike the EMG in ECG recordings, the pink noise level can be reduced by proper instrumentation design. For the measurement of time intervals between both signals, an acceptable level of uncertainty due to pink noise in the IPG would be the

same than the uncertainty introduced by the EMG calculated in section 2.1.2, *i.e.*, 1 ms. As with the ECG R-wave timing, several parameters of the signal acquisition system, such as the phase response of analog filters, sampling frequency, interpolation, and the number of bits of the ADC, can introduce significant errors to the measurement that must be characterized to maintain the uncertainty below the 1 ms level.

The effect of pink noise on the uncertainty of the pressure-pulse timing has been evaluated from the timing shifts in a noise-free recording with different levels of added simulated pink noise [87]. Several successive levels of pink noise were added to a 100 ms PPG recording obtained from a single subject with the system described in section 2.4.2 simulating a noise-free IPG recording. The uncertainty of the pressure-pulse timing was estimated from the standard deviation of the timing shifts of the foot of the pressure pulse on the recordings with added pink noise with respect to the original recordings, $\sigma(\Delta t)$. Fig. 2.15 shows the effect of pink noise on the standard uncertainty of the pressure-pulse timing.

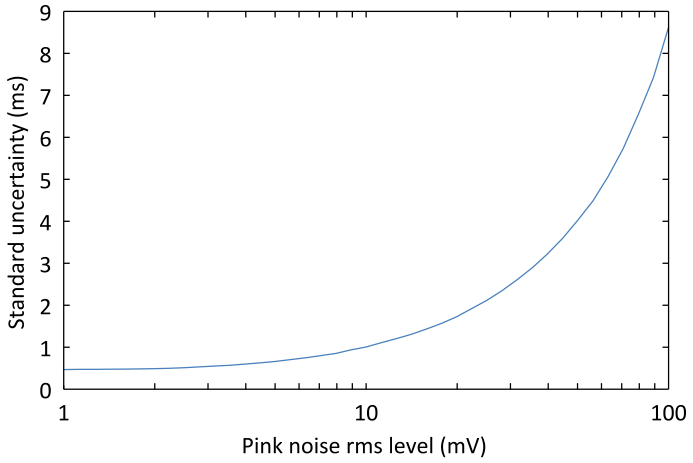

Fig. 2.15. Effect of the pink noise level on the standard uncertainty of the pressure-pulse timing.

The maximal pink noise rms to assure for the foot of the pressure pulse an uncertainty of 1 ms similar to that of the ECG R-wave timing calculated in section 2.1.2 is 10 mV.

As described for the ECG in section 2.1.2, another source of uncertainty in IPG recordings is the phase response of analog filters, which can introduce systematic shifts on the pressure-pulse timing. The influence of the cutoff frequency of the IPG high-pass and low-pass filters was estimated from 14 healthy subjects using the system described in section 2.2.3. In order to induce hemodynamic changes, the subjects were asked to perform a paced respiration maneuver at 0.1 Hz for 50 s. The signals were acquired and sent to a PC using the system described in section 2.4.1. Several cutoff frequencies in the range of interest where simulated by using three common analog filters: first order, second order Butterworth, and second order Bessel. The systematic shift introduced in the pressure-pulse timing introduced by the simulated analog filters is shown in Fig. 2.16.

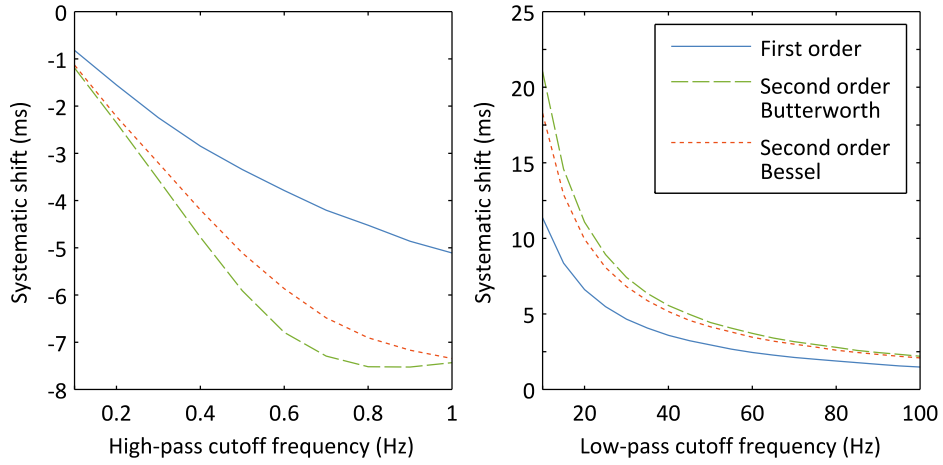

Fig. 2.16. Systematic shift of the IPG pressure-pulse timing introduced by analog filters.

The systematic shift on the pressure-pulse timing introduced by analog high-pass and low-pass filters is several times greater than the standard uncertainty of 1 ms previously reported for the ECG R-wave timing in section 2.1.2 hence absolute timing measurements between the IPG and other signals should be calibrated in order to achieve minimal uncertainty.

The previously described uncertainty introduced by the ADC also affects the timing of the IPG pressure-pulse. The effect of interpolation was estimated from the 100 s recording previously used to characterize the uncertainty introduced by pink noise. The signal was down-sampled at several factors and then interpolated to the original frequency by using two common interpolators: linear and spline. The standard uncertainty was calculated from the pressure-pulse timing differences between the foot of the original pressure pulse and that of the interpolated recording. Fig. 2.17 shows the standard uncertainty of the IPG pressure-pulse timing introduced by interpolation.

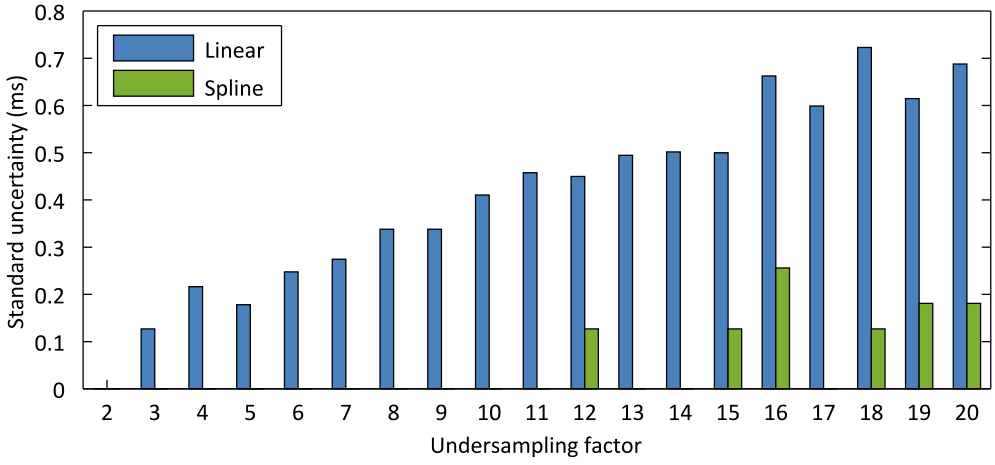

Fig. 2.17. Standard uncertainty of the IPG pressure-pulse timing introduced by interpolation.

The sampling frequency can be reduced up to 50 Hz without introducing an uncertainty in the pressure-pulse timing above the standard uncertainty of 1 ms previously reported for the ECG R-wave timing in section 2.1.2 by using any of the two interpolation methods studied.

The effect of amplitude quantization was evaluated from the previous recording by decreasing the number of quantization levels. After that, the recording was band-pass filtered with a first-order filter with cutoff frequencies 0.2 Hz and 20 Hz applied forward and reverse and the standard uncertainty was calculated from the differences between the foot of the pressure-pulse and that of the original recording. Fig. 2.18 shows the standard uncertainty as a function of the resolution of the ADC.

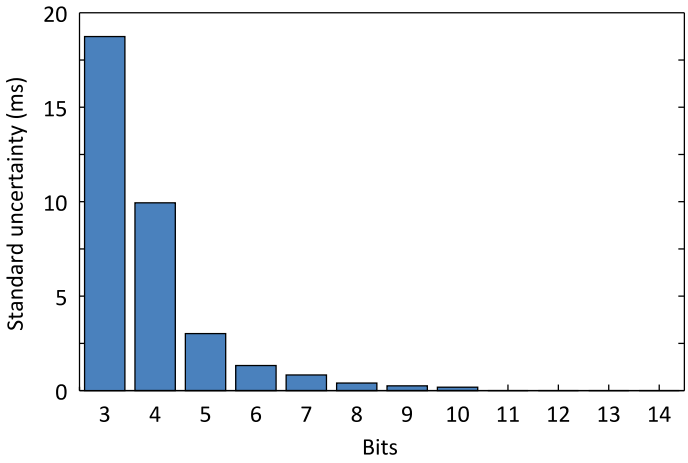

Fig. 2.18. Standard uncertainty of the IPG pressure-pulse timing with respect to the ADC resolution.

A minimum of 7 bits in the ADC are required in order to achieve a standard uncertainty below the standard uncertainty of 1 ms previously reported for the ECG R-wave timing in section 2.1.2.

2.2.3.IPG analog front-end design

As in the ECG case, the IPG analog front-end has been designed to operate in ambulatory scenarios while having a minimal number of active components, which results in a lower cost and lower power consumption, in addition to the requirements for a minimal uncertainty in the measurement of the pressure-pulse timing established in section 2.2.2. The current and gain were set according to common values in IPG systems, and the bandwidth was set according to [95] and [96]. The maximal output noise was set according to the results in Fig. 2.15 whereas the resolution of the ADC was set to 8 bits to match the capabilities of common cost-effective acquisition systems, and the sampling frequency was set to 1 kHz, which introduces an uncertainty in the pressure-pulse timing below 1 ms without requiring interpolation.

The design specifications for the IPG analog front-end are summarized in Table 2.2.

Table 2.2. IPG analog front-end specifications.

Parameter	Value
Frequency	20 kHz
Current	0.5 mA_p
Gain	2200
Bandwidth	0.2-20 Hz [95][96]
Maximal rms output noise	10 mV
Resolution	8 bits
Sampling frequency	1 kHz
Additional considerations	Compatible with dry electrodes.

The IPG measurement frequency was 20 kHz, which is a good tradeoff between interference with baseband signals, such as the ECG, and performance yet does not need costly components. The current source was built from a 20 kHz oscillator connected to a Howland current source designed to inject 0.5 mA peak current, which is suited to typical impedances measured including those of the electrodes.

At this frequency it is not necessary to connect the dry electrodes to voltage buffers to assure an optimal performance as the electrode impedance is only a few kilohms. Instead of using a capacitor in series with the gain-setting resistor [100], which requires a large gain for optimal performance, the measurement electrodes were ac-coupled to the amplifier to reject electrode drifts, low-frequency noise, and power line interference by using the fully-differential high-pass filter described in [89]. The resistors were selected large enough to achieve an input impedance about 100 times larger than electrode impedances [100]. Basal impedances limit the maximal gain of this stage, which was set to 50.

The signal was downshifted to the baseband with a coherent demodulator based on a switched-gain amplifier [60], as synchronous sampling requires a more complex setup and diode-based rectification has worse SNR. Further, coherent demodulators are especially suited to low-noise designs as they keep the pink noise of previous stages outside the band of interest. An integrator was added in a feedback loop from the output to the reference terminal of the instrumentation amplifier to reject the offset at the output of the switched gain amplifier caused by basal impedances thus allowing maximal gain on the next stages. This setup performs like a high-pass filter [89] with corner frequency set to 0.15 Hz and also increases the performance of the signal that drives the switch, which is highly sensitive to offsets.

Finally, the output from the demodulator was filtered and amplified to remove high-frequency components with a second-order Sallen-Key filter with gain set to 220 and a cutoff frequency of 20 Hz. This configuration was enough to reject the 20 kHz carrier and the power-line interference.

Fig. 2.19 shows the full analog front-end designed for IPG acquisition.

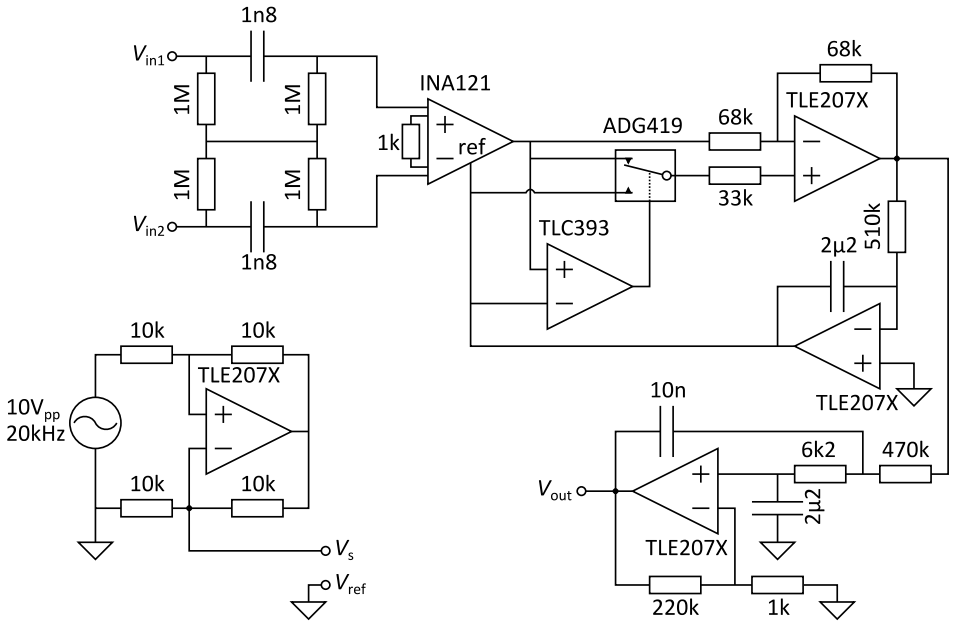

Fig. 2.19. Designed IPG analog front-end.

2.2.4.IPG analog front-end characterization: IPG to PPG comparison

Since IPG acquisition systems are not standardized, the designed system has been characterized and evaluated in comparison to a commercial PPG sensor, which is the most used technology to record pressure-pulse waveforms in research and clinical settings [5]. Even though both signals are sensitive to plethysmographic changes, other factors such as the blood flow, orientation of the erythrocytes, and the contact pressure of the PPG sensor have influence on the measured waveform and must be characterized in order to grant an adequate performance of the IPG in measurements typically performed with the PPG.

The uncertainty in the pressure-pulse timing introduced by the noise of the IPG system was estimated from a 100 s recording with the injection and detection electrodes connected to a 100 Ω resistor, simulating typical basal impedances of local IPG measurements. The rms value of the measured signal, completely attributed to pink noise, was 9 mV, which means that the standard uncertainty introduced on the pressure-pulse timings by the system noise according to the results shown in Fig. 2.15 is about 1 ms.

The performance of the IPG as a surrogate of the PPG was evaluated by simultaneously measuring the PAT from the ECG R-wave to the two signals obtained at the finger. The ECG was obtained from the standard ECG system described in [89] connected to attachable wet-gel electrodes placed in the shoulders. The IPG and the PPG were obtained from the system described in section 2.2.3 and the system described in section 2.4.2, respectively. The IPG injection electrodes were placed in the distal and proximal phalanxes whereas the measurement electrodes were placed at the intermediate phalanx, as close as possible to the PPG sensor placed at the distal phalanx, as shown in Fig. 2.20.

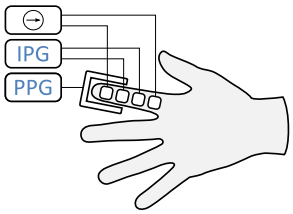

Fig. 2.20. Setup for the IPG system characterization.

The IPG, PPG, and the ECG were simultaneously recorded from three healthy subjects, all of them without any medical condition. In order to avoid the effect of motion artifacts that could hinder the analysis, the IPG was obtained from attachable wet-gel electrodes. In order to induce hemodynamic changes, the subjects were asked to perform a paced respiration maneuver at 0.1 Hz for 100 s. The signals were acquired and sent to a PC using the system described in section 2.4.1. The ECG R-wave timing was measured by applying a modified Pan-Tompkins algorithm, whereas pressure-pulse timings were measured by applying the tangent intersection method. Fig. 2.21 shows a PAT sample measured from the ECG, PPG, and the IPG representative of the measured traces.

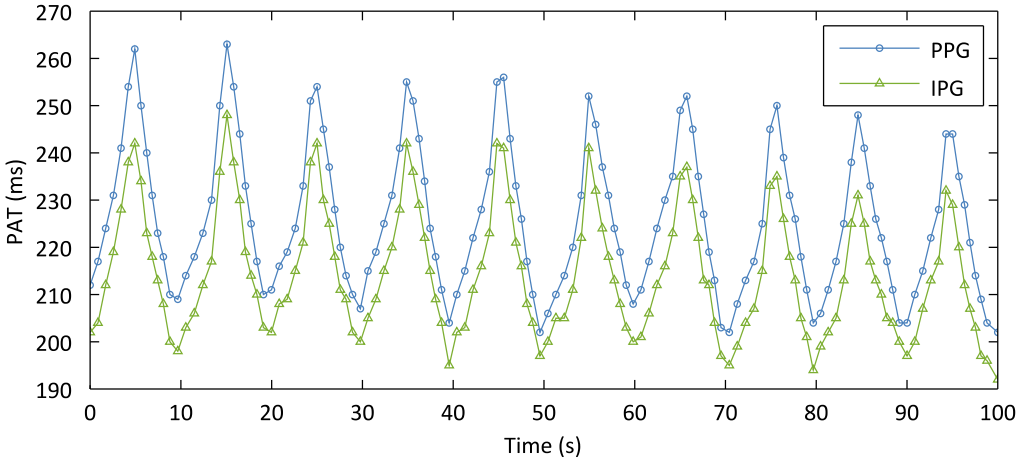

Fig. 2.21. Example of the PAT traces from the ECG, PPG, and the IPG obtained during paced respiration.

The hemodynamic changes induced by paced respiration in the three samples were in phase and had similar amplitudes. The correlation coefficients between the PAT measured from the PPG and from the IPG for each subject were 0.99, 0.99, and 0.94 respectively.

The uncertainty introduced by the IPG was calculated as the difference in PAT with respect to the PPG. The systematic shifts measured were -11.2 ms, -9.3 ms, and -13.4 ms, which are too large to be attributed to the distance between sensors or mismatches in the cutoff frequency of analog filters. Further, these differences cannot be attributed to different sensitivities of the IPG and the PPG to volume and flow, as both magnitudes are in phase at the upstroke.

The standard uncertainties measured were 2.9 ms, 2.0 ms, and 3.3 ms, which are higher than the maximal uncertainty introduced by the system noise at the output and represent about 1.5 % of the total PAT and 10 % of the respiratory-induced variations in PAT.

Fig. 2.22 shows the aggregated 407 pairs of PAT values measured from the ECG R wave to the PPG pressure pulse, PAT_{PPG}, and to the IPG pressure pulse, PAT_{IPG}, obtained from the 3 subjects during the experiments.

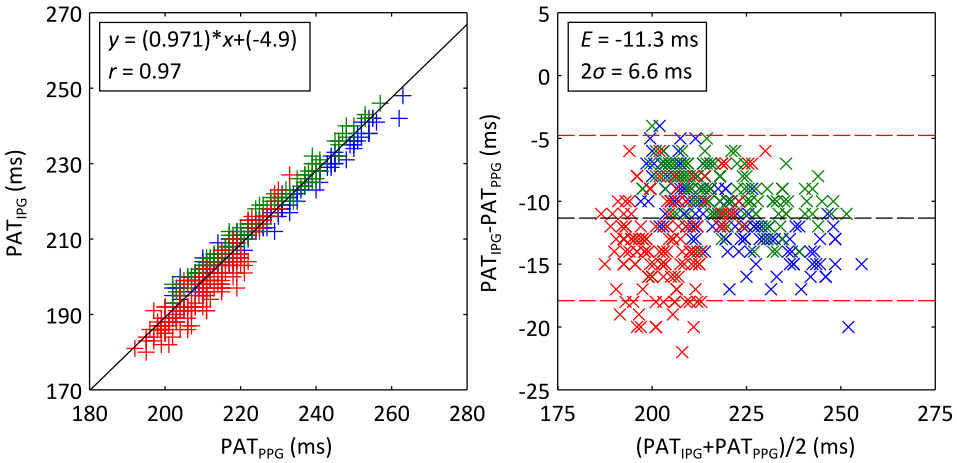

Fig. 2.22. PAT_{IPG} vs. PAT_{PPG}, and Bland-Altman analysis of PAT_{IPG} vs. PAT_{PPG} during paced respiration.

The agreement between PAT values in the aggregated analysis is good, although the mean and standard deviation of the difference is slightly larger with respect to the values reported for individual subjects.

The reasons for this higher uncertainty compared to the expected uncertainty introduced by the system noise can be better explained by examining the uncertainty traces. Fig. 2.23 shows an example of the uncertainty of the PAT measured from the IPG as a surrogate of the PPG, obtained from the same subject of Fig. 2.21.

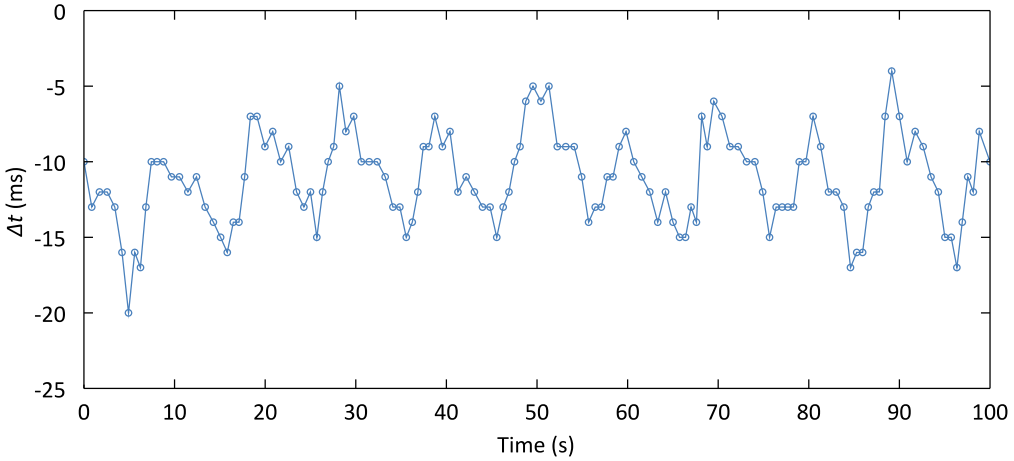

Fig. 2.23. Example of the uncertainty of the PAT measured from the IPG as a surrogate of the PPG.

The uncertainty of the pressure-pulse timing shows a component synchronous with the respiration-induced changes in PAT, with a maximal delay coincident with the shortest PAT, and a low-power random component attributable to noise and artifacts. A plausible explanation of this effect is the influence of the PPG sensor contact pressure, which is known to cause changes in the amplitude and morphology of the measured waveforms [11], and cause time shifts on the measured features [12].

Two additional recordings were obtained from the subjects of Fig. 2.21 and Fig. 2.23, with the PPG sensor set intentionally looser in the first recording and tighter in the second. The mean uncertainties measured were -2.1 ms and -36.3 ms respectively. Fig. 2.24 shows an example of the waveforms recorded with normal, high, and low contact pressure with the difference between maxima and minima of the waveforms.

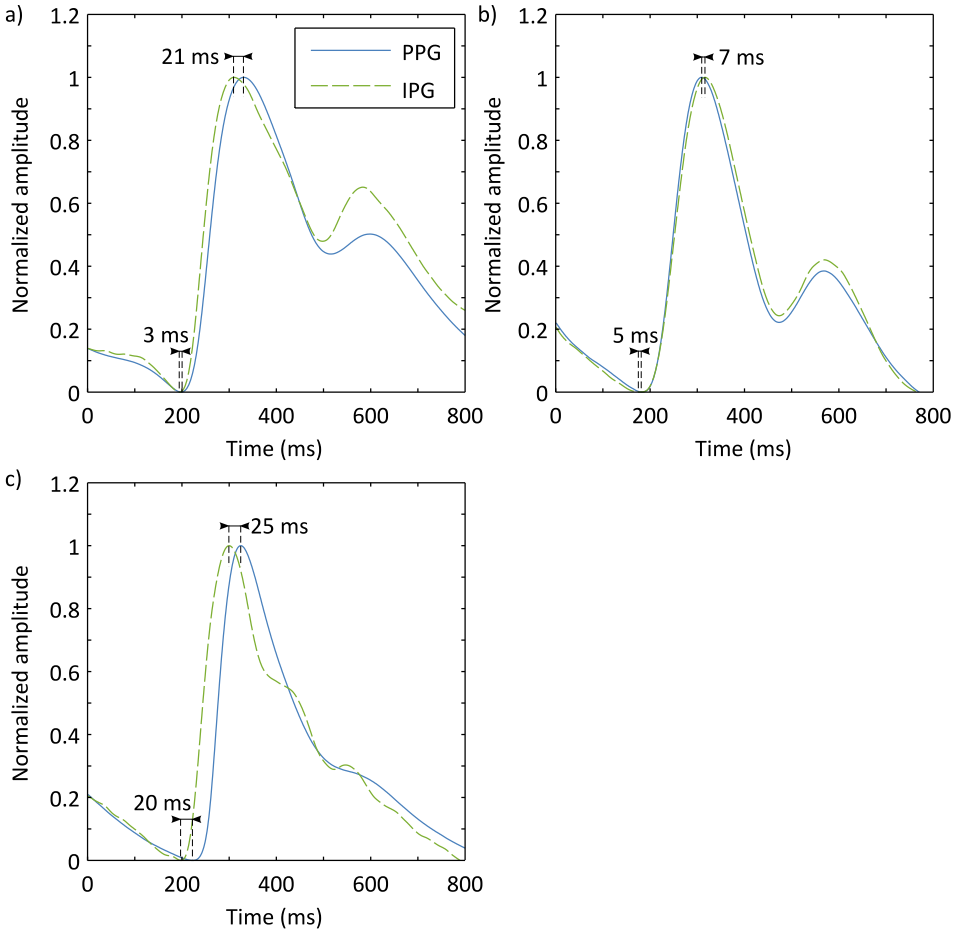

Fig. 2.24. Example of the PPG and IPG waves measured with normal (a), low (b), and high (c) sensor contact pressure and the difference between their maxima and minima.

By comparison with the IPG, an increase of contact pressure causes a decrease of amplitude of the dicrotic notch and a delay of the upstroke in the PPG. The recording with low contact pressure shows the best agreement between IPG and PPG waveforms, although this configuration is extremely sensitive to motion artifacts. In the recording with high contact pressure, the IPG signal also seems influenced as both signals are clearly overdamped.

This experiment shows that the contact pressure of the PPG sensor not only affects the amplitude of the waveform but also the timing of the upstroke by acting like a mechanical low-pass filter. As the PPG sensor used in the tests is mounted on a fixed-length strap, the increase of blood volume induced by paced respiration causes an increase of contact pressure, which could explain the results shown in Fig. 2.23.

Similar results were obtained by using other commercial systems including a transmission PPG system and a glued PPG system hence it can be concluded that the PPG is not a reliable source for absolute time interval measurements if contact pressure is not well controlled, since the uncertainty introduced by this phenomena is potentially higher than the uncertainty attributable to noise in the PPG.

In order to separate this effect, which is intrinsic to the PPG system but not to the IPG system, and estimate the uncertainty introduced by the IPG system, the uncertainty traces were filtered by using a fourth-order Butterworth low-pass filter with cutoff frequency set to 0.2 Hz applied forward and reverse to estimate respiration-induced uncertainty introduced by the PPG. The uncertainty introduced by the IPG system was obtained from the difference between the original uncertainty and that estimated for the PPG. Fig. 2.25 shows the estimated contributions of the IPG and the PPG in the uncertainty trace in Fig. 2.23.

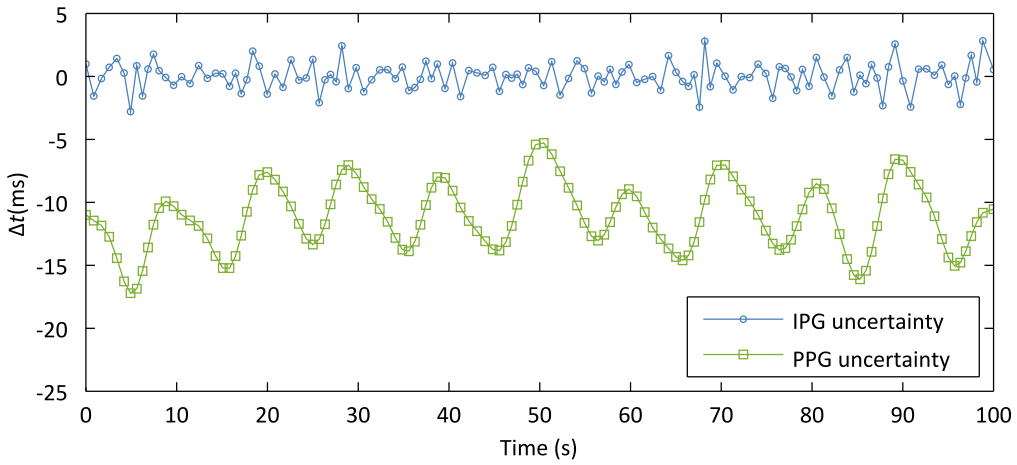

Fig. 2.25. Estimation of the contributions of the IPG and the PPG to the uncertainty of the PAT obtained from the IPG as a surrogate of the PPG shown in Fig. 2.23.

The estimated contributions of the IPG to the uncertainty of the PAT of each subject were 1.1 ms, 0.9 ms, and 1.8 ms respectively, which are coherent with the voltage noise measured at the output and the effect of pink noise predicted from Fig. 2.15. On the other hand, the estimated contribution of the PPG to the uncertainty of the PAT due to changes in the contact pressure under paced respiration was 2.6 ms, 1.9 ms, and 2.7 ms respectively, and clearly predominates over the uncertainty attributed to the IPG.

2.3. The ballistocardiogram (BCG)

The BCG is the recording of forces caused by blood displacements through the arterial tree as a result of cardiac ejection. These forces can be measured from the displacement, velocity or acceleration of the gravity center of the body and have components in all three geometric axes. The first observations of the BCG were performed in 1877 [62] although the technique remained unpublished until some years later [63]. The practical limitations of early BCG recorders, which were cumbersome fully-mechanical devices, combined with the advent of the ECG and, later, catheters and ultrasound techniques, lead to the progressive abandonment of the technology until recent times, when technological advancements made possible the measurement from simple and cost-effective modified weighing scales [66], which are especially suited to periodic monitoring in ambulatory scenarios since only require the subject to stand motionless on the scale to record the BCG in the head-feet axis, the so-called longitudinal BCG

The weighing-scale BCG waveform and its main waves are named using alphabetically consecutive letters from H to N, as shown in Fig. 2.26,

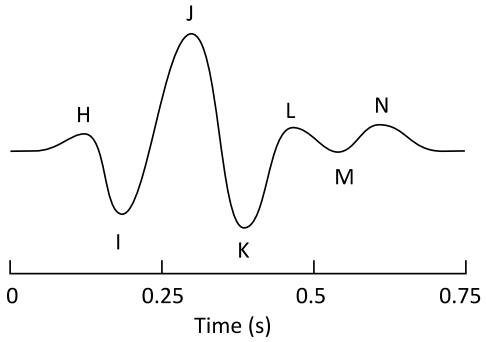

Fig. 2.26. Representation of the weighing-scale BCG waveform and its waves.

Several studies have been carried out to relate the main BCG waves to physiological events in the cardiac cycle [101] [102] although most of these are referred to the ultra-low-frequency BCG obtained from instrumented beds [73], in which the body of the subject is weakly coupled to the environment and the BCG is recorded from the displacement of the body centre of gravity [8], and do not necessarily apply to the waves of the weighing-scale BCG due to their different nature. The weighing-scale BCG waveform starts with the H wave followed by the IJK complex, which is its most clearly identifiable feature and is generally attributed to cardiac ejection. The ensuing L, M, and N waves are mostly attributed to the superposition of pressure-pulse reflections in peripheral arteries and secondary reflections in the aorta.

There are currently no standards for the acquisition of the BCG although it is known that the frequency components of the signal are mostly in the band from 1 Hz to 10 Hz [103]. In order to avoid possible waveform distortions due to the phase response of analog filters, early studies recommended a low-pass frequency of 30 Hz [104] or a minimal bandwidth of 0.5-50 Hz [105],

although systems intended for time interval measurements usually have narrower bandwidths, such as 0.1-10 Hz [66], 0.2-25 Hz [70], 0.5-30 Hz [14], and 0.1-25 Hz [106].

Motion artifacts, in the frequency band from 1 to 10 Hz, are the most relevant noise source in BCG recordings, especially in recordings obtained from standing subjects.

2.3.1. An overview of BCG instrumentation

BCG systems built from weighing scales use their strain gauges, mounted in a Wheatstone bridge, to transform vertical forces into an electrical voltage. The differential signal is usually ac-coupled to a differential amplifier to remove the dc component due to body weight, which is often implemented with an integrator in a feedback loop to the reference node of the instrumentation amplifier [107], or the same plus a differential filter [66]. Typical gains of this stage are in the range from 10 to 1,000.

Afterwards, the signal is usually band-pass filtered to remove offsets caused by bias currents and to reduce high-frequency noise and interference. Finally, the signal is amplified by about 10 to 100 times to obtain an output voltage in the range of a few volts. Some systems include an additional low-pass filter to further reject high-frequency noise.

Alternatively, the Wheatstone bridge can be ac-driven to achieve better noise performance [108]. This design uses a similar structure with the only addition of a demodulation block after the instrumentation amplifier.

2.3.2. Determination of error sources in the BCG J-wave timing

Time intervals measured from the BCG usually take the J wave as a reference as it is the most prominent feature of the waveform. The simplest algorithms for its detection relay on a windowed detection of the maximum by using other reference signals such as the ECG. The uncertainty in these measurements is usually limited by motion artifacts, which are comparatively stronger and more frequent than in other biomedical signals. As motion artifacts are subject-dependent rather than system-dependent, typical values of uncertainty in the J-wave timing are calculated in section 2.3.4 below. For the measurement of intervals between both signals, an acceptable level of uncertainty would be the same than the uncertainty introduced by the EMG calculated in section 2.1.2 that was also proposed for the IPG pressure-pulse timing in section 2.2.2, that is, 1 ms. As with the ECG R-wave timing and the IPG pressure-pulse timing, several parameters of the signal acquisition system, such as the phase response of analog filters, sampling frequency, interpolation and the number of bits of the ADC, can introduce significant errors to the measurement that must be characterized to maintain the uncertainty below the 1 ms level.

Unlike the ECG and the IPG, there seems to be no consensus about the minimal bandwidth for BCG acquisition required to analyze the influence of the phase response of analog filters. In order to estimate its bandwidth, the BCG has been acquired from the modification of the system described in section 2.3.3 shown in Fig. 2.27.

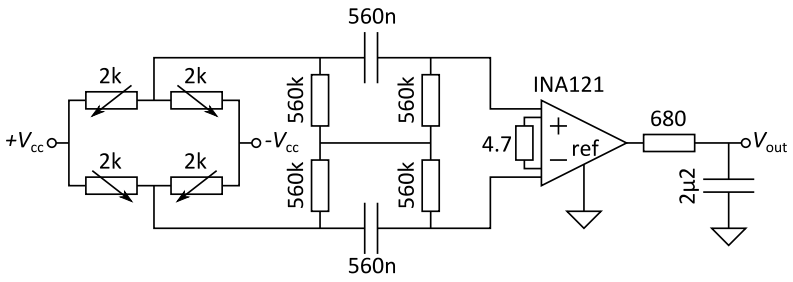

Fig. 2.27. System to study the BCG bandwidth.

This system has a relatively wide bandwidth from 0.5 Hz to 100 Hz to allow up to 50 harmonics considering regular heart rates from 60 beats per minute to 120 beats per minute, although the high gain of the instrumentation amplifier causes an undesired output offset of about 0.5 V. The BCG was recorded from 5 healthy volunteers in order to include different waveform morphologies in the analysis. The subjects were asked to stand motionless for 25 s to obtain recordings with a minimal degree of artifacts. The ECG was simultaneously recorded with the system described in section 2.1.3 and the signals were acquired and sent to a PC using the system described in section 2.4.1. Fig. 2.28 shows the mean of the BCG power spectrum estimations.

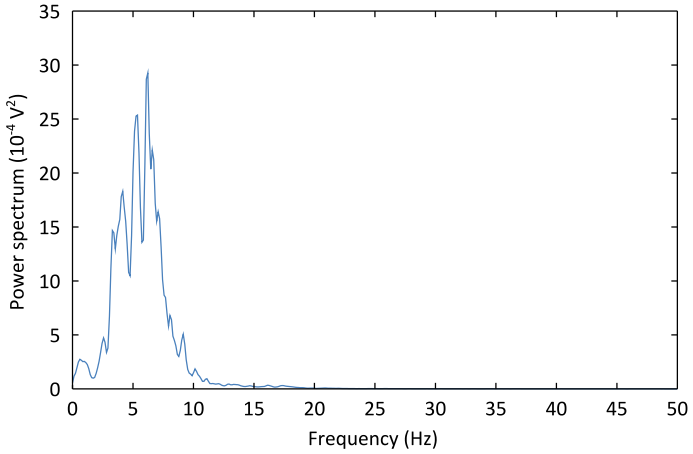

Fig. 2.28. Mean of the BCG power spectrum estimations.

As stated in [103], 95 % of the power of the mean BCG spectrum was in the band from 0.5 Hz to 12.5 Hz although there was some power up to 20 Hz. In some recordings, up to 11 harmonics were clearly identifiable, as shown in the example in Fig. 2.29.

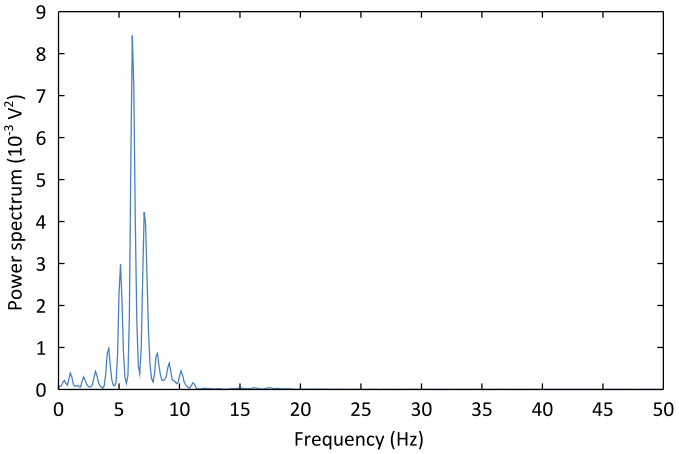

Fig. 2.29. Example of BCG power spectrum estimation with 11 harmonics.

Therefore, assuming that regular heart rates for standing subjects are in the range from 50 beats per minute to 120 beats per minute, which implies that fundamental frequencies are between 0.8 Hz and 2 Hz, the minimal bandwidth for BCG acquisition systems to include 11 harmonics should be 0.5-25 Hz.

The influence of the cutoff frequency of the BCG high-pass and low-pass filters was estimated from 14 healthy subjects, all of them without any medical condition, using the system described in section 2.3.3. In order to induce hemodynamic changes, the subjects were asked to perform a paced respiration maneuver at 0.1 Hz for 50 s. The signals were acquired and sent to a PC using the system described in section 2.4.1. Several cutoff frequencies in the range of interest where simulated by using three common analog filters: first order, second order Butterworth, and second order Bessel. The systematic shift in the J-wave timing introduced by the simulated analog filters is shown in Fig. 2.30.

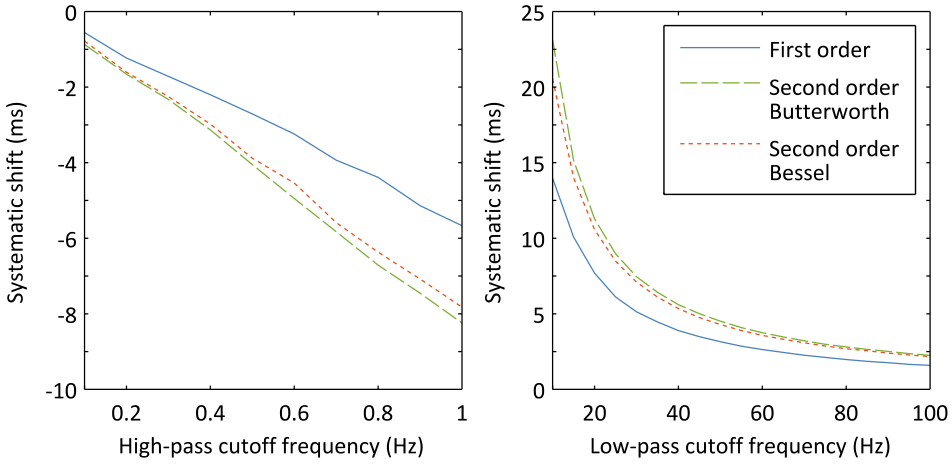

Fig. 2.30. Systematic shift in the J-wave timing introduced by analog filters.

The systematic shift introduced in the J-wave timing by analog high-pass and low-pass filters is several times larger than the standard uncertainty of 1 ms previously reported for the ECG R-wave timing in section 2.1.2 and the IPG pressure-pulse timing in section 2.2.4 hence absolute timing

measurements between the BCG and other signals should be calibrated in order to achieve minimal uncertainty.

The uncertainty introduced by the ADC in timing measurements can also increase the uncertainty in the J-wave timing. The effect of interpolation was estimated from the five 25 s recordings previously used to characterize the BCG spectrum. The signal was down-sampled at several factors and then interpolated to the original frequency by using two common interpolators: linear and spline. The standard uncertainty was calculated from the J-wave timing differences between the original and the interpolated recording. Fig. 2.31 shows the standard uncertainty of the pressure-pulse timing introduced by interpolation.

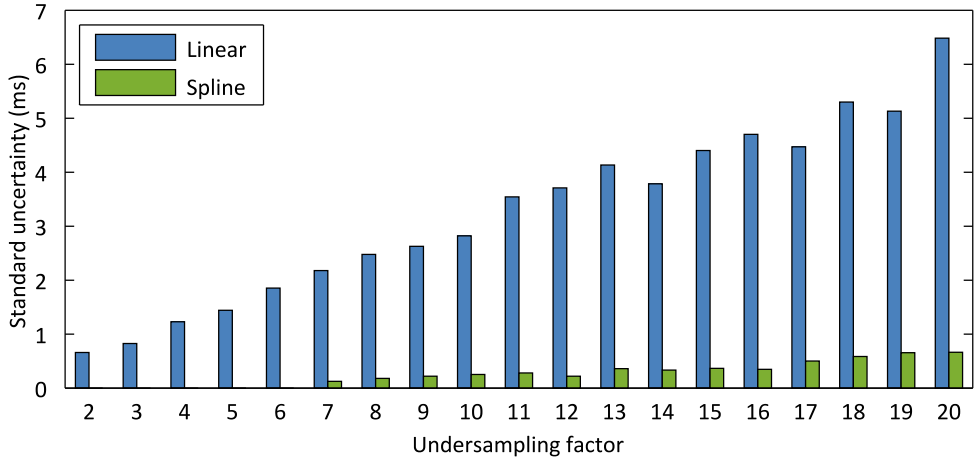

Fig. 2.31. Standard uncertainty of the J-wave timing introduced by interpolation.

In order to achieve an uncertainty lower than the standard uncertainty of 1 ms previously reported for the ECG R-wave timing in section 2.1.2 and the IPG pressure-pulse timing in section 2.2.4, the sampling frequency can be reduced up to 333 Hz with linear interpolation and up to 50 Hz with a spline interpolation.

The effect of amplitude quantization was evaluated from the previous recordings by decreasing the number of quantization levels. After that, the recordings were band-pass filtered with a first-order Butterworth filter with cutoff frequencies 0.5 Hz and 25 Hz applied forward and reverse and the standard uncertainty was calculated from the pressure-pulse timing differences between these and the original recording. Fig. 2.32 shows the standard uncertainty of the J-wave timing with respect to the resolution of the ADC.

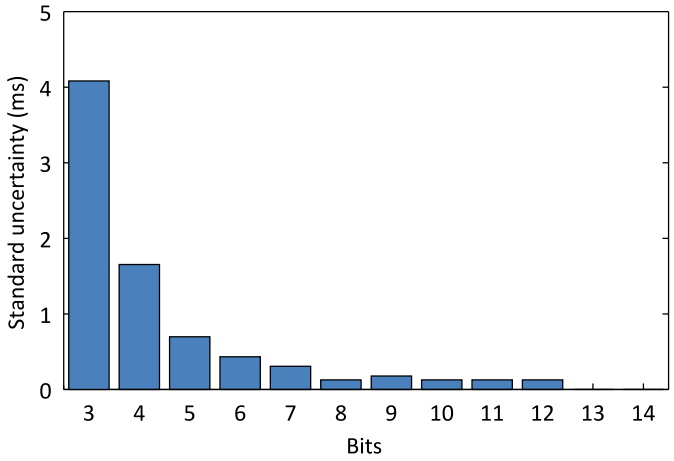

Fig. 2.32. Standard uncertainty of the J-wave timing with respect to the ADC resolution.

A minimum of 4 bits in the ADC are required in order to achieve a standard uncertainty of the J-wave timing below the standard uncertainty of 1 ms previously reported for the ECG R-wave timing in section 2.1.2 and the IPG pressure-pulse timing in section 2.2.4.

Some of the results presented on this section in were reported in [C4] and [J2] as a first step towards standardization of BCG systems.

2.3.3.BCG analog front-end design

As in the ECG and IPG case, the BCG analog front-end has been designed to operate in ambulatory scenarios while having a minimal number of active components, which results in a lower cost and lower power consumption, in addition to the requirements for a minimal uncertainty in the measurement of the J-wave timing established in section 2.3.2. The gain was set according to common values in BCG systems, and the bandwidth was set according to the results reported in section 2.3.2. The resolution of the ADC was set to 8 bits to match the capabilities of common cost-effective acquisition systems, and the sampling frequency was set to 1 kHz, which introduces an uncertainty in the J-wave timing below 1 ms without requiring interpolation. The maximal output noise has been not analyzed since motion artifacts are constant and several orders larger than typical levels of noise BCG recordings from standing subjects.

The design specifications for the BCG analog front-end are summarized in Table 2.3.

Table 2.3. BCG analog front-end specifications.

Parameter	Value
Gain	25,000
Bandwidth	0.5-25 Hz (see section 2.3.2)
Resolution	8 bits
Sampling frequency	1 kHz

The BCG is a force signal superimposed to a large offset caused by the body weight hence it requires high-pass filtering before amplification to avoid amplifier saturation or an ADC with a very large dynamic range. High-pass filtering can be achieved with a differential filter or with an

integrator in the feedback loop of the reference node of the instrumentation amplifier, although this second option is less desirable as it cannot handle large offsets and requires an additional amplifier.

The high-pass filtering block has been built with the fully-differential first-order high-pass filter described in [89], with corner frequency set to 0.5 Hz to reject offset and some motion artifacts, and with resistors several times larger than the strain gauges to avoid excessive voltage loading effect.

The gain of the instrumentation amplifier was set to 5,000, which causes an output offset of a few hundreds of millivolts due to non-ideal amplifier characteristics. In order to remove it, the final stage was ac-coupled to an inverter amplifier with gain 5 and corner frequency 0.5 Hz, and connected to a first-order low-pass filter with corner frequency set to 25 Hz to remove typical values of high-frequency noise and interference in BCG systems. The equivalent output impedance of the filter is small enough as compared to the input impedance of the following stage.

Fig. 2.33 shows the full analog front-end designed for BCG acquisition.

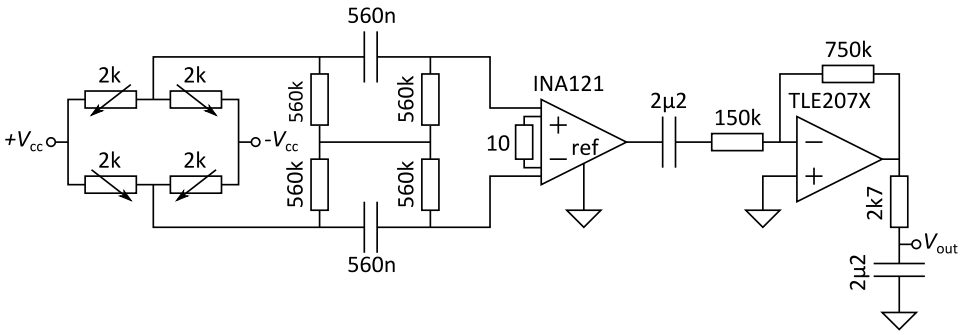

Fig. 2.33. Designed BCG analog front-end.

2.3.4.BCG analog front-end characterization

Since BCG acquisition systems are not standardized and similar waveforms cannot be obtained from other reference systems, the uncertainty of the J-wave timing in BCG recordings from the designed system has been characterized from the high-frequency component of the RJ interval in the two sets of measurements described in section 2.3.2, obtained by filtering the low-frequency component induced by maneuvers or hemodynamic regulation.

The first set of 5 BCG recordings, which were recorded with a low level of artifacts, were digitally filtered to simulate an analog band-pass filter with cutoff frequencies 0.5 Hz and 25 Hz and match the bandwidth of the system designed whereas the second set of 14 recordings under paced respiration was left unadjusted. RJ changes induced by respiration and hemodynamic regulation were estimated by filtering the RJ intervals with a fourth-order Butterworth low-pass filter with cutoff frequency set to 0.2 Hz applied forward and reverse. The uncertainty in the J-wave timing introduced by motion artifacts was calculated as the difference between the original RJ interval and the estimated maneuver-induced changes in the RJ interval. Fig. 2.34 shows an example of the

measured RJ and the estimation of maneuver-induced changes, extracted from the second set of recordings.

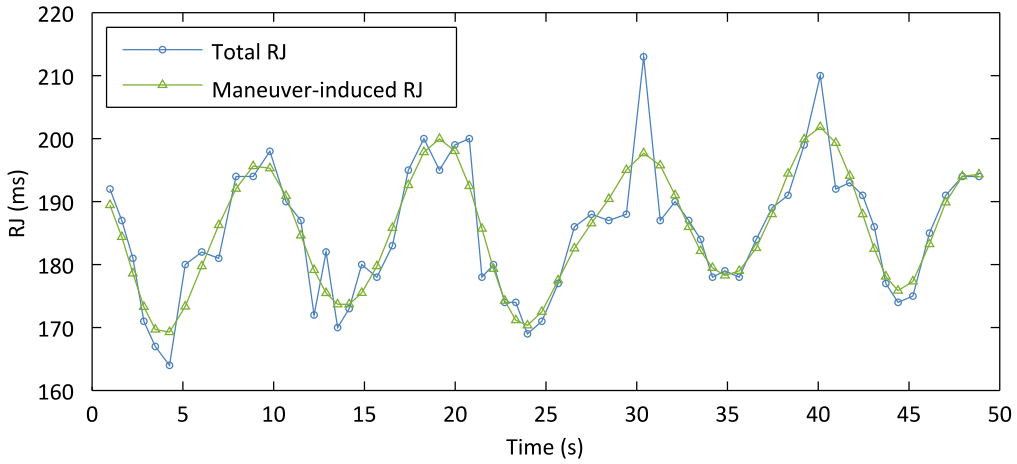

Fig. 2.34. Example of the total RJ interval and estimation of the maneuver-induced part during paced respiration.

The mean standard uncertainty in the first set with a low degree of motion artifacts was 1.7 ms and the maximum was 3.1 ms, whereas in the second set with a higher level of motion artifacts due to the paced respiration maneuver the mean standard uncertainty was 10.4 ms and the maximum was 17.6 ms. The values in the second set are about 10 times greater than the uncertainty of 1 ms previously reported for the ECG R-wave timing in section 2.1.4 or the IPG pressure-pulse timing in section 2.2.4, and constitute a challenge for the measurement of the RJ interval as they are of the same order of the maneuver-induced changes.

Additionally, the RJ interval was calculated from the R wave of the ECG and the J wave of an ensemble average composed from several consecutive BCG heartbeats, including an equal number between previous and consecutive. This technique, which is widely used to analyze evoked potentials in electroencephalography (EEG), can be applied to the BCG [106][109] to reduce random effects by $1/N$, N being the number of samples of the ensemble average, while keeping the power of the signal of interest. The main advantage of this technique is that it provides low-noise waveforms for feature-extraction algorithms that otherwise would fail. Fig. 2.35 shows the mean standard uncertainty of the RJ interval obtained from the second set of recordings measured with this alternative method, for different number of heartbeats of the ensemble average.

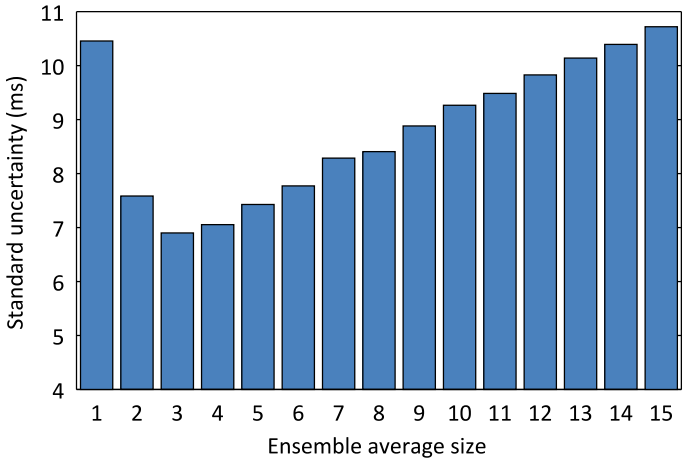

Fig. 2.35. Standard uncertainty of the RJ interval for different sizes of the ensemble average.

The increase of the number of heartbeats in the ensemble average causes a decrease of the standard uncertainty due to artifact filtering and an increase of the standard uncertainty due to the misalignment of the BCG samples with respect to the ECG, which causes a filtering of the high-frequency features of the BCG waveform. The minimal standard uncertainty achieved is 6.9 ms and corresponds to an ensemble average of 3 heartbeats. Fig. 2.36 shows the same RJ trace of Fig. 2.34 calculated from a 3-heartbeat ensemble average.

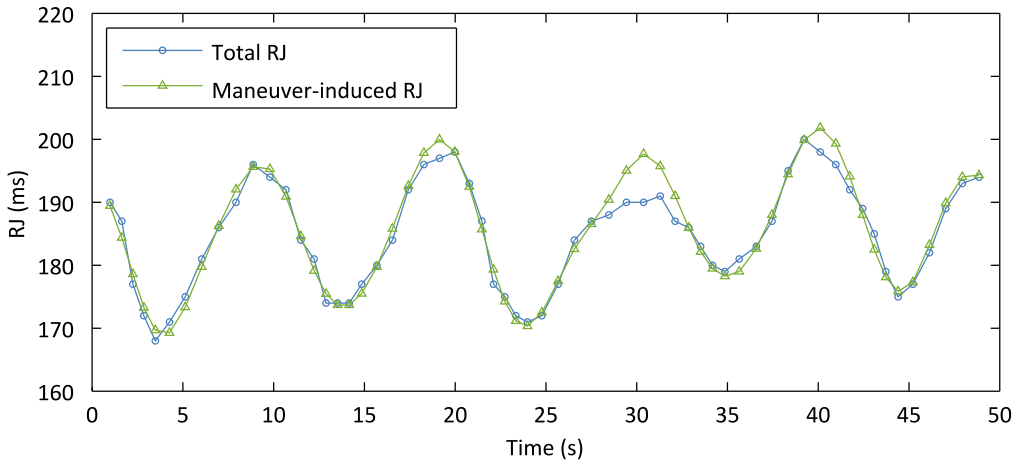

Fig. 2.36. Example of the total RJ interval measured from a 3-heartbeat ensemble average and estimation of the maneuver-induced part during paced respiration.

The agreement between the RJ interval and the estimated maneuver-induced changes in the RJ is much greater by using a 3-heartbeat ensemble average, although a higher number of intervals could be used to achieve lower standard uncertainties in RJ traces with slower variations. Further, sample misalignments as a result of RJ interval fluctuations that cause a smoothening of the BCG waveform can be corrected by using a realignment algorithm such as the one proposed by Woody for evoked potentials in EEG [110]. This method was used to reduce the level of artifacts in the BCG, and EMG noise in the ECG obtained from the feet in [C2].

2.4. Data acquisition system and additional reference systems

This section describes the data acquisition system and other additional systems that have been used to obtain additional reference physiological signals throughout the experiments.

2.4.1. Data acquisition system

The signals were acquired with a 10-channel 14-bit DAQ (μDAQ USB-26/30-BNC, Eagle Technology, Auckland, New Zealand) with input range set to ±5V and sampling frequency set to 1 kHz, so that the sampling interval (1 ms) was somewhat below typical standard uncertainties of timing measurements found in preliminary tests.

The DAQ was controlled from a custom LabVIEW® interface and the recorded signals were processed offline with Matlab®.

2.4.2. Photoplethysmogram (PPG)

The PPG system was designed from a commercial reflective PPG sensor (model 1020, UFI, Morro Bay, California). The sensor output was ac-coupled (0.1 Hz cutoff frequency) to a non-inverting amplifier with gain 51, as shown in Fig. 2.37.

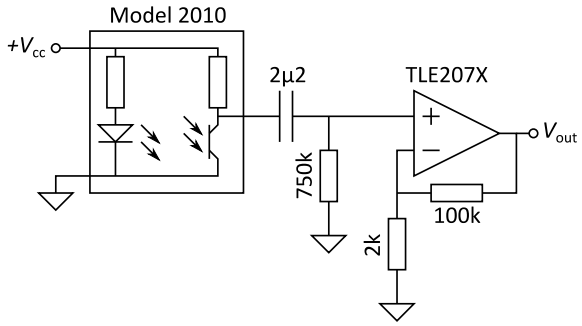

Fig. 2.37. Analog front-end for the PPG sensor.

The high-frequency response of the sensor, not specified by its manufacturer, was found by characterizing the amplitude and phase response of the system. The result was manually adjusted to a simulated system with variable cutoff frequencies to found the best fit. Fig. 2.38 shows the measured and simulated amplitude and phase response.

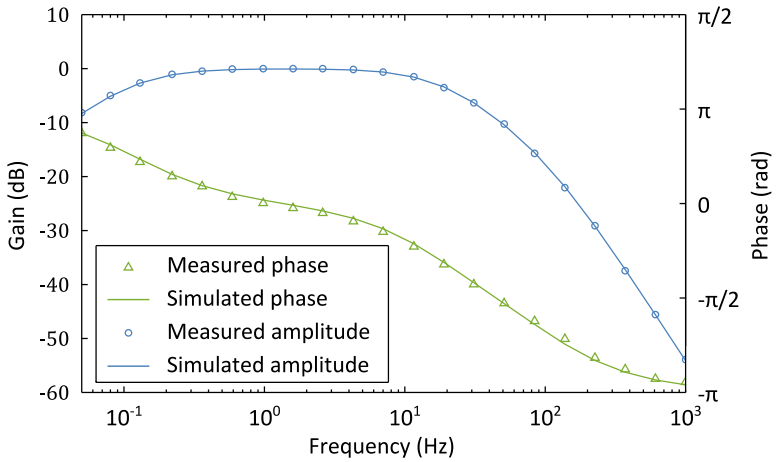

Fig. 2.38. Measured (markers) and simulated (lines) amplitude and phase response of the PPG system used.

The best fit to the measured amplitude and phase response of the PPG was a system with a first-order high-pass filter with cutoff frequency 0.11 Hz, a first-order low-pass filter with cutoff frequency 18 Hz, and a first-order low-pass filter with a cutoff frequency of 110 Hz.

2.4.3. Pressure pulse transducer (PPT)

The PPT system was designed from a commercial piezoelectric sensor (model 1010, UFI, Morro Bay, California). The sensor was conditioned with the circuit proposed by its manufacturer, with an additional amplification stage with gain 10, as shown in Fig. 2.39.

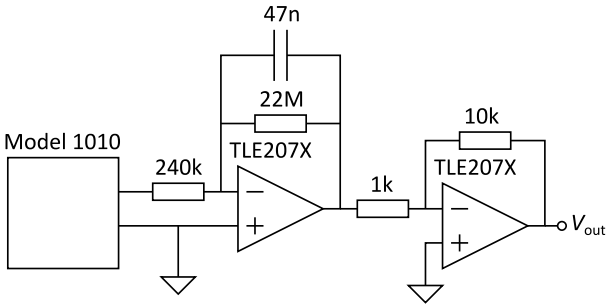

Fig. 2.39. Analog front-end for the pressure pulse transducer (PPT).

The high-pass and low-pass cutoff frequencies of the PPT system were experimentally determined from the discharge times of the sensor and the circuit respectively, and the values obtained were 0.15 Hz and 22 Hz.

The uncertainty of the pressure-pulse timing from this PPT system was estimated by using the PPG as a reference from a single healthy subject, which was asked to perform a paced respiration maneuver at 0.1 Hz for 100 s. The PPT and the PPG were simultaneously obtained from the left hand index and middle fingers respectively using the PPT and the PPG system described in section 2.4.2. The signals were acquired and sent to a PC using the system described in section 2.4.1 and the timing of the pressure-pulse was determined with the tangent intersection method.

The systematic shift of the foot of the pressure-pulse was 3.2 ms, which was expected from the bandwidth mismatch, and the standard uncertainty was 1.5 ms, which can be attributed to noise and artifacts.

2.5. Summary

This chapter has been devoted to the analysis of the uncertainty in time interval measurements from the ECG, IPG, and the BCG. First, the main sources of error in the timing of the most widely-measured fiducial points for each signal have been analyzed and the results show that standard uncertainties below 1 ms are hard to achieve in ambulatory scenarios, mostly because of EMG noise for the ECG, the pink noise for the IPG, and motion artifacts for the BCG, but this is still far below current uncertainties in several time interval measurements [29][30][31][32] that are of the order of tens of milliseconds.

Afterwards, we have characterized the effect of several parameters of data acquisition systems to establish the minimal design requirements to assure that the uncertainties they introduce are below that level. Table 2.4 shows a summary of the minimal specifications required for ECG, IPG, and BCG acquisition systems.

Table 2.4. Summary of specifications for ECG, IPG, and BCG acquisition systems intended for time interval measurements.

Parameter	ECG	IPG	BCG
Bandwidth (Hz)	0.5-40	0.2-20	0.5-25
rms output noise (mV)	30	10	-
Resolution (bits)	4	7	4
Sampling frequency (linear interpolation)(Hz)	333	50	333
Sampling frequency (spline interpolation)(Hz)	125	50	50

We have found that analog filters at these frequency bands introduce significant shifts that must be calibrated in absolute time measurements. On the other hand, the requirements for ADC are not especially demanding hence costly high-performance systems are not required to achieve uncertainties below 1 ms.

After the state of the art of the instrumentation circuits to process those signals has been reviewed, we have designed a data acquisition system tailored to each signal according to the specifications previously developed and oriented to measurements in ambulatory scenarios, which demand cost-effective low-power designs.

For the ECG, we have designed a system compatible with an IPG system based on a novel passive first-order fully-differential band-pass filter that requires a minimal number of amplifiers, hence has lower cost and power consumption.

The IPG characterization revealed that the uncertainty in timing measurements for the widely-used PPG strongly depends on contact pressure, which induces higher uncertainty in timing

measurements than that due to pink noise in the IPG. Therefore, the IPG can be a better tool for the assessment of the pressure-pulse timing in spite of the popularity of the PPG.

After analyzing some BCG traces during paced respiration, we have found that motion artifacts are almost 10 times larger than the minimal uncertainties achieved in other timing measurements from the ECG and the IPG, and become an important drawback. We have characterized a method based on sample averaging that reduces that uncertainty in the BCG J-wave timing at the cost of its ability to reflect beat-to-beat changes.

The results described in this chapter are a necessary step towards standardization of systems intended for timing measurements, as several common timing measurements are currently being performed with systems unintended for that purpose whose impact on the measurement performance is unknown.

Chapter 3

The IPG from limb to limb

THE IPG obtained from limb to limb is better suited to measurements in ambulatory scenarios than local IPG measurements as the placement of two electrodes on each limb is easier than placing four electrodes on a single limb. In addition, IPG systems are obtained from electrodes that can be shared with systems that obtain additional signals such as the ECG, and can be easily integrated on the surface of daily-use objects. However, there is no model able to describe the response of the limb-to-limb IPG to different hemodynamic changes and therefore its usefulness is currently limited to obtaining the heart rate although the signal is sensitive to changes along the whole current path and can potentially reflect hemodynamic changes in proximal sites complementary to those commonly obtained from distal sites. This chapter proposes and evaluates a model for hand-to-hand and foot-to-foot IPG signals based on the geometry of the arterial tree. This novel model is built from anatomical data collected from living subjects reported in the literature and predicts the sensitivity of the different body segments along the current path to pressure changes and the effect of that sensitivity on the timing of the pressure pulse. Afterwards, the performance of the PAT measured from the ECG to the hand-to-hand IPG and to the foot-to-foot IPG is evaluated in a small group of subjects.

3.1. The potential of limb-to-limb IPG measurements

In addition to local measurements with electrodes clustered in a small area of interest, the IPG can be obtained by measuring between distant sites, which yields information about the aggregated plethysmographic changes along the current path. The ICG is probably the most common of these measurements and is routinely used in research and clinical care to gain information about

volumetric changes in the aorta [49] by measuring impedance changes between the neck and the abdomen.

Impedance measurements based on electrodes placed on wrists and ankles, the so-called whole-body impedance measurement [58], are assumed to have performance similar to that of the ICG in spite that it includes the impedance of the limbs. However, the reported systematic overestimation of PWV when using the whole-body waveform as a proximal signal suggests that the upstroke of the waveform is delayed with respect to the ICG upstroke and causes an underestimation of PTT. This delay can be attributed to the influence of distal impedance changes that also contribute to other whole-body impedance measurements [59].

Even though whole-body impedance measurements fit the criteria identified for noninvasive measurement of cardiovascular parameters, other impedance measurements from limbs can be easily integrated in common daily-use devices to yield information of interest. The IPG measured from foot to foot has been proposed to detect heart rate [13][60] or to increase the reliability in heartbeat detection combined with other signals [15], and can be obtained from the electrodes of modern weighing scales intended for body composition analysis. Even though the physiological basis of the foot-to-foot IPG has been not reported, this signal could be sensitive to the arrival of the pressure-pulse to the abdomen as the current flows through it from leg to leg, and the abdomen is currently one of the two reference measurement sites specified by the gold standard measurement of arterial stiffness [17]. Analogously, the measurement of impedance from hand to hand [61] could be sensitive to volume changes in the arteries of the thorax that reflect the earliest volume changes caused by cardiac ejection, the same as with the whole-body impedance measurement.

These two IPG measurements between limbs are of great interest as they can potentially deliver information about the pressure-pulse arrival to proximal sites complementary to the information from other signals typically obtained at the hands such as the ECG or local pressure-pulse waveforms. This makes it interesting to elaborate a model able to predict the contributions of the different body segments along the current path to the waveform obtained and could corroborate that hypothesis and support further studies.

3.2. A model for limb-to-limb IPG measurements

Limb-to-limb IPG measurements are the aggregated contribution of impedance changes in the different body segments along the current path hence the logical steps to build a model are first to identify the current path and afterwards to calculate the effect of impedance changes in each segment.

The IPG should theoretically rely only on physiological properties of the large arteries, as only these have a pulsatile behavior, which decreases to a steady flow in the smaller arteries and capillaries. However, some of the current injected can flow through adjacent tissues or fluids with non-pulsatile behavior such as veins, muscles, or fat causing a decrease of sensitivity on the

different segments of the current path. Therefore, as the amount of non-pulsatile tissue surrounding arteries in limb-to-limb measurements is different along the current path, it cannot be assumed that the sensitivity is evenly distributed.

Table 3.1, adapted from [111], summarizes the electrical properties of some of the human body tissues and fluids that can be found in the current path from limb-to-limb.

Table 3.1. Summary of electrical properties of human body tissues and fluids, adapted from [111].

Tissue	Conductivity (S/m) at low frequencies (from 1 Hz to 10 kHz)	Anisotropy
Human skin, dry	10^{-7}	Unknown
Human skin, wet	10^{-5}	Unknown
Bone	0.005-0.06	Strong
Fat	0.02-0.05	Small
Lung	0.05-0.4	Local
Brain (grey matter)	0.03-0.4	Small
Brain (white matter)	0.03-0.3	Strong
Liver	0.2	Unknown
Muscle	0.05-0.4	Strong
Whole blood	0.7	Flow dependent
Urine	0.5-2.6	No
Cerebrospinal fluid	1.6	No

Blood conductivity is at least an order of magnitude higher than that of the other tissues and fluids that can be found in limbs excluding muscles, whose maximal conductivity is about half that of the blood. As muscles constitute mostly of the cross-section in human limbs it could be expected that a significant amount of current would flow through them.

However, limbs are complex structures and cannot be analyzed as a simple aggregation of tissues. Individual muscles are surrounded by the fascia, a large macromembrane that separates them from each other, and are connected to bones through tendons. These structures show much higher impedance than the muscular tissue itself and increase the impedance of muscles from end to end. Further, muscular tissue is strongly anisotropic, which means that its conductivity is dependent on the direction of the current. As muscular cells are stretched, the current crosses a higher number of cellular membranes when traveling in perpendicular direction, which show higher impedance [111] and hinder the current flow to adjacent tissues.

On the other hand, blood vessels offer a continuous low-impedance path along the human body, which suggests that a significant amount of electric current injected between two limbs will flow through them. Consequently, variations of the amount of tissue surrounding large arteries have a small effect and the current flowing through them during the cardiac cycle can be assumed constant.

Considering only the influence of the large arteries, the measurement sensitivity is dominated by two phenomena reflected in equation (2.6). First, the increase of impedance is inversely proportional to the square of the cross-sectional area hence a given cross-sectional area change in

distal arteries will have a higher impact on the total measured impedance, as the cross-sectional area decreases from proximal to distal sites.

Second, the increase of impedance is proportional to the increase of cross-sectional area, which is related to the increase of pressure by the particular geometry and elasticity of the artery. The compliance C of an artery defines the ratio of increase of cross-sectional area ΔA per increase of pressure ΔP, and depends on the elastic modulus E, radius r, and wall thickness h of the artery [112], according to

$$C = \frac{\Delta A}{\Delta P} = \frac{2\pi r^3}{hE}. \tag{3.1}$$

The elastic modulus increases from proximal to distal arteries as a result of the decrease of the relative amount of elastic tissue whereas the vessel radius and wall thickness decrease [113]. In consequence, compliance decreases from proximal to distal arteries, which implies that pressure changes in proximal arteries result in higher increases of volume than in proximal sites.

The cross-sectional sensitivity of an artery S, defined as the ratio of increase of resistance ΔR per increase of pressure ΔP per unit length l, can be obtained from equations (2.6) and (3.1) according to

$$S = \frac{\Delta R}{l\Delta P} = \frac{-\rho_e \Delta V}{A^2}\frac{1}{l\Delta P} = \frac{-\rho_e \Delta A}{A^2 \Delta P} = \frac{-\rho_e C}{A^2} = \frac{-2\rho_e}{hrE}, \tag{3.2}$$

where ρ_e is the resistivity of blood, which is typically 1.43 Ω m (see Table 3.1).

Therefore, the sensitivity in a body segment is a tradeoff between arterial cross-sectional area and compliance, which have opposite effects in proximal and distal vessels and whose dominance can only be calculated from real physiological data. Reference values of radius, wall thickness, and length can be obtained from corpses [114] whereas the elastic modulus to obtain the compliance can be calculated from the arterial distensibility D measured *in vivo* [115], according to

$$E = \frac{0.75 \cdot 2r}{hD}, \tag{3.3}$$

where 0.75 is a correction coefficient to compensate for the thickness of the arterial wall [116], which is assumed to be much smaller than r in equation (3.3).

3.3. Time intervals from the hand-to-hand IPG

Fig. 3.1 shows the large arteries that can be found in the current path from hand to hand, adapted from [114].

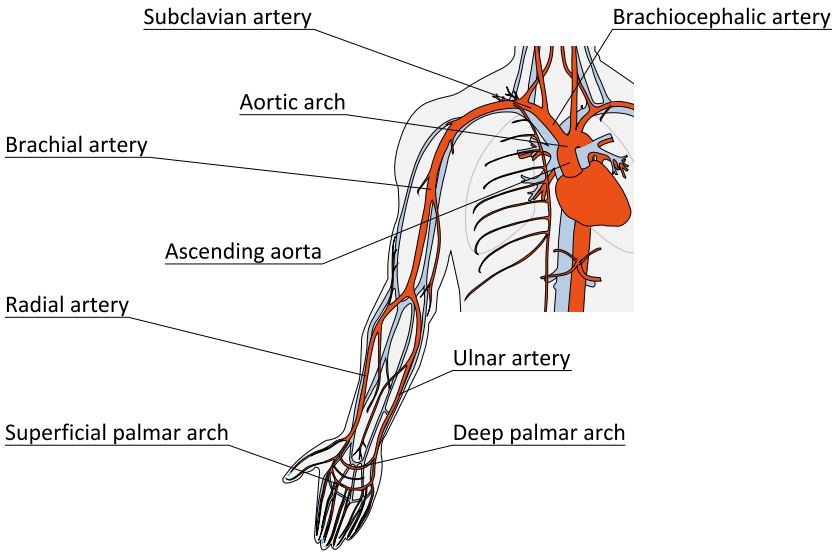

Fig. 3.1. Large arteries in the current path from hand to hand, adapted from [114].

According to the observations made in section 3.2, the most of the current injected from hand to hand flows through the deep and superficial palmar arches, radial artery, ulnar artery, brachial artery, subclavian artery, brachiocephalic artery, and the aortic arch. Table 3.2 summarizes the physiological parameters of these arteries and others involved in the propagation of the pressure pulse measured from real subjects in [114] and [115]. An additional coefficient x is used to represent the fraction of the total current flowing through each large artery, which has been calculated by modeling arteries in parallel as parallel resistors.

Table 3.2. Physiological properties of the large arteries involved in the hand-to-hand IPG measurement, extracted from [114] and [115].

Artery	r (cm)	h (cm)	l (cm)	D (10^{-3} mmHg^{-1})	E (10^{6} Pa)	x (Ø)
Ascending aorta	1.470	0.163	4.0	5.49	0.33	0
Aortic arch	1.263	0.126	2.0	5.32	0.38	0.5
Brachiocephalic	0.699	0.080	3.4	3.30	0.53	0.5
Subclavian	0.541	0.067	3.4	3.08	0.52	1
Brachial	0.515	0.067	42.2	2.09	0.74	1
Radial	0.367	0.043	23.5	1.21	1.41	0.41
Ulnar A	0.454	0.046	6.7	1.25	1.58	0.59
Ulnar B	0.433	0.046	17.1	1.13	1.67	0.59

The cross-sectional sensitivity of the large arteries in the current path from hand to hand, calculated from equation (3.3) and the data in Table 3.2, is shown in Fig. 3.2.

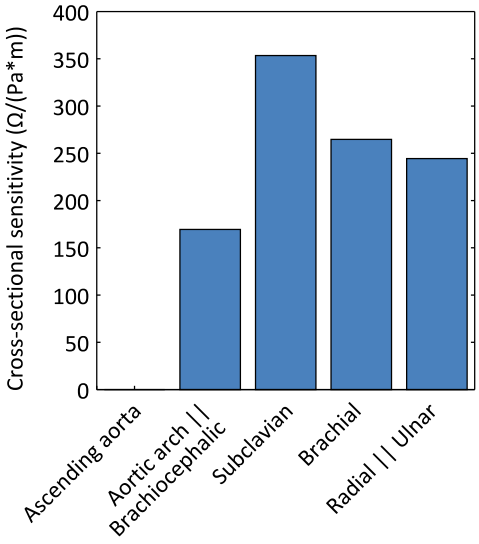

Fig. 3.2. Cross-sectional sensitivity of the large arteries in the current path from hand-to-hand.

The cross-sectional sensitivity is low in proximal arteries due to their high cross-sectional area and in distal arteries due to their low compliance whereas the best trade-off is found in the subclavian artery. As the available data does not include the palmar arch, its sensitivity cannot be calculated although it is expected to decrease according to the trend observed in Fig. 3.2. Arterioles have less elastic tissue than larger arteries and capillaries have no elastic tissue at all and therefore their cross-sectional sensitivity is expected to be negligible.

The system response to an impulse-shaped pressure pulse traveling through an artery has a base equal to the length of the artery divided by the PWV and a height equal to the cross-sectional sensitivity multiplied by the PWV, which can be calculated from several physiological properties of the arteries and the blood density ρ_b (1060 kg/m^3) by using the Moens-Korteweg equation

$$\mathrm{PWV} = \sqrt{\frac{Eh}{2r\rho_b}}. \tag{3.4}$$

The total impulse response of the system $h(t)$ is the concatenated response of the different large arteries in the current path, as shown in Fig. 3.3.

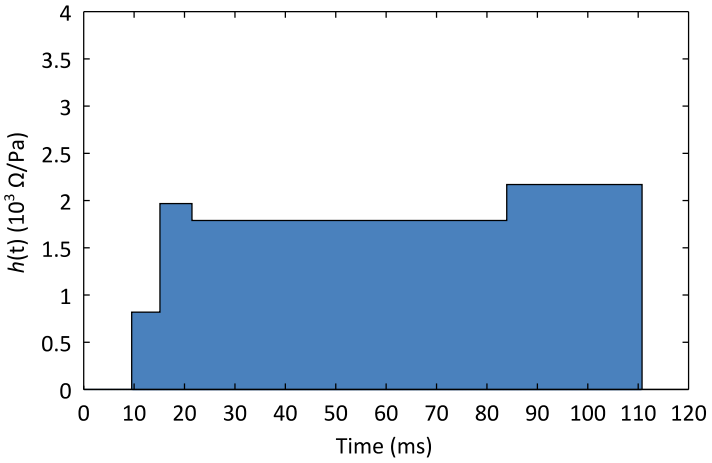

Fig. 3.3. Impulse response of the hand-to-hand IPG.

PWV compensates for the decrease of sensitivity in distal arteries and the system response is almost flat, which implies that the measured waveform is a summation of pressure changes along the path from the brachiocephalic artery to the end of the radial and ulnar arteries. The shape of h(t) can be approximated to the impulse response of a delayed rectangular window filter hence it is expected to cause a delay and low-pass filter to the input signal. However, the length of the impulse response of the hand-to-hand IPG depends on the PWV, which changes with the mean BP, and the time dependency of h(t) can only be properly evaluated by simulation.

The upstroke of the hand-to-hand IPG has been simulated by convoluting $h(t)$ with a synthetic waveform $x(t)$, defined as

$$x(t) = \begin{cases} 0, & t \geq 0 \\ \dfrac{-\cos\left(\dfrac{\pi}{0.12}t\right)+1}{2}, & 0 < t \leq 0.12 \\ 1, & t \geq 0.12 \end{cases}, \qquad \textbf{(3.5)}$$

which has been selected for having a shape similar to that typical pressure-pulse upstrokes [117], assuming that the pressure pulse waveform remains unaltered at the upstroke during the propagation.

Fig. 3.4 shows the simulated upstroke of the hand-to-hand IPG with other simulated local IPG upstrokes obtained from different reference sites such as the shoulder (end of the subclavian artery), elbow (end of the brachial artery), and the wrist (end of the radial and ulnar arteries). Waveforms amplitudes are normalized with respect to their respective maximum to ease their comparison.

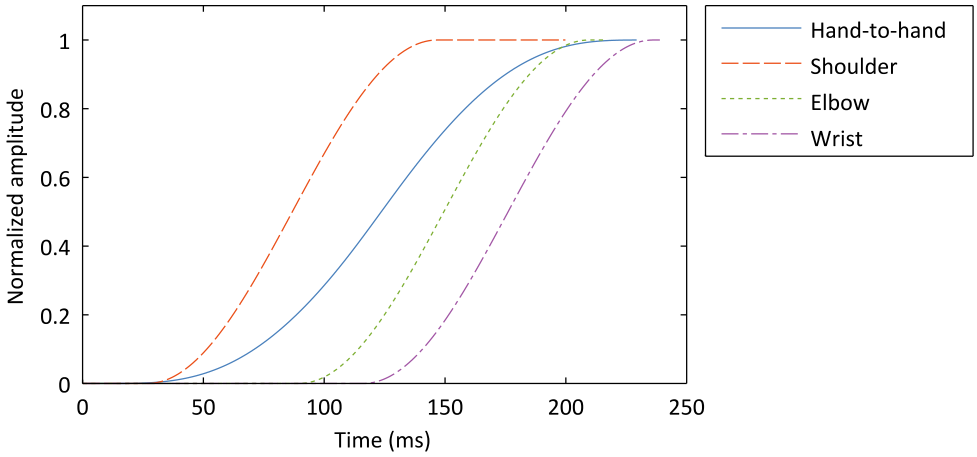

Fig. 3.4. Simulated hand-to-hand IPG upstroke and local IPG upstrokes at the shoulder, elbow, and the wrist.

As expected from the impulse response in Fig. 3.3, the hand-to-hand IPG upstroke is smoothed compared to other local IPG waveforms, especially in the area of the pulse foot, which indicates that the signal is sensitive to changes in proximal vessels in this area.

The elastic modulus E, which according to (3.4) affects PWV, can be related to the mean blood pressure P [118], according to

$$E = E_0 e^{\xi P}, \tag{3.6}$$

where E_0 is the elastic modulus at reference mean BP and ξ is a constant that depends on the particular vessel and ranges from 0.016 mmHg^{-1} to 0.018 mmHg^{-1}. Fig. 3.5 shows several hand-to-hand IPG waveforms simulated for different values of mean BP normalized with respect to their maximum. E_0 has been obtained from Table 3.2, which values correspond to P = 100 mmHg, and ξ is assumed to be 0.017 mmHg^{-1}. Higher pressures yield faster upstrokes but otherwise the foot undergoes minimal change.

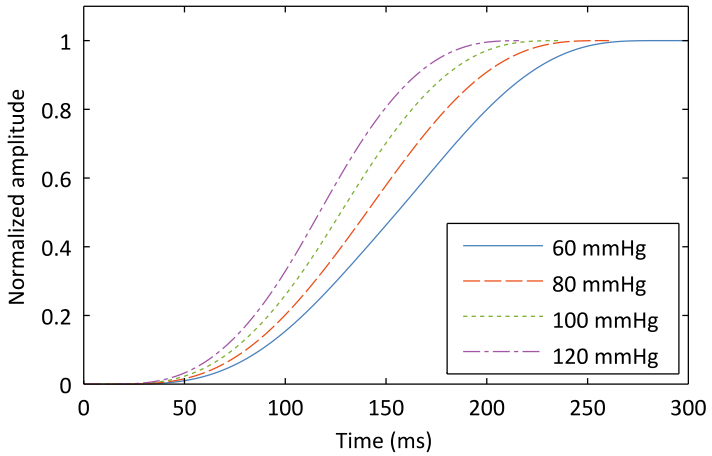

Fig. 3.5. Simulated hand-to-hand IPG upstrokes for different mean BP values.

Changes in mean BP are mostly reflected on the slope of the upstroke of the hand-to-hand IPG although the foot of the wave is also slightly delayed.

The pressure-pulse timing was measured in the simulated waves for different values of mean BP by using the intersecting tangents method and the results were compared to the pressure-pulse timing of the simulated wrist and carotid (end of the brachiocephalic artery) IPG. Fig. 3.6 shows the PTT measured from cardiac ejection to the simulated hand-to-hand, carotid, and wrist IPG.

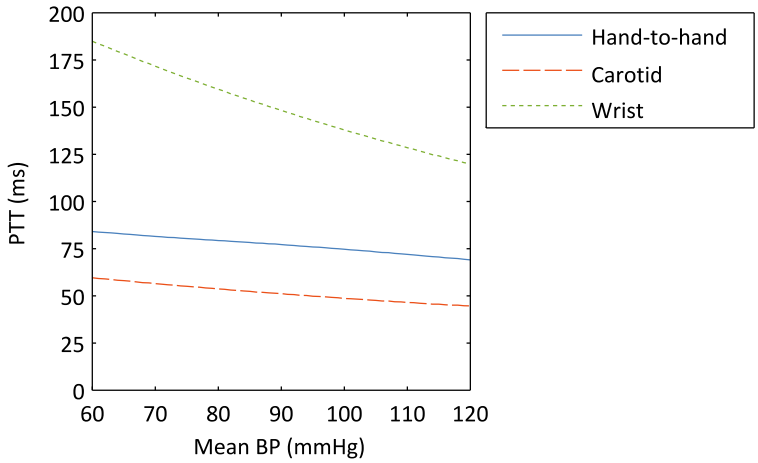

Fig. 3.6. PTT from the opening of the aortic valve to the simulated hand-to-hand, carotid, and wrist IPG.

The sensitivity of the pressure-pulse timing to changes in the PTT caused by changes in BP is lower than the sensitivity of the pressure-pulse timing at the finger and similar to the sensitivity of the pressure-pulse at the carotid, despite of the higher offset. This low sensitivity with respect to the higher delay can be attributed to the change in slope that counteracts the displacement of the foot of the wave when using the tangent intersection method. Consequently, the interval from the ECG R wave to the hand-to-hand IPG pressure-pulse timing using this method includes the PEP (see Fig. 1.3) plus a constant delay weakly sensitive to the PTT hence constitutes a good candidate to estimate changes in the PEP, as it is commonly performed with the carotid PAT [119] or the earlobe PAT [120].

3.3.1. Hand-to-hand IPG model verification

This model for the hand-to-hand IPG has been verified by a novel four-electrode system able to simultaneously obtain the ECG and the hand-to-hand IPG [P1]. The IPG system was built according to the design described in section 2.2.3, which was adapted to hand-to-hand measurements by setting the gain of the instrumentation amplifier to 10. The ECG system was built according to the design described in section 2.1.3. The current injection electrodes were contacted by index fingers whereas the measurement electrodes were contacted by middle fingers. An additional IPG obtained from the system described in section 2.2.3 was used to measure simultaneous reference pressure-pulse waveforms at the shoulder, elbow, wrist, and the finger by using the current injected by the hand-to-hand IPG system, as shown in Fig. 3.7.

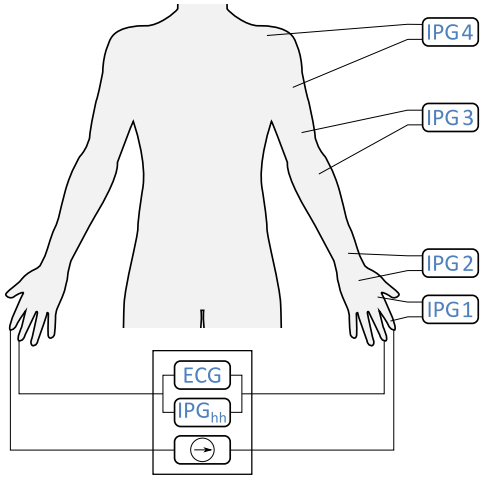

Fig. 3.7. Measurement setup for hand-to-hand IPG model verification.

The signals, which were acquired and sent to a PC using the system described in section 2.4.1, were sequentially recorded from a single subject for 10 s from each reference site. Fig. 3.8 shows a sample of the IPG waveforms obtained, normalized with respect to its maximum and synchronized with respect to the R wave of the ECG.

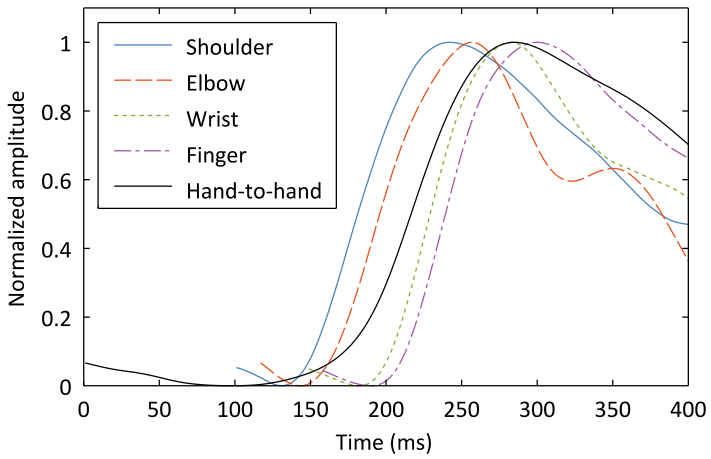

Fig. 3.8. Simultaneous hand-to-hand IPG and local IPG at the shoulder, elbow, wrist, and the finger.

The shoulder IPG is delayed with respect to the simulated waveforms in Fig. 3.4, perhaps because the beginning of the brachial artery (in the shoulder) is not accessible with surface electrodes. The elbow IPG upstroke precedes the hand-to-hand IPG upstroke, which indicates that impedance changes at distal sites are slightly underestimated by the model. This can be attributed to the pressure pulse amplification in distal sites [121], which has been not included in the model. Another plausible explanation could be the lower proportion of tissues such as muscle or fat surrounding distal arteries, which could cause an increase of current flowing through it and justify this increased sensitivity. However, the signal obtained still reflects the smoothed foot and the slower slope of the upstroke, which suggests that the waveform is sensitive to changes in proximal sites and supports the validity of the assumptions made for the design of the model.

3.3.2. Assessment of PEP changes from the ECG and the hand-to-hand IPG

The performance of the PAT to the hand-to-hand IPG in assessing changes in the PEP suggested by the model has been evaluated in 14 healthy subjects. The hand-to-hand IPG and the ECG were obtained from the four-electrode system described in section 3.3.1 whereas reference changes in the PEP were obtained from the PAT to the PPT system described in section 2.4.3 placed over the left carotid artery. Even though the PAT to this artery includes about 30 ms of PTT [122], this site has proven to be a good surrogate for the measurement of changes in PEP [119] and is the proximal reference site specified in the standard aortic PTT measurement [17]. Since an increase of PTT can be related to an increase in mean BP according to

$$\Delta\mathrm{PTT} = \mathrm{PTT}_0\left(\sqrt{e^{(-0.017*\Delta P)}} - 1\right), \tag{3.7}$$

derived from equations (3.4) and (3.6), a large change in mean BP of 40 mmHg would result in a decrease in carotid PAT of only 8.5 ms, which implies that the interval is mostly dominated by changes in the PEP. An additional reference PAT to the left annular finger was obtained from the PPG system described in section 2.4.2. Fig. 3.9 shows the measurement setup for the assessment of changes in the PEP from the ECG and the hand-to-hand IPG.

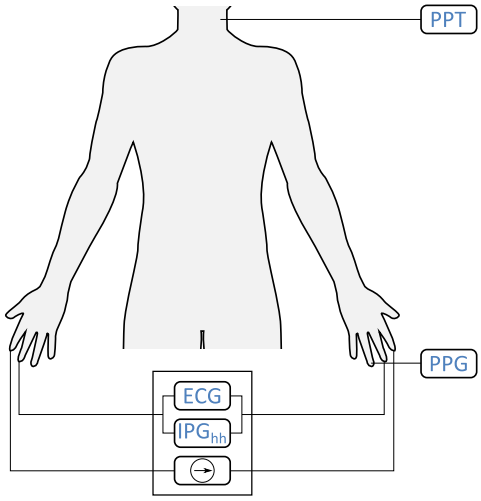

Fig. 3.9. Measurement setup for the assessment of PEP changes from the ECG and the hand-to-hand IPG.

In order to induce hemodynamic changes, the subjects were asked to perform a paced respiration maneuver at 0.1 Hz for 50 s. The signals were acquired and sent to a PC using the system described in section 2.4.1. The ECG R-wave timing was measured by applying a modified Pan-Tompkins algorithm, whereas pressure-pulse timings were measured by applying the tangent intersection method.

Fig. 3.10 shows an example of the finger, hand-to-hand, and carotid PAT traces obtained during the experiment.

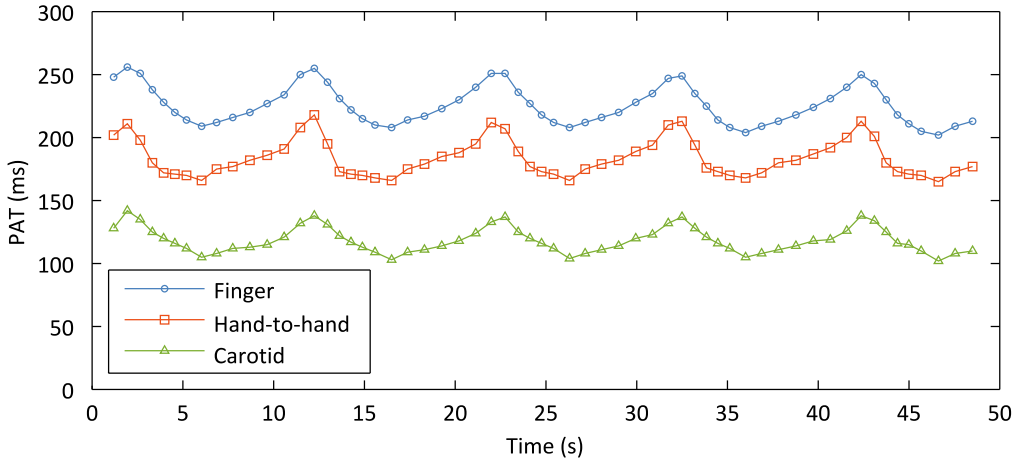

Fig. 3.10. Example of the finger, hand-to-hand, and carotid PAT traces obtained during paced respiration.

From the amplitude and phase of the carotid PAT and the finger PAT traces, it follows that paced respiration induces changes in the PEP, as it has been previously reported for other short-term maneuvers [72]. As predicted by Fig. 3.6, the hand-to-hand PAT is longer than the carotid PAT and shorter than the finger PAT. However, these timings cannot be considered an absolute reference as the PPG and the PPT have an offset caused by the contact pressure, described in section 2.2.4 and reported in [12]. The mean of the correlation coefficients between the hand-to-hand PAT and the carotid PAT was 0.72 with a standard deviation of 0.14 whereas the mean of the correlation coefficients between hand-to-hand PAT and finger PAT was 0.76 with a standard deviation of 0.12. A total of three carotid PAT recordings and two finger PAT recordings were excluded for having $p > 0.05$ attributable to excessively soft hemodynamic changes induced by paced respiration.

Fig. 3.11 shows the aggregated 780 hand-to-hand PAT and carotid PAT pairs of values obtained from the 14 subjects during the experiment.

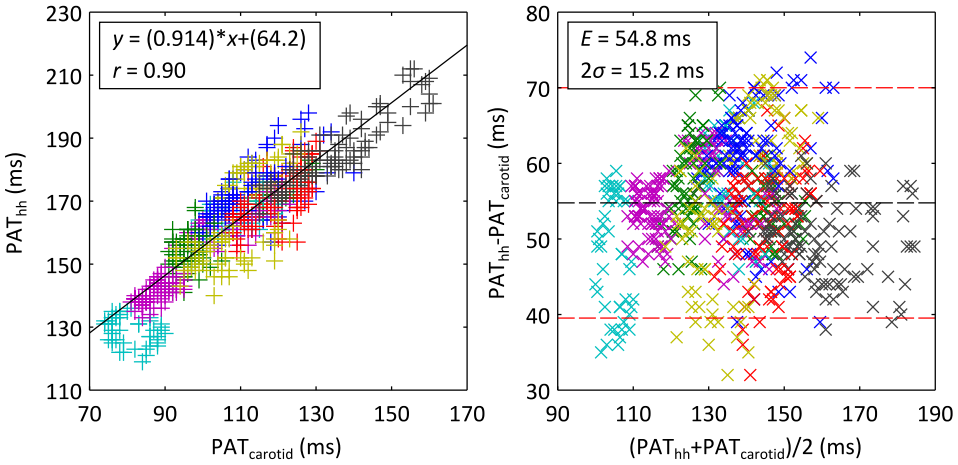

Fig. 3.11. Hand-to-hand PAT vs. carotid PAT, and Bland Altman analysis of hand-to-hand PAT vs. carotid PAT during paced respiration.

The correlation between the hand-to-hand PAT and the carotid PAT is strong and the slope of the regression line is close to 1, which proves that the sensitivity of the hand-to-hand PAT to PEP changes is high. The offset is higher than the model prediction in Fig. 3.6, perhaps as a result of the underestimation of sensitivity in distal sites already observed in Fig. 3.8.

The standard deviation of the difference between the hand-to-hand PAT and the carotid PAT during paced respiration was 7.6 ms, which is twice as large as the standard uncertainty of 3.3 ms reported when using the IPG as a surrogate of the PPG in section 2.2.4. This larger uncertainty can be attributed to a higher degree of motion artifacts on the carotid PPT signal, which is especially sensitive to subtle head and neck movements performed during respiration. Further, the non-zero sensitivity to PTT changes in both the carotid PPT and hand-to-hand IPG signals cause small displacements of the measured points and increase the uncertainty.

Fig. 3.12 shows the aggregated 780 hand-to-hand PAT and finger PAT pairs of values obtained from the 14 subjects during the experiment.

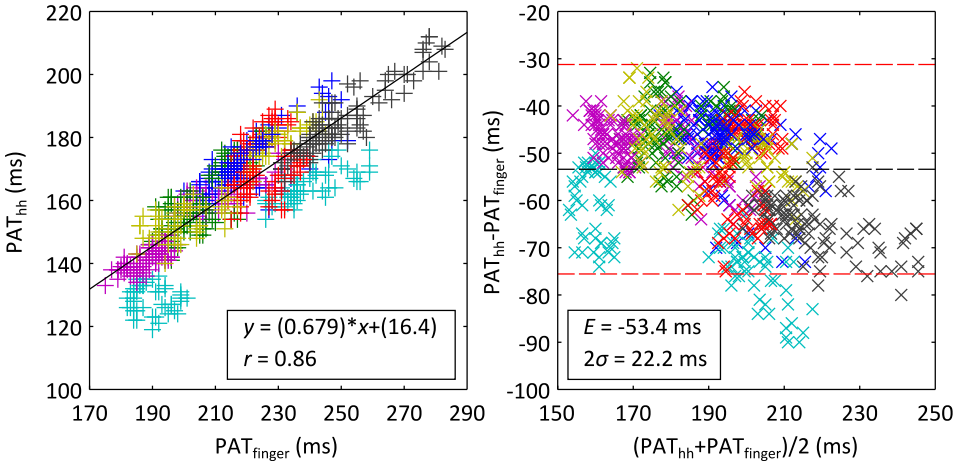

Fig. 3.12. Hand-to-hand PAT vs. finger PAT, and Bland Altman analysis of hand-to-hand PAT vs. finger PAT during paced respiration.

Even though the correlation between the hand-to-hand PAT and the finger PAT is still strong [C5], the slope of the regression line is lower than 1, thus suggesting that the finger PAT includes a higher amount of PTT that changes synchronously with PEP changes and causes a displacement of the pairs of values to the right. Therefore, it can be concluded that the hand-to-hand PAT reflects the arrival of the pressure pulse at proximal sites rather than distal sites even though it is obtained from distal electrodes.

3.4. Time intervals from the foot-to-foot IPG

Fig. 3.13 shows the large arteries that can be found in the current path from foot to foot, adapted from [114].

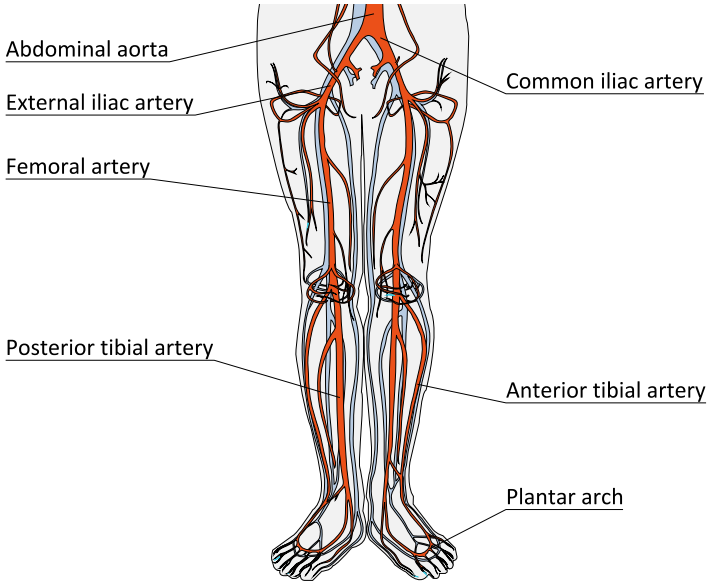

Fig. 3.13. Large arteries in the current path from foot to foot, adapted from [114].

According to the observations made in section 3.2, the most of the current injected from foot to foot flows through the pedal arch, anterior tibial artery, posterior tibial artery, femoral artery, external iliac artery, and the common iliac artery. Table 3.3 summarizes the physiological parameters of these arteries and others involved in the propagation of the pressure pulse measured from real subjects in [114] and [115]. An additional coefficient x is used to represent the fraction of the total current flowing through each artery, which has been calculated by modeling arteries in parallel as parallel resistors.

Table 3.3. Physiological properties of the large arteries involved in the foot-to-foot IPG measurement, extracted from [114] and [115].

Artery	r (cm)	h (cm)	l (cm)	D (10^{-3} mmHg^{-1})	E (10^{6} Pa)	x (Ø)
Ascending aorta	1.470	0.163	4.0	5.49	0.33	0
Aortic arch	1.229	0.120	5.9	5.30	0.39	0
Thoracic aorta	1.096	0.105	15.6	4.58	0.46	0
Abdominal aorta	0.770	0.078	18.9	4.01	0.49	0
Common iliac	0.470	0.060	5.9	3.10	0.51	1
External iliac	0.482	0.053	14.5	2.84	0.64	1
Femoral	0.361	0.050	44.4	2.44	0.59	1
Posterior tibial	0.375	0.045	32.2	1.41	1.18	0.79
Anterior tibial	0.197	0.039	34.4	1.24	0.85	0.21

The cross-sectional sensitivity of the large arteries in the current path from foot to foot, calculated from equation (3.3) and the data in Table 3.3, is shown Fig. 3.14.

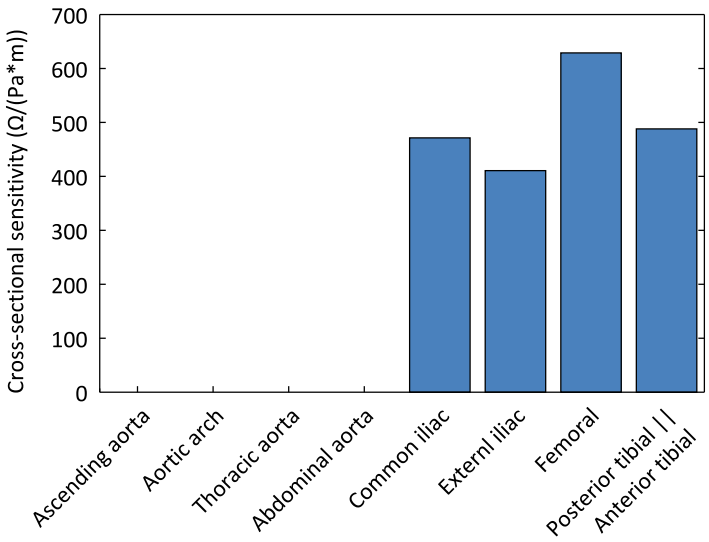

Fig. 3.14. Cross-sectional sensitivity of the large arteries in the current path from foot-to-foot.

Unlike the IPG from hand to hand, proximal arteries have no influence on the foot-to-foot IPG. Even though the sensitivity increases when approaching to more distal arteries, the difference is not as high as in the hand-to-hand measurement.

The total impulse response of the system $h(t)$, calculated as the concatenated response of the different large arteries in the current path, is shown in Fig. 3.15.

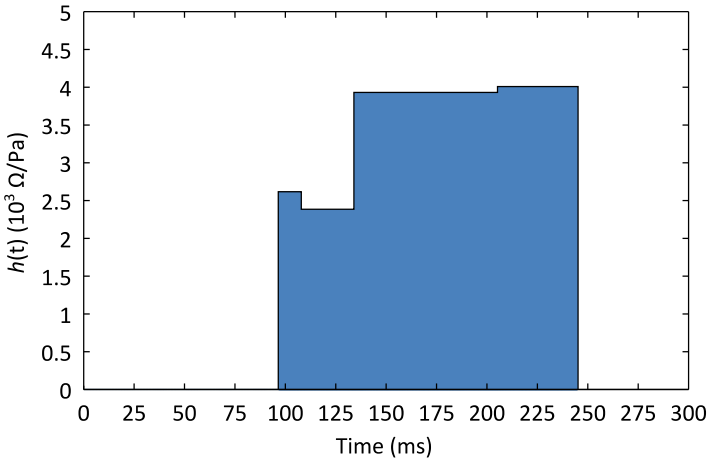

Fig. 3.15. Impulse response of the foot-to-foot IPG.

Similarly to the hand-to-hand IPG, the PWV compensates for the decrease of sensitivity in distal arteries and the system response is similar to the system response of a delayed rectangular window filter, which implies that the measured waveform is sensitive to the summation of pressure changes along the path from the common iliac artery to the end of the tibial arteries, and is expected to be smoothed and delayed with respect to the BP waveform.

Fig. 3.16 shows the simulated upstroke of the foot-to-foot IPG with other simulated local IPG upstrokes obtained from different reference sites such as the femoral artery (end of the external iliac artery), knee (end of the femoral artery), and the ankle (end of the anterior and posterior tibial

arteries). The waveforms are normalized with respect to their respective maximum to ease the comparison.

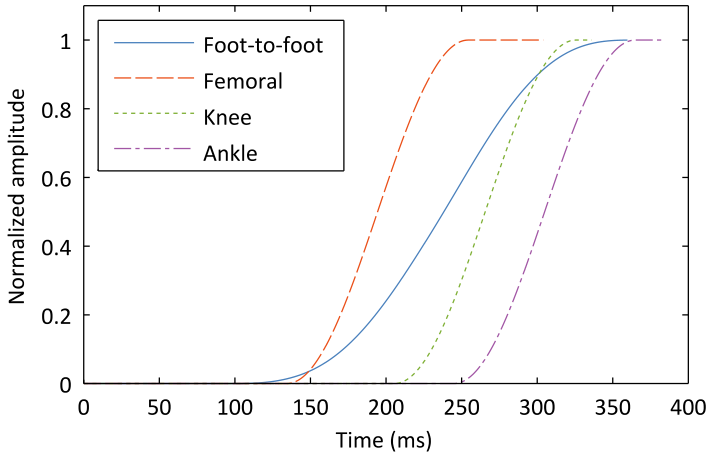

Fig. 3.16. Simulated hand-to-hand IPG upstroke and local IPG upstrokes at the femoral artery, knee, and the ankle.

Similarly to the hand-to-hand IPG, the rectangular shape of the transfer function causes a smoothening of the foot-to-foot IPG upstroke and there is also some change in the foot of the wave.

Fig. 3.17 shows several foot-to-foot IPG upstrokes simulated for different values of BP. The same as with the hand-to-hand IPG, when the mean BP increases the slope of the upstroke of the foot-to-foot IPG also increases, but here the displacement of the foot of the wave is significantly higher.

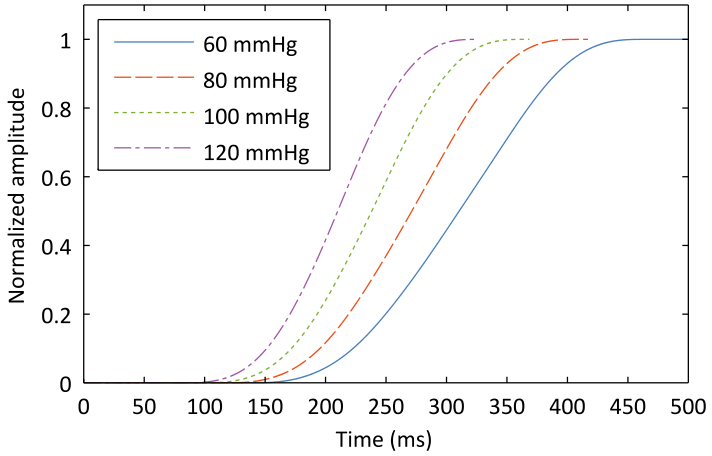

Fig. 3.17. Simulated foot-to-foot IPG waveforms for different mean BP values.

Fig. 3.18 shows the pressure-pulse timing measured from the simulated waves for different values of mean BP compared to the pressure-pulse timing of the simulated femoral and ankle IPG.

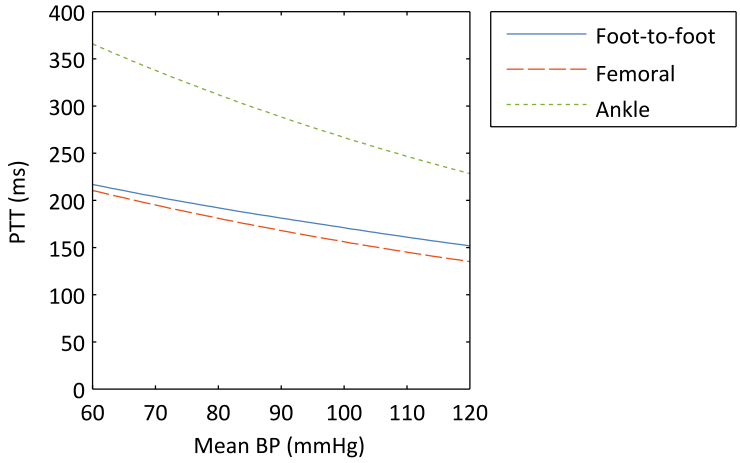

Fig. 3.18. PTT from the opening of the aortic valve to the simulated foot-to-foot, femoral artery, and ankle IPG.

Unlike the hand-to-hand IPG, the pressure-pulse timing of the foot-to-foot IPG is sensitive to PTT changes caused by changes in mean BP although its dependence is similar to that of the femoral pressure-pulse timing rather than to the ankle pressure-pulse timing. Therefore, the foot-to-foot PAT is of great interest as it could be used to assess changes in the femoral pulse, which is one of the reference sites specified by the gold standard measurement of arterial stiffness [17].

3.4.1. Foot-to-foot IPG model verification

The foot-to-foot IPG model has been verified by a four-electrode system built according to the design described in section 2.2.3, which was adapted to foot-to-foot measurements by setting the gain of the instrumentation amplifier to 10. Each current injection electrode was contacted by one forefoot whereas each measurement electrode was contacted by one heel. The ECG was simultaneously obtained from the system described in section 2.1.3 connected to the left and right hands. An additional IPG obtained from the system described in section 2.2.3 was used to measure simultaneous reference pressure-pulse waveforms at the femoral artery, knee, and the ankle by using the current injected by the foot-to-foot IPG system, as shown in Fig. 3.19.

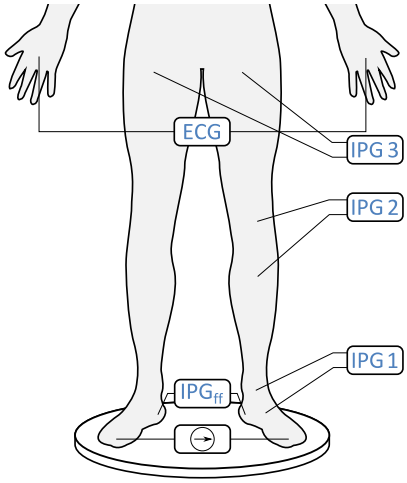

Fig. 3.19. Measurement setup for foot-to-foot IPG model verification.

The signals, which were acquired and sent to a PC using the system described in section 2.4.1, were sequentially recorded from a single subject for 10 s from each reference site. Fig. 3.20 shows a sample of the IPG waveforms obtained, synchronized from the ECG R wave.

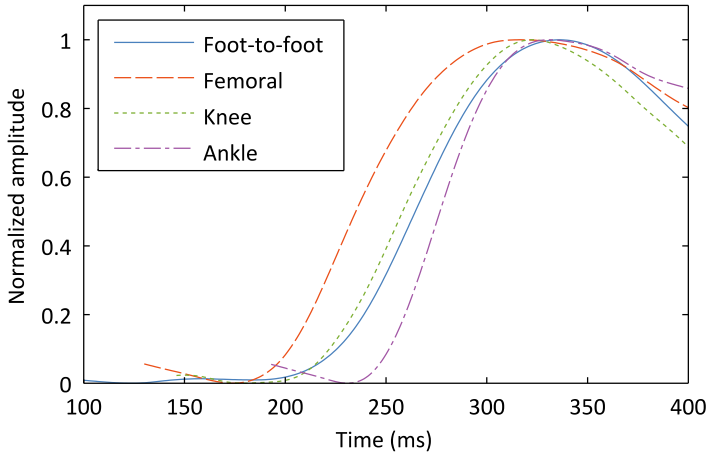

Fig. 3.20. Simultaneous foot-to-foot IPG and local IPG at the femoral artery, knee, and the ankle.

The femoral, knee and ankle IPG waveforms are roughly comparable to those simulated in Fig. 3.16 with regard to the timing of the wave foot and the slope of the upstroke. The foot-to-foot IPG waveform, however, is considerably delayed as compared to the upstrokes simulated in Fig. 3.16. It seems that, similarly to the hand-to-hand IPG, the model underestimates changes in distal sites, which can be as well attributed to the pressure pulse amplification phenomena or to a lower proportion of tissues surrounding distal arteries. However, the effect is higher in this case and the foot of the waveform obtained is not as smoothed as it was in the hand-to-hand waveform whereas the slope of the upstroke is similar to that of the three local IPG waveforms.

3.4.2. Assessment of the femoral PAT from the ECG and the foot-to-foot IPG

The performance of the foot-to-foot IPG to determine the arrival of the pressure pulse at the femoral artery suggested by the model has been evaluated on three healthy subjects, which were asked to perform a paced respiration maneuver at 0.1 Hz for 100 s in order to induce hemodynamic changes. The ECG, foot-to-foot IPG, and a femoral IPG were obtained by the measurement setup shown in Fig. 3.19. The signals were acquired and sent to a PC using the system described in section 2.4.1. The ECG R-wave timing was measured by applying a modified Pan-Tompkins algorithm whereas pressure-pulse timings were measured by applying the tangent intersection method.

Fig. 3.21 shows an example of the femoral PAT and foot-to-foot PAT traces obtained during the experiment.

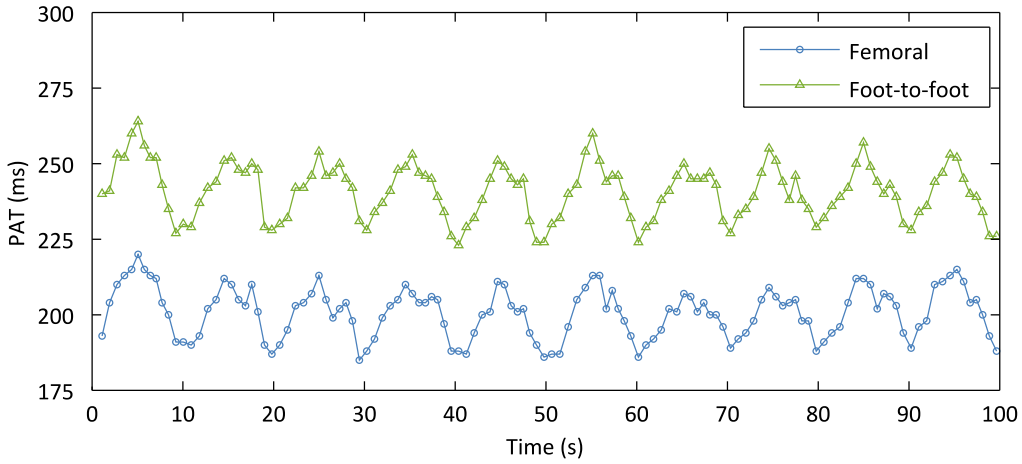

Fig. 3.21. Example of the foot-to-foot PAT and femoral PAT traces obtained during paced respiration.

The same as in Fig. 3.20, the foot-to-foot PAT is significantly longer than the femoral PAT hence the foot-to-foot IPG cannot be used as a direct surrogate of the femoral pulse. However, individual correlations were strong, with correlation coefficients of 0.93, 0.86, and 0.89 respectively.

Fig. 3.22 shows the aggregated 408 foot-to-foot PAT and femoral PAT pairs of values obtained from the 3 subjects during the experiment and the Bland-Altman analysis.

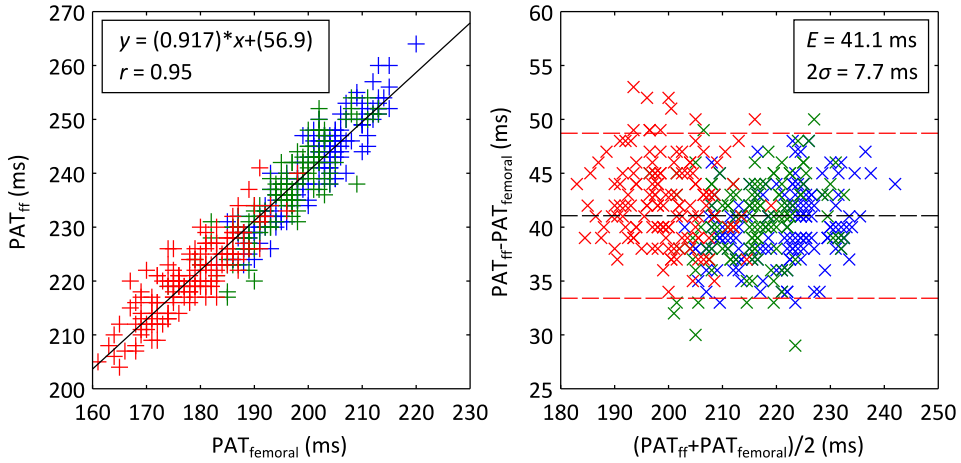

Fig. 3.22. Foot-to-foot PAT vs. femoral PAT, and Bland-Altman analysis of foot-to-foot PAT vs. femoral PAT during paced respiration.

The correlation between foot-to-foot PAT and femoral PAT is strong and the slope of the regression line is close to 1, which proves that the sensitivity of the foot-to-foot PAT to changes in PEP and PTT is similar to that of the femoral pulse even though the offset is higher for the foot-to-foot PAT. The standard deviation of the difference between foot-to-foot PAT and femoral PAT during paced respiration was 3.8 ms, which is not significantly larger than the standard uncertainty of 3.3 ms reported when using the IPG as a surrogate of the PPG in section 2.2.4.

3.5. Summary

This chapter has been devoted to the measurement of time intervals from the IPG measured from hand to hand and from foot to foot, which had never been analyzed before. First, we studied how the different body segments along the current path contribute to the measured signal. We have found that the contribution of the large arteries relies on the tradeoff between arterial cross-sectional area and compliance, which have opposite effects in proximal and distal vessels. As a result of this, the upstrokes of the measured waveforms reflect the pressure-pulse arrival to proximal sites but after a constant delay.

Second, we have found that the PAT to the hand-to-hand IPG reflects changes in the PEP rather than in the PTT and can be used as a surrogate of the carotid PAT with an uncertainty below the uncertainties reported for other pressure-pulse timing measurements [29][30][31][32] that are of the order of tens of milliseconds. This measurement is of great interest since the carotid PAT is the proximal reference signals in standard aortic PTT measurements and can be obtained from the timing of the hand-to-hand IPG by a single-point calibration to account for a constant delay. The performance of the PAT to the hand-to-hand IPG was analyzed from a novel four-electrode system able to simultaneously obtain the ECG and the IPG, which is especially suitable for monitoring devices due to its reduced number of electrodes.

Finally, we have found that the sensitivity of the foot-to-foot IPG pressure-pulse timing to changes in PEP and aortic PTT is similar to that of the femoral PAT, which is the distal reference

signal in standard aortic PTT measurements. The foot-to-foot PAT can be used as a surrogate of femoral PAT with a standard uncertainty below the uncertainties reported for other pressure-pulse timing measurements, although the interval includes an offset that must be calibrated.

Further, since the IPG signals analyzed do not suffer from any delays introduced by the sensor contact pressure, these constitute a more reliable tool for pressure-pulse timing measurements while the need of calibration to measure intervals such as the PTT does not represent a major drawback, as these often require calibration in any case. Further, IPG signals are obtained from electrodes, which can be easily embedded in common objects and shared with other systems, hence these are especially suited for cardiovascular parameter measurements in ambulatory scenarios.

Chapter 4

Time intervals from the BCG

THE measurement of time intervals between the weighing-scale BCG and other signals to obtain cardiovascular parameters is a promising field as the signal can be noninvasively obtained from simple and cost-effective weighing scales in ambulatory scenarios. Due to the abundance of motion artifacts typically present BCG recordings from standing subjects, most of the efforts carried out until now focus on the measurement of the J-wave timing, which is the most prominent feature of the BCG and therefore has the highest SNR, as a surrogate measurement of the cardiac-ejection timing. However, the particular intra-waveform dynamics of the weighing-scale BCG have not been yet reported and could be sensitive to other cardiovascular parameters. This chapter analyzes the performance of the I wave as a surrogate of the cardiac-ejection timing and the response of the IJ interval to changes in the PTT. Finally, the performance of the interval from the BCG I wave to the foot-to-foot IPG pressure-pulse timing in assessing the aortic PTT is evaluated.

4.1. The relative timing of the BCG waves

The development of several BCG systems embedded in weighing scales [66] in the last years has prompted a renewed interest on this signal because these devices are already common in the daily routine of many homes and are periodically used to monitor the health status from the body weight.

The BCG waveform is originated from the forces caused by cardiac ejection of blood hence any interval measured from the ECG QRS complex to the BCG depends on the PEP, the time from the electric activation of the heart to the beginning of cardiac ejection (see Fig. 1.3). As the physiological origin of the BCG waves is still controversial, the J wave is usually the reference BCG

waveform feature used to assess the PEP because its SNR is higher than that of other BCG waves. The capability of the RJ interval, measured from the ECG R wave instead of the Q wave because of its higher SNR, in assessing the PEP [70] and contractility [71], which is inversely proportional to the PEP under stable conditions of preload and afterload, is good. The RJ can also be used to assess changes in systolic BP [14], which are strongly correlated with changes in PEP during short effort tests [72], and the strong correspondence between the RJ interval and systolic BP during the four phases of a Valsalva maneuver was reported in [C6].

Despite of the strong correlations reported, the performance of the RJ interval in assessing the PEP relies on the underlying hypothesis that the timing from cardiac ejection to the J wave is constant, which is not supported by any reported model or systematic observation and cannot be assumed to be true in all circumstances. BCG waves result from a superposition of forces caused by events during the propagation of the pressure-pulse along the arterial tree hence it is reasonable to assume that the later waves, which are originated by events in distal sites, are dependent on the PTT besides of the cardiac-ejection timing. Fig. 4.1 shows a representation of the ECG, BCG, and the BP at the aorta, carotid, and femoral arteries with different intervals of interest measured between its waves.

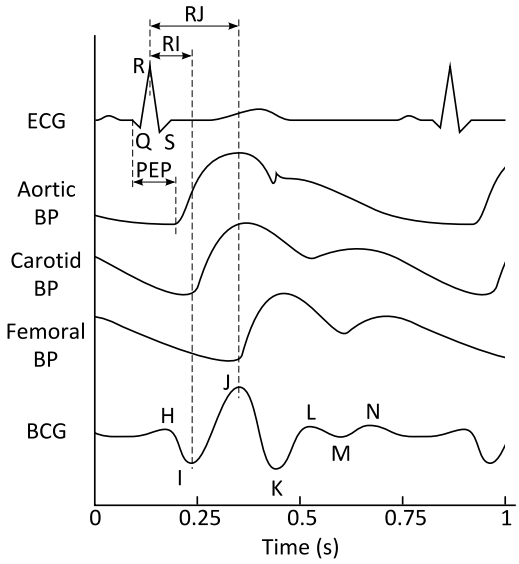

Fig. 4.1. Representation of the ECG, aortic BP, carotid BP, femoral BP, and the BCG.

The RJ interval typically lasts about 210 ms [106] whereas the PEP usually lasts about 100 ms [18]. If it is assumed that the interval between the Q and R is roughly half of the QRS, which typically lasts about 80 ms [18], the J-wave timing appears to be about 150 ms later than the opening of the aortic valve, which is similar than the pressure-pulse timing at the finger or the femoral artery (see Fig. 3.8 and Fig. 3.20) and suggests that the wave is influenced by the PTT in addition to the PEP.

Earlier waves such as the H wave and the I wave should include a lesser amount of PTT and better assess the cardiac-ejection timing. However, the H wave, whose use to assess the PEP was

suggested in [74] and is nearly simultaneous with the aortic valve opening, is better attributed to ventricular movements due to its absence in recordings without ventricular contraction [75]. Alternatively, the I-wave timing is typically about 90 ms after the ECG R wave [106], which is only about 30 ms after cardiac ejection and is similar to the pressure-pulse timing at the carotid artery (see Fig. 3.10), hence it is reasonable to assume that the I-wave timing is less influenced by superposed earlier waves and the PTT. Therefore, the I-wave timing should assess the cardiac-ejection timing better than the J-wave timing in spite of the higher SNR of this wave.

Further, the observations made above imply that the difference in timings of the I and J waves of the BCG, that is, the IJ interval, should be sensitive to the PTT in a manner analogous to other timing measurements from other proximal to distal signals. Therefore, as the I-wave timing and the J-wave timing are dependent to the carotid ejection timing and the J wave presumably includes a higher amount of PTT, it is reasonable to assume that the difference is sensitive to the PTT, and more particularly to changes in aortic PTT, as the greatest vertical forces recorded in the longitudinal BCG are originated there. The different dynamics of the RJ, RI, and IJ intervals during a paced respiration maneuver reported in [C7] suggest that the intervals could be sensitive to different cardiovascular parameters.

Finally, the ability of the BCG in assessing the cardiac-ejection timing has still not been fully exploited since the signal can be used to measure the PTT combined with a distal pressure-pulse waveform integrated in a weighing scale such as an IPG. Similar measurement have not been performed until very recent times [76], even though some systems reported are theoretically capable of performing this measurement [15] and use the information from both signals to improve heartbeat detection [123][124]. The results reported in section 3.4.2 suggest that the IPG from foot-to-foot is a very interesting signal that can be obtained from a weighing scale, as the pressure-pulse timing of this signal is insensitive to PTT changes in limbs and therefore the interval measured from the BCG I wave to it should be sensitive only to the aortic PTT, which is of great interest since this is currently the gold standard measurement of PTT for the assessment of regional arterial stiffness [17].

4.2. Cardiac-ejection timing assessment from the I wave of the BCG

The validity of the RI interval to assess the cardiac-ejection timing has been evaluated in 14 healthy subjects. The RI interval was obtained from the ECG system described in section 2.1.3 and the BCG system described in section 2.3.3 whereas reference cardiac-ejection timings were obtained from the PPT system described in section 2.4.3 placed over the left carotid artery. The pressure-pulse timing at this site is strongly sensitive to changes in the PEP compared to changes in the PTT, as explained in section 3.3.2. Fig. 4.2 shows the measurement setup for the assessment of the cardiac-ejection timing from the ECG and the BCG.

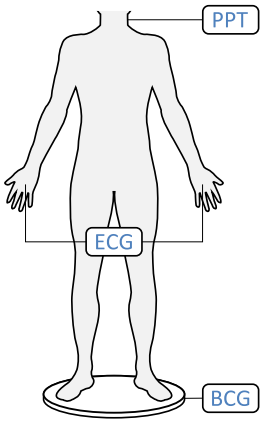

Fig. 4.2. Measurement setup for the assessment of the cardiac-ejection timing.

In order to induce hemodynamic changes, the subjects were asked to perform a paced respiration maneuver at 0.1 Hz for 50 s. The signals were acquired and sent to a PC using the system described in section 2.4.1. The ECG R-wave timing was measured by applying a modified Pan-Tompkins algorithm whereas the pressure-pulse timing was measured by applying the tangent intersection method to detect its foot. The I and J wave timings were measured from a windowed maximum and minimum detection algorithm in an ensemble average composed of three consecutive heartbeats, as described in section 2.3.4, to decrease the uncertainty of the timing measurement.

The mean of the correlation coefficients between the RI interval and the carotid PAT was 0.71 and the standard deviation was 0.16 whereas the mean of the correlation coefficients between the RJ interval and the carotid PAT was 0.37 and the standard deviation was 0.44. A total of six RI recordings and nine RJ recordings were considered not statistically significant and were excluded of these calculations for having $p > 0.05$. The reasons for these apparently weaker correlations compared to those reported between the RJ interval and the PEP reported during a Valsalva maneuver (0.87 [71], 0.93 [74]) can be better explained by examining the traces obtained during the experiments, a sample of which is shown in Fig. 4.3.

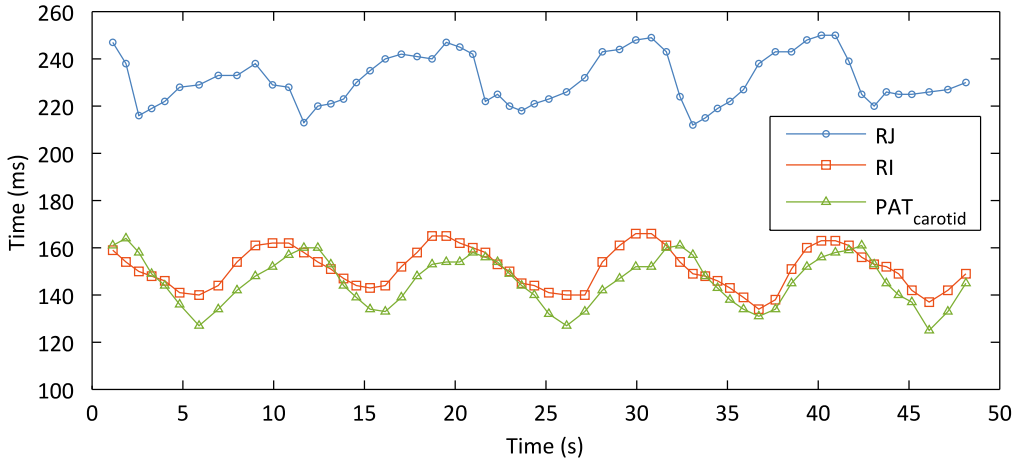

Fig. 4.3. Example of the RJ interval, RI interval, and carotid PAT traces obtained during paced respiration.

The RJ trace has a delay of about 5 heartbeats compared to the carotid PAT trace, which together with the high degree of motion artifacts typically found on standing BCG recordings obtained from weighing scales is responsible for the low correlation coefficients obtained. This delay was different for each subject, ranging from 0 to 6 heartbeats.

A plausible explanation for the delay in RJ traces with respect to the carotid PAT is the hypothesized dependence of the RJ interval on the PTT in addition to the PEP. During inspiration, the filling of air in the lungs expels blood to the systemic arterial system that raises the BP and shortens the PPT as a result of the increase of arterial elasticity (see equation (3.6)). This increase in pressure is counteracted by the hemodynamic regulation system by increasing the stroke volume of the right ventricle [125], which results in a shortening of the PEP. This regulation process takes a few heartbeats to stabilize and it could be responsible for the delay between PTT and PEP traces during paced respiration. In slower maneuvers that induce stronger hemodynamic changes in PEP, such as the Valsalva or tilt-up maneuvers, this delay is less perceptible and has a lesser effect on the correlation between the PEP and the RJ interval. It was also observed that subjects that performed excessively soft paced respiration maneuvers had a nearly constant PTT while the hemodynamic changes were only induced in the PEP.

On the other hand, the carotid PAT and RI interval traces are almost synchronous, which explains the stronger correlation compared to the RJ interval, the small differences being attributable to the different PTT included in carotid PAT with respect to the RI interval or to other factors such as the overlap of the I wave with earlier waves.

Fig. 4.4 shows the aggregated 804 RJ and carotid PAT pairs of values obtained from the 14 subjects during the experiments.

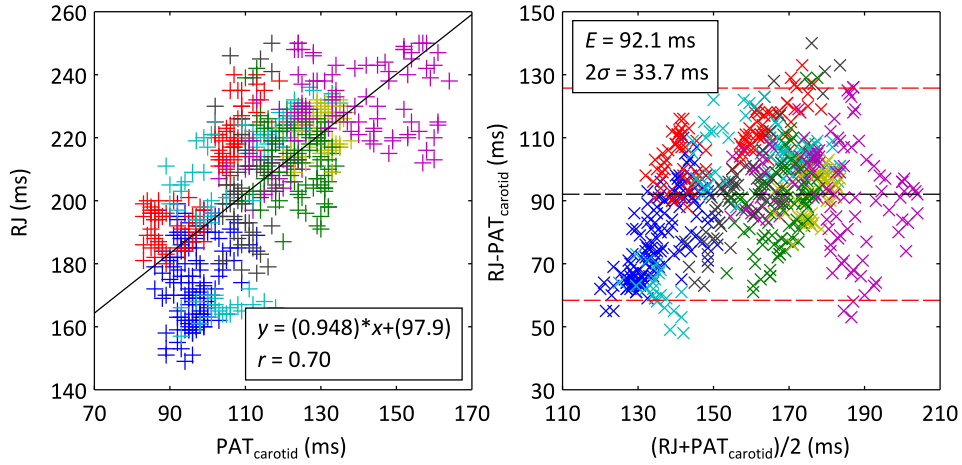

Fig. 4.4. RJ interval vs. carotid PAT, and Bland-Altman analysis of RJ interval vs. carotid PAT during paced respiration.

The correlation between the RJ interval and carotid PAT during paced respiration increases significantly in the aggregated analysis but the delay between traces scatters the points around and this yields a low correlation coefficient and a higher σ in the Bland-Altman analysis compared to those reported during a Valsalva maneuver [71][74]. The slope, y-intercept, and mean of the Bland-Altman analysis are consistent with the values reported in the literature.

Fig. 4.5 shows the aggregated 804 RI and carotid PAT pairs of values obtained from the 14 subjects during the same experiments.

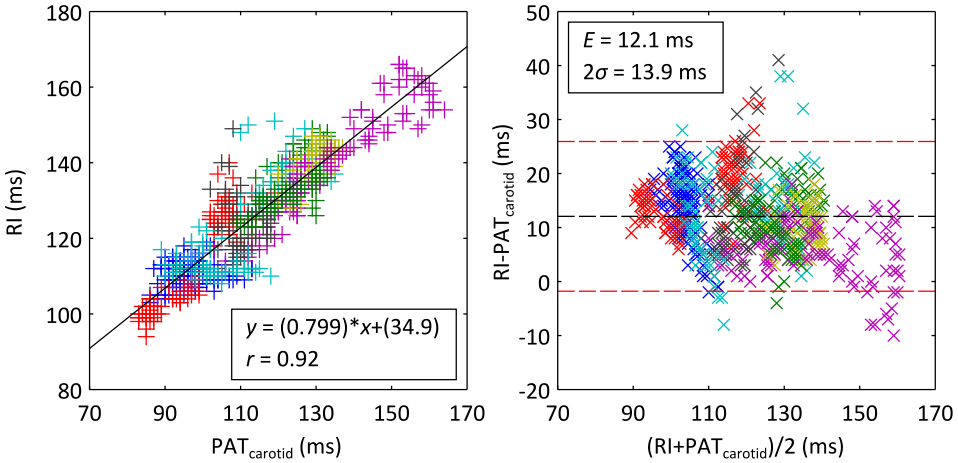

Fig. 4.5. RI interval vs. carotid PAT, and Bland-Altman analysis of RI interval vs. carotid PAT during paced respiration.

The correlation between the RI interval and carotid PAT during paced respiration also increases in the aggregated analysis and, despite of its lower SNR, the RI interval shows stronger correlation than the RJ interval during paced respiration, which suggests that the I wave is less influenced by the PTT and a better surrogate of the cardiac-ejection timing than the J wave. The RI interval can be used as a surrogate of the carotid PAT with a standard uncertainty of 6.9 ms, which is similar to the minimum uncertainty of 6.9 ms achieved in the J-wave timing in section 2.3.4, and

the low mean difference of only 12.1 ms implies that the measured timings do not require any calibration in applications where a low uncertainty is not required.

4.3. Aortic PTT assessment from the IJ interval

The validity of the IJ interval in assessing the aortic PTT has been evaluated in 3 healthy subjects. The IJ interval was obtained from the BCG system described in section 2.3.3 whereas reference aortic PTT values were obtained from the PPT system described in section 2.4.3 placed over the left carotid artery and the IPG system described in section 2.2.3 with the injection electrodes connected to the forefeet and the measurement electrodes placed about the beginning of the femoral artery. The ECG system described in section 2.1.3 was connected to the hands to be used as a timing reference. The IPG_{ff} was simultaneously obtained from the system described in section 3.4.1 with the injection electrodes connected to the forefeet and the detection electrodes connected to the heels for further use in section 4.4. Fig. 4.6 shows the measurement setup for the assessment of aortic PTT from the BCG.

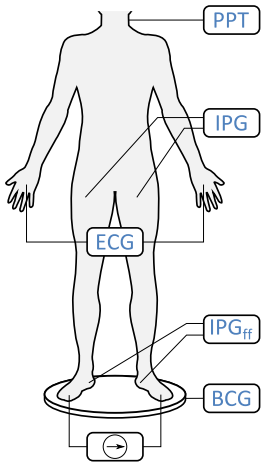

Fig. 4.6. Measurement setup for the assessment of the PTT from the BCG.

In order to induce hemodynamic changes, the subjects were asked to perform a paced respiration maneuver at 0.1 Hz for 100 s. The signals were acquired and sent to a PC using the system described in section 2.4.1. The ECG R-wave timing was measured by applying a modified Pan-Tompkins algorithm whereas the pressure-pulse timings were measured by applying the tangent intersection method to detect its foot. The I and J wave timings were measured from a windowed maximum and minimum detection algorithm in an ensemble average composed of three consecutive heartbeats, as described in section 2.3.4, to decrease the uncertainty of the timing measurement.

The individual correlations between the IJ interval and the aortic PTT were moderate, with correlation coefficients of 0.65, 0.62, and 0.65. Unlike the correlations reported in section 4.2, these low values were a result of the abundant artifacts typically present on standing BCG rather than a consequence of any delay between traces, which was apparently zero.

Fig. 4.7 shows a sample of the traces obtained during the experiment.

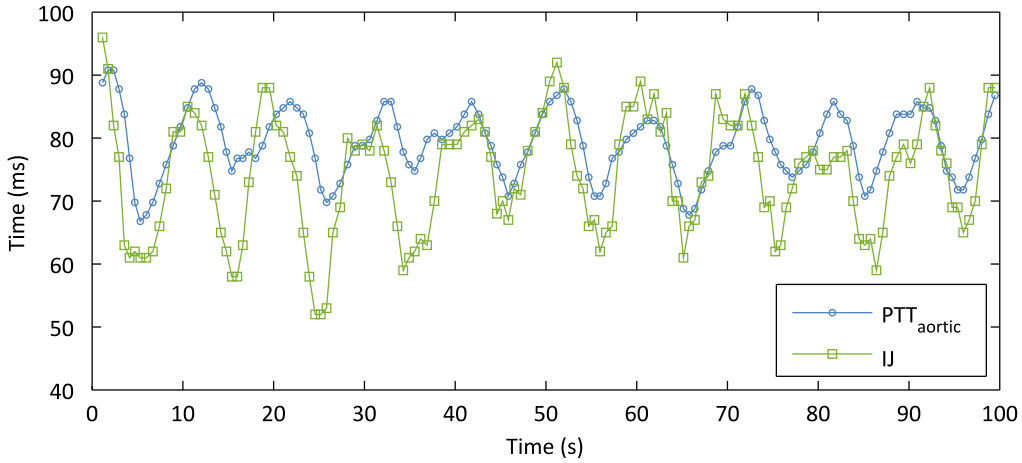

Fig. 4.7. Sample of the IJ interval and aortic PTT traces obtained during paced respiration.

The approximate synchronism between the IJ interval and aortic PTT traces during paced respiration suggests that the IJ interval strongly depends on the PTT and it is responsible for the low correlation between the RJ interval and the PEP during this maneuver, as reported in section 4.2. The slightly larger changes in the IJ interval compared to the changes in the aortic PTT indicate that the IJ interval could be more sensitive to PTT than the aortic PTT, which can be attributed to the different overlap between the I and J waves during changes of the IJ interval.

Fig. 4.8 shows the aggregated 407 IJ and aortic PTT pairs of values obtained from the 3 subjects during the experiments.

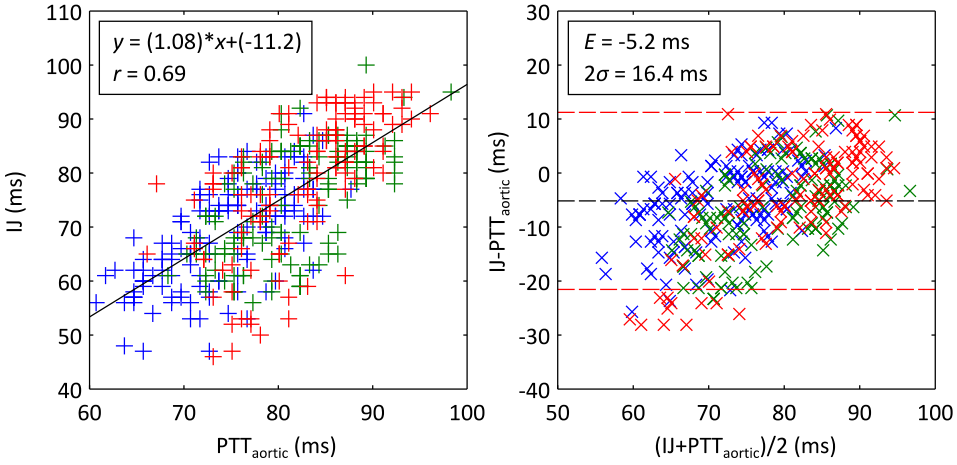

Fig. 4.8. IJ interval vs. aortic PTT, and Bland-Altman analysis of IJ interval vs. aortic PTT during paced respiration.

The correlation between the IJ interval and the aortic PTT during paced respiration slightly increases in the aggregated analysis but it is limited by the abundant motion artifacts present in BCG recordings compared to the range of variation in aortic PTT. The slope close to 1 and the low mean of the difference indicates that the IJ interval has a similar sensitivity to changes in arterial stiffness than the aortic PTT and can be used as a surrogate of aortic PAT without calibration in

applications where a low uncertainty is not required. The standard deviation of the difference between intervals is in the range expected from the uncertainties in the I-wave timing of 6.9 ms, and the J-wave timing of 6.9 ms reported in sections 4.1 and 2.3.4, respectively, and the general equation (2.4).

4.4. Aortic PTT assessment from the BCG and the foot-to-foot IPG

The validity of the time interval between the BCG I wave and the pressure-pulse timing of the foot-to-foot IPG in assessing the carotid PAT has been evaluated from the data collected in the experiments preformed to assess the aortic PTT from the IJ interval described in section 4.3.

The individual correlations between the interval from the BCG I wave to the foot-to-foot IPG pressure-pulse timing, from here named PTT_{a_est}, and the aortic PTT were moderately strong, with correlation coefficients of 0.52, 0.68, and 0.72, and slightly higher than the correlations between the aortic PTT and the IJ interval reported for the same recordings. Fig. 4.9 shows a sample of the traces obtained during the experiment for the same subject in Fig. 4.7.

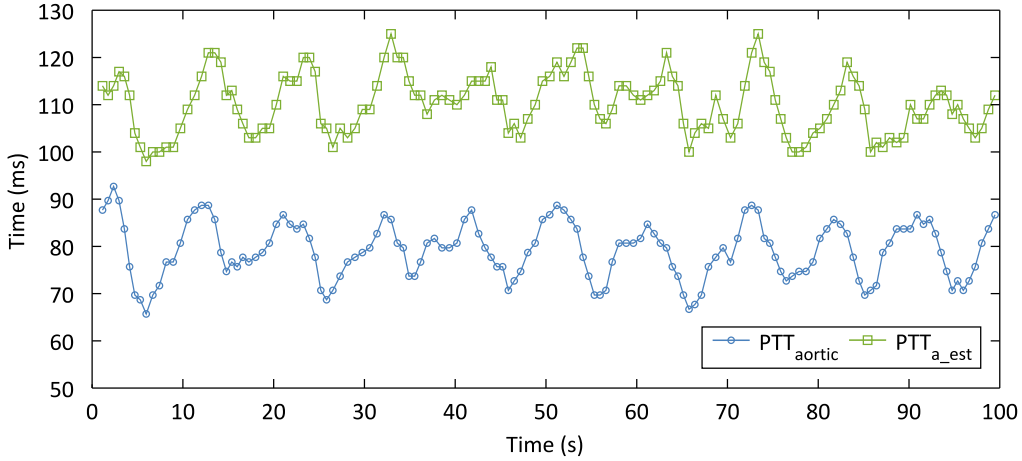

Fig. 4.9. Sample of the PTT_{a_est} and aortic PTT traces obtained during paced respiration.

Despite of the offset between traces, the magnitude and phase of the changes induced by paced respiration is similar for both traces, which indicates that PTT_{a_est} contains a similar amount of PTT than the aortic PTT and can be used as a surrogate by a single-point calibration.

Fig. 4.10 shows the aggregated 407 PTT_{a_est} and aortic PTT pairs of values obtained from the 3 subjects during the experiments.

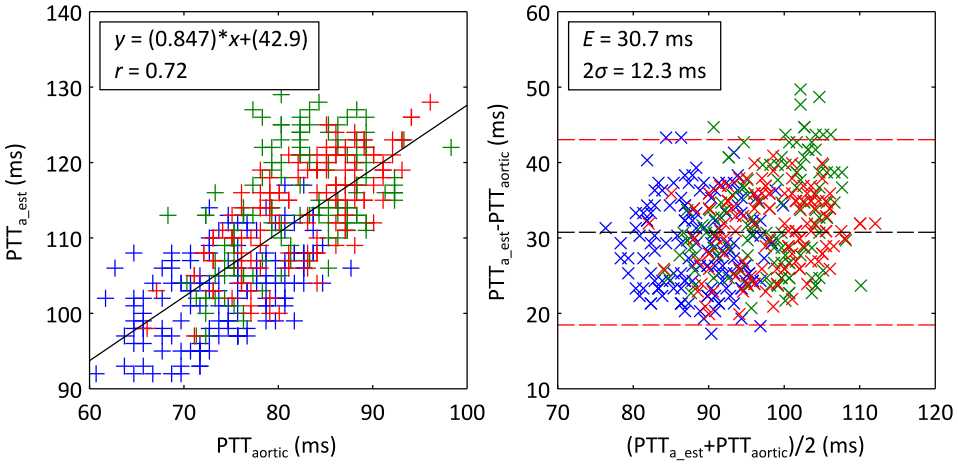

Fig. 4.10. PTT_{a_est} vs. aortic PTT, and Bland-Altman analysis of PTT_{a_est} vs. aortic PTT during paced respiration.

The correlation between the PTT_{a_est} and aortic PTT during paced respiration somewhat improves in the aggregated analysis, and indicates that the performance of the PTT_{a_est} as a surrogate of the aortic PTT is good. The mean and standard deviation of the difference is consistent with the values reported for the I-wave timing of 6.9 ms and the pressure-pulse timing of the foot-to-foot IPG of 3.9 ms in sections 4.2 and 3.4.2, respectively, and the general equation (2.4).

4.5. Summary

This chapter has been devoted to the measurement of several time intervals that involve BCG waves. First, we have proved that, in spite of its lower SNR, the I wave is a better marker of cardiac ejection than the commonly used J wave. We have found that the correlation between the RJ interval and the PEP under paced respiration is weaker than during alternative maneuvers such as the Valsalva's, which indicates that the RJ interval includes, in addition to the PEP, a delay that cannot be assumed to be constant in all circumstances. On the contrary, the performance of the RI interval during the same experiments is significantly superior and the correlation coefficients and uncertainties obtained are similar to those previously reported between the RJ interval and the PEP under other maneuvers. These results suggest that the RI interval performs similarly to the RJ interval in a wider range of circumstances hence it constitutes a better option to assess the carotid ejection timing. Further, we have found that the RI interval can be used to assess the carotid PAT without any calibration hence it is a good candidate to be used as a surrogate of this proximal measurement.

Second, we have found that the IJ interval is sensitive to changes in the PTT, which explains the worse performance of the RJ interval in assessing the PEP compared to the RI interval. The correlations found are moderately strong and the uncertainty is comparable to that of the aortic PTT measured with by other systems [29][30][31][32] that are of the order of tens of milliseconds. Even though the aggregate analysis suggests that the IJ interval could be a good surrogate of the aortic PTT without any calibration, individual traces show a slightly overestimation of the changes

in PTT that can be attributed to the change in overlap between the I and J waves and could require a calibration to properly estimate aortic PTT. These results are of particular interest since the dynamics of the BCG waves no yet explained is sensible to a parameter whose periodic monitoring is of great interest.

Finally, we have proposed and tested a novel method to estimate the aortic PTT from the timing between the BCG I wave as a proximal site to the foot-to-foot IPG pressure-pulse timing as a distal site. The timing measurement between the BCG and a distal pressure-pulse waveform, not proposed until very recent times, constitute an optimal solution to assess the aortic PTT in ambulatory scenarios since both signals can be obtained from a weighing scale. This method yields a stronger correlation with aortic PTT and a lower standard uncertainty than the IJ interval even though the measured interval contains some offset, which could presumably be calibrated from the body height analogously to the estimation of the aortic length [126].

These results can help in achieving a better comprehension of the physiological origin of the BCG waves, and reinforce the role of weighing scales as a tool for the noninvasive assessment of cardiovascular parameters in ambulatory scenarios.

Chapter 5

Conclusions

THE work presented in this thesis analyzes some systems and methods to assess cardiovascular parameters in ambulatory scenarios from the measurement of time intervals between or within the waves of physiological signals. Three signals, the ECG, IPG, and the BCG have been identified as the most suitable for that purpose as these can be acquired with simple, noninvasive, and cost-effective devices in ambulatory scenarios. Several cardiovascular parameters of interest can be assessed from time intervals between the proposed signals, some of them currently being used in research and clinical practice, since the signals contain information about different events associated to proximal and distal sites of the arterial tree. However, most of these intervals are measured in signals obtained from systems designed for broader purposes whose influence on the performance of timing measurements is often omitted.

The first main goal of this work was to analyze the influence of the signal acquisition system on timing measurements from the proposed signals, in order to establish the repeatability of the intervals typically measured from it such as the PTT, PAT, or the PEP. Otherwise, the validity of the conclusions extracted from these intervals throughout this thesis or others in future works could be questionable.

The second main goal was to propose novel methods to obtain cardiovascular parameters of interest using two signals whose physiological origin is still under debate: the IPG from limb to limb and the BCG. Due to the novelty of the hypotheses tested with respect to the prior knowledge about the signals, the objective was to prove the feasibility of the proposed measurements and to identify the main engineering challenges.

The conclusions achieved during this thesis related to the main topics discussed and their implications are summarized below.

Error sources in time interval measurements using cardiovascular signals

The measurement of time intervals between physiological signals is a broad field with many applications of interest hence it is mandatory to know the factors that affect the reproducibility and repeatability of timing measurements. We have analyzed the effect of several parameters of the signal acquisition system such as the phase response of analog filters, noise level, sampling frequency, and the resolution of the ADC that can affect the uncertainty in timing measurements, and reported the minimal specifications for signal acquisition systems intended for time interval measurements in ambulatory scenarios. Further, we have designed and characterized custom signal acquisition systems that fulfill these specifications and are intended to be used as a reference in further works.

Even though our methods were tested in small groups of subjects, the results reported show that whereas some uncertainties are unavoidable, others can be reduced with a careful design. The minimal requirements for signal acquisition systems found are not specially demanding yet some of the systems currently being used do not fulfill them, which degrades the uncertainty in their measurements. Conversely, some capabilities of common signal acquisition systems can be downgraded without degrading the uncertainty, which can contribute to design more cost-effective systems intended to be distributed in large population groups.

The uncertainties measured throughout this document are in the range of milliseconds, which is significantly lower than typical uncertainties reported in time interval measurements and suggests that these could be much lower if they were obtained from systems especially intended for time interval measurements instead of general-purpose systems. Even though the results presented only include a limited number of subjects and the most common timing algorithms for each signal, the values reported constitute a reference value for systems intended for time interval measurements.

Further, the evidence that timings obtained from the PPG are dependent to the sensor contact pressure found during the IPG characterization has strong implications, since the PPG is nowadays the most widely-used method to measure the pressure-pulse timing in clinical care. The results show that the uncertainty in timings from the PPG can be higher than the uncertainty introduced by the signal acquisition system. This, together with the inherent advantages of the IPG reinforces the role of this signal as a reliable tool for the pressure-pulse timing despite of its lower SNR as compared to the PPG.

The IPG from limb to limb

The limb-to-limb IPG has not received much attention and its only application is monitoring the heart rate in weighing scales. Compared to other pulsatile signals, it has the main advantage that it is obtained from electrodes that can be easily embedded in common objects of daily use such as a

phone case or a weighing scale. As the same electrodes can be shared with other systems to obtain other signals such as the ECG and the local IPG, the signal significantly increases the potential capabilities of multi-signal devices to assess cardiovascular parameters in ambulatory scenarios.

We have hypothesized that the IPG from limb to limb is sensitive to changes in proximal sites even though it is obtained at distal sites, and we have proposed and evaluated a model to estimate the contributions of each body segment in the current path for the hand-to-hand and foot-to-foot IPG. After that, we have analyzed its validity to assess changes in the PEP and femoral PAT, two intervals of great interest since these can be used for the measurement of the aortic PTT.

The strong correlation between the hand-to-hand IPG with the carotid pulse and the foot-to-foot IPG with the femoral pulse found, strengthened by the model presented, show that the IPG from limb to limb can reflect changes in proximal sites with good uncertainty despite the need for offset calibration, which is otherwise common in several measurements based on time interval such as the PWV from the PTT. Combined with other signals obtained from distal sites that provide complementary information, the IPG from limb to limb substantially increases the spectrum of time intervals that can be measured noninvasively to assess cardiovascular parameters in ambulatory scenarios.

Time intervals from the BCG

The BCG has been known since long ago but the physiological origin of its waves is still controversial. We have hypothesized and demonstrated the enhanced performance of the RI interval compared to the RJ interval in assessing the PEP due to dependence of the IJ interval on the PTT, and we have proposed a novel method to assess the aortic PTT from the BCG and the foot-to-foot IPG.

The strong dependency of the I wave to cardiac ejection, and the strong correlation between the IJ interval and the aortic PTT found can help in achieving a better comprehension of the signal. The hypotheses formulated are simple enough to stand even without a model and the results suggest that several parameters of great interest can be obtained from the timings of the BCG waves.

Combined with the diffusion of weighing scales in modern households, the results presented consolidate the role of weighing scales as a platform for multi-signal acquisition in ambulatory scenarios since the main parameters and signals targeted on this thesis can be acquired from systems integrated in them. Even though measurements from weighing scales are limited to only standing subjects, monitoring cardiovascular parameters in a daily basis is attractive enough to consider this new scenario for future approaches to cardiovascular disease treatment.

The main results described above show that the initial objectives of this thesis have been achieved. Nevertheless, the work presented constitutes only a first step towards further research. As

described earlier, clinical trials should confirm some of the results obtained for a limited cohort. Further, some technical improvements could enhance the capabilities of the systems presented.

First, the IPG has proved to be a reliable tool for pressure-pulse timing measurement, as it is almost insensitive to the sensor contact pressure. However, a low-noise design able to match the capabilities of common PPG systems would consolidate the IPG as the preferred option for time interval measurements.

The BCG has shown a great potential in assessing cardiovascular parameters although these are strongly blurred by the high level of motion artifacts typically present on recordings. Reducing motion artifacts would increase the interest on the signal for cardiovascular parameter monitoring in ambulatory scenarios.

Even though the ECG can be obtained in a weighing scale through a handheld device, a system to obtain it from the feet would turn weighing scales in a more integrated and easy-to-use solution.

The increasing need for simple, noninvasive, and cost-effective solutions to provide a better medical access to the population defined the goals of this thesis. The systems and methods here described constitute a basis for the future development of platforms to monitor cardiovascular parameters in ambulatory scenarios and, hopefully, contribute to substantially improve life quality of healthy and diseased people in the world.

References

[1] World Health Organization (WHO), "World Health Statistics 2012," Geneve, 2012.

[2] World Health Organization (WHO), "Global Atlas of Cardiovascular Disease Prevention and Control," Geneve, 2011.

[3] J. T. Cohen, P. J. Neumann, and M. C. Weinstein, "Does Preventive Care Save Money? Health Economics and the Presidential Candidates," *N. Engl. J. Med.*, vol. 358, no. 7, pp. 661–663, Feb. 2008.

[4] World Health Organization (WHO), "A Prioritized Research Agenda for Prevention and Control of Noncomunicable Diseases," Geneve, 2011.

[5] J. Allen, "Photoplethysmography and Its Application in Clinical Physiological Measurement," *Physiol. Meas.*, vol. 28, no. 3, Feb. 2007.

[6] L. Sörnmo and P. Laguna, *Bioelectrical Signal Processing in Cardiac and Neurological Applications*, 1st ed. Amsterdam, The Netherlands: Elsevier Academic Press, 2005.

[7] J. Nyboer, M. M. Kreider, and L. Hannapel, "Electrical Impedance Plethysmography: a Physical and Physiologic Approach to Peripheral Vascular Study," *Circulation*, vol. 2, no. 6, pp. 811–821, Dec. 1950.

[8] O. T. Inan, P. F. Migeotte, K.-S. Park, M. Etemadi, K. Tavakolian, et al., "Ballistocardiography and Seismocardiography: a Review of Recent Advances," *Biomed. Heal. Informatics, IEEE J.*, pending publication, 2014.

[9] R. M. Rangayyan and R. J. Lehner, "Phonocardiogram Signal Analysis: A Review," *Crit. Rev. Biomed. Eng.*, vol. 15, no. 3, pp. 211–236, 1987.

[10] K. Matthys and P. Verdonck, "Development and Modelling of Arterial Applanation Tonometry: A Review," *Technol. Heal. Care*, vol. 10, no. 1, pp. 65–76, Jan. 2002.

[11] A. Grabovskis, Z. Marcinkevics, U. Rubins, and E. Kviesis-Kipge, "Effect of Probe Contact Pressure on the Photoplethysmographic Assessment of Conduit Artery Stiffness," *J. Biomed. Opt.*, vol. 18, no. 2, p. 27004, 2013.

[12] X. F. Teng and Y. T. Zhang, "Theoretical Study on the Effect of Sensor Contact Force on Pulse Transit Time," *Biomed. Eng. IEEE Trans.*, vol. 54, no. 8, pp. 1490–1498, Aug. 2007.

[13] R. Gonzalez-Landaeta, O. Casas, and R. Pallas-Areny, "Heart Rate Detection From Plantar Bioimpedance Measurements," *Biomed. Eng. IEEE Trans.*, vol. 55, no. 3, pp. 1163–1167, Mar. 2008.

[14] J. H. Shin, K. M. Lee, and K. S. Park, "Non-constrained Monitoring of Systolic Blood Pressure on a Weighing Scale," *Physiol. Meas.*, vol. 30, no. 7, p. 679, 2009.

[15] O. T. Inan, D. Park, G. T. A. Kovacs, and L. Giovangrandi, "Multi-Signal Electromechanical Cardiovascular Monitoring on a Modified Home Bathroom Scale," in *Engineering in Medicine and Biology Society, EMBC, 2011 Annual International Conference of the IEEE*, 2011, pp. 2472–2475.

[16] S. Laurent, J. Cockcroft, L. Van Bortel, P. Boutouyrie, C. Giannattasio, et al., "Expert Consensus Document on Arterial Stiffness: Methodological Issues and Clinical Applications," *Eur. Heart J.*, vol. 27, no. 21, pp. 2588–2605, Sep. 2006.

[17] P. Boutouyrie, M. Briet, C. Collin, S. Vermeersch, and B. Pannier, "Assessment of Pulse Wave Velocity," *Artery Res.*, vol. 3, no. 1, pp. 3–8, Feb. 2009.

[18] A. M. Weissler, W. S. Harris, and C. D. Schoenfeld, "Systolic Time Intervals in Heart Failure in Man," *Circulation*, vol. 37, no. 2, pp. 149–159, 1968.

[19] D. Buxi, J. M. Redouté, and M. R. Yuce, "A Survey on Signals and Systems in Ambulatory Blood Pressure Monitoring Using Pulse Transit Time," *Physiol. Meas.*, vol. 36, no. 3, pp. R1–R26, Mar. 2015.

[20] J. Naschitz, S. Bezobchuk, R. Mussafia-Priselac, S. Sundick, D. Dreyfuss, et al., "Pulse Transit Time by R-wave-gated Infrared Photoplethysmography: Review of the Literature and Personal Experience," *J. Clin. Monit. Comput.*, vol. 18, no. 5–6, pp. 333–342, Dec. 2004.

[21] J. Argod, J.-L. Pépin, and P. Lévy, "Differentiating Obstructive and Central Sleep Respiratory Events through Pulse Transit Time," *Am. J. Respir. Crit. Care Med.*, vol. 158, no. 6, pp. 1778–1783, Dec. 1998.

[22] T. Weiss, A. Del Bo, N. Reichek, and K. Engelman, "Pulse Transit Time in the Analysis of Autonomic Nervous System Effects on the Cardiovascular System," *Psychophysiology*, vol. 17, no. 2, pp. 202–207, Mar. 1980.

[23] W. Chen, T. Kobayashi, S. Ichikawa, Y. Takeuchi, and T. Togawa, "Continuous Estimation of Systolic Blood Pressure Using the Pulse Arrival Time and Intermittent Calibration," *Med. Biol. Eng. Comput.*, vol. 38, no. 5, pp. 569–574, Sep. 2000.

[24] H. Gesche, D. Grosskurth, G. Küchler, and A. Patzak, "Continuous Blood Pressure Measurement by Using the Pulse Transit Time: Comparison to a Cuff-based Method," *Eur. J. Appl. Physiol.*, vol. 112, no. 1, pp. 309–315, May 2012.

[25] J. G. Kips, A. E. Schutte, S. J. Vermeersch, H. W. Huisman, J. M. Van Rooyen, et al., "Comparison of Central Pressure Estimates Obtained From SphygmoCor, Omron HEM-9000AI and Carotid Applanation Tonometry," *J. Hypertens.*, vol. 29, no. 6, pp. 1115–1120, 2011.

[26] S. S. Ahmed, G. E. Levinson, C. J. Schwartz, and P. O. Ettinger, "Systolic Time Intervals as Measures of the Contractile State of the Left Ventricular Myocardium in Man," *Circulation*, vol. 46, no. 3, pp. 559–571, Sep. 1972.

[27] D. B. Newlin and R. W. Levenson, "Pre-ejection Period: Measuring Beta-adrenergic Influences Upon the Heart," *Psychophysiology*, vol. 16, no. 6, pp. 546–552, Nov. 1979.

[28] R. P. Lewis, S. E. Rittogers, W. F. Froester, and H. Boudoulas, "A Critical Review of the Systolic Time Intervals," *Circulation*, vol. 56, no. 2, pp. 146–158, Aug. 1977.

[29] T. Weber, M. Ammer, M. Rammer, A. Adji, M. F. O'Rourke, et al., "Noninvasive Determination of Carotid–Femoral Pulse Wave Velocity Depends Critically on Assessment of Travel Distance: A Comparison with Invasive Measurement," *J. Hypertens.*, vol. 27, no. 8, pp. 1624–1630, Aug. 2009.

[30] P. Salvi, E. Magnani, F. Valbusa, D. Agnoletti, C. Alecu, et al., "Comparative Study of Methodologies for Pulse Wave Velocity Estimation," *J. Hum. Hypertens.*, vol. 22, no. 10, pp. 669–677, Oct. 2008.

[31] N. A. Jatoi, A. Mahmud, K. Bennett, and J. Feely, "Assessment of Arterial Stiffness in Hypertension: Comparison of Oscillometric (Arteriograph), Piezoelectronic (Complior) and Tonometric (SphygmoCor) techniques*," *J. Hypertens.*, vol. 27, no. 11, 2009.

[32] S. C. Millasseau, A. D. Stewart, S. J. Patel, S. R. Redwood, and P. J. Chowienczyk, "Evaluation of Carotid-femoral Pulse Wave Velocity: Influence of Timing Algorithm and Heart Rate," *Hypertension*, vol. 45, no. 2, pp. 222–226, Feb. 2005.

[33] M. Merri, D. C. Farden, J. G. Mottley, and E. L. Titlebaum, "Sampling Frequency of the Electrocardiogram for Spectral Analysis of the Heart Rate Variability," *Biomed. Eng. IEEE Trans.*, vol. 37, no. 1, pp. 99–106, Jan. 1990.

[34] S. Mittal, C. Movsowitz, and J. S. Steinberg, "Ambulatory External Electrocardiographic Monitoring. Focus on Atrial Fibrillation," *J. Am. Coll. Cardiol.*, vol. 58, no. 17, pp. 1741–1749, Oct. 2011.

[35] American National Standards Institute, "Ambulatory Electrocardiographs (ANSI/AAMI EC38:1998)." Arlington, VA: Association for the Advancement of Medical Instrumentation, 1998.

[36] American National Standards Institute, "Diagnostic Electrocardiographic Devices (ANSI/AAMI EC11:1991/(R)2001)." Arlington, VA: Association for the Advancement of Medical Instrumentation, 2000.

[37] A. Ueno, Y. Akabane, T. Kato, H. Hoshino, S. Kataoka, et al., "Capacitive Sensing of Electrocardiographic Potential Through Cloth From the Dorsal Surface of the Body in a Supine Position: A Preliminary Study," *Biomed. Eng. IEEE Trans.*, vol. 54, no. 4, pp. 759–766, Apr. 2007.

[38] A. S. and L. Kirkup, "A Direct Comparison of Wet, Dry and Insulating Bioelectric Recording Electrodes," *Physiol. Meas.*, vol. 21, no. 2, p. 271, 2000.

[39] Y. M. Chi, T. P. Jung, and G. Cauwenberghs, "Dry-contact and Noncontact Biopotential Electrodes: Methodological Review," *Biomed. Eng. IEEE Rev.*, vol. 3, pp. 106–119, 2010.

[40] P. S. Luna-Lozano and R. Pallas-Areny, "Microphonics in Biopotential Measurements With Capacitive Electrodes," in *Engineering in Medicine and Biology Society (EMBS), 2010. 32th Annual International Conference of the IEEE*, Aug. 2010, pp. 3487–3490.

[41] G. Ascher and J. P. Coustenoble, "Portable apparatus for recording electrocardiograms," US Patent 4,596,256, Jun. 24th, 1986.

[42] S. R. Inciardi, S. D. Elliott, F. Einberg, and K. Svensson, "eCard ECG Monitor," US Patent Application 2014/0073979, Mar. 13th, 2014.

[43] A. Benini, M. Donati, F. Iacopetti, and L. Fanucci, "User-friendly Single-lead ECG Device for Home Telemonitoring Applications," in *2014 8th International Symposium on Medical Information and Communication Technology (ISMICT)*, Apr. 2014, pp. 1–5.

[44] M. Kohls, "ECG Recording Device and Method of Use," US Patent Application 2007/0149886, Jun. 28th, 2007.

[45] C. A. Chou, "Handheld Electrocardiographic Device," US Patent 8,644,915 B2, Feb. 4th, 2014.

[46] H. L. Chan, P. K. Chao, and J. C. Jheng, "Device and method for measuring three-lead ECG in a wristwatch," US Patent Application 2010/0076331, Mar. 25th, 2010.

[47] G. Andreoni, A. Pedotti, and M. Di Rienzo, "ECG Monitoring through Environmental Electrodes," in *1st Annual International IEEE-EMBS Special Topic Conference on Microtechnologies in Medicine and Biology. Proceedings*, 2000, pp. 615–618.

[48] H. B. Wheeler, "Diagnosis of Deep Vein Thrombosis. Review of Clinical Evaluation and Impedance Plethysmography," *Am. J. Surg.*, vol. 150, no. 4A, pp. 7–13, 1985.

[49] L. Jensen, J. Yakimets, and K. K. Teo, "A Review of Impedance Cardiography," *Hear. Lung J. Acute Crit. Care*, vol. 24, no. 3, pp. 183–193, May 1995.

[50] M. D. Reisner Andrew, P. D. Shaltis Phillip A., D. McCombie, and P. D. Asada H Harry, "Utility of the Photoplethysmogram in Circulatory Monitoring," *J. Am. Soc. Anesthesiol.*, vol. 108, no. 5, pp. 950–958, May 2008.

[51] T. M. R. Shankar, J. G. Webster, and S. Y. Shao, "The Contribution of Vessel Volume Change and Blood Resistivity Change to the Electrical Impedance Pulse," *Biomed. Eng. IEEE Trans.*, vol. BME-32, no. 3, pp. 192–198, Mar. 1985.

[52] S. Bang, C. Lee, J. Park, M. C. Cho, Y. G. Yoon, et al., "A Pulse Transit Time Measurement Method Based on Electrocardiography and Bioimpedance," in *2009 IEEE Biomedical Circuits and Systems Conference*, Nov. 2009, pp. 153–156.

[53] F. Risacher, J. Jossinet, E. McAdams, C. Eynard, J. McLaughlin, et al., "Computation of the Pulse Wave Velocity in Limbs From Multichannel Impedance Plethysmography," in *Engineering in Medicine and Biology Society (EMBS), 1992. 14th Annual International Conference of the IEEE*, Oct. 1992, vol. 5, pp. 1744–1745.

[54] B. A. Friedman, R. Medero, L. T. Hersh, and S. Kolluri, "Continuous, Non-invasive Technique for Measuring Blood Pressure Using Impedance Plethysmography," U.S. patent: US6648828 B2, issued, Nov. 18th, 2003.

[55] M. C. Cho, J. Y. Kim, and S. Cho, "A Bio-impedance Measurement System for Portable Monitoring of Heart Rate and Pulse Wave Velocity Using Small Body Area," in *2009 IEEE International Symposium on Circuits and Systems*, May 2009, pp. 3106–3109.

[56] F. Risacher, J. Jossinet, E. T. McAdams, J. McLaughlin, Y. Mann, et al., "Impedance Plethysmography for the Evaluation of Pulse Wave Velocity in Limbs," *Med. Biol. Eng. Comput.*, vol. 31, no. 3, pp. 318–322, 1993.

[57] N. K. Kristiansen, J. Fleischer, M. S. Jensen, K. S. Andersen, and H. Nygaard, "Design and Evaluation of a Handheld Impedance Plethysmograph for Measuring Heart Rate Variability," *Med. Biol. Eng. Comput.*, vol. 43, no. 4, pp. 516–521, 2005.

[58] T. Kööbi, M. Kähönen, T. Iivainen, and V. Turjanmaa, "Simultaneous Non-invasive Assessment of Arterial Stiffness and Haemodynamics – A Validation Study," *Clin. Physiol. Funct. Imaging*, vol. 23, no. 1, pp. 31–36, Jan. 2003.

[59] K. R. Foster and H. C. Lukaski, "Whole-body Impedance - What Does It Measure?," *Am. J. Clin. Nutr.*, vol. 64, no. 3, p. 388S–396S, Sep. 1996.

[60] D. H. Diaz, O. Casas, and R. Pallas-Areny, "Heart rate detection from single-foot plantar bioimpedance measurements in a weighing scale," in *Engineering in Medicine and Biology Society, 2010. EMBS 2010. 32th Annual International Conference of the IEEE*, 2010, pp. 6489–6492.

[61] O. Casas and R. Pallas-Areny, "Signal to Noise Ratio in Bioelectrical Impedance Measurements Using Synchronous Sampling," in *Engineering in Medicine and Biology Society (EMBC), 1994 Annual International Conference of the IEEE*, 1994, vol. 2, pp. 890–891.

[62] J. W. Gordon, "Certain Molar Movements of the Human Body Produced by the Circulation of the Blood," *J. Anat. Physiol.*, vol. 11, no. Pt 3, pp. 533–536, Apr. 1877.

[63] I. Starr, A. J. Rawson, H. A. Schroeder, and N. R. Joseph, "Studies on the Estimation of Cardiac Ouptut in Man, and of Abnormalities in Cardiac Function, From the Heart's Recoil and the Blood's Impacts; the Ballistocardiogram," *Am. J. Physiol. - Leg. Content*, vol. 127, no. 1, pp. 1–28, 1939.

[64] E. Pinheiro, O. Postolache, and P. Girão, "Theory and Developments in an Unobtrusive Cardiovascular System Representation: Ballistocardiography," *Open Biomed. Eng. J.*, vol. 4, pp. 201–216, Oct. 2010.

[65] A. Akhbardeh, S. Junnila, M. Koivuluoma, T. Koivistoinen, V. Turjanmaa, et al., "Towards a Heart Disease Diagnosing System Based on Force Sensitive Chair's Measurement, Biorthogonal Wavelets and Neural Networks," *Eng. Appl. Artif. Intell.*, vol. 20, no. 4, pp. 493–502, Jun. 2007.

[66] R. Gonzalez-Landaeta, O. Casas, and R. Pallas-Areny, "Heart Rate Detection from an Electronic Weighing Scale," in *Engineering in Medicine and Biology Society (EMBS), 2007. 29th Annual International Conference of the IEEE*, Aug. 2007, vol. 2007, pp. 6283–6.

[67] J. Alihanka, K. Vaahtoranta, and I. Saarikivi, "A New Method for Long-term Monitoring of the Ballistocardiogram, Heart Rate, and Respiration," *Am. J. Physiol. - Regul. Integr. Comp. Physiol.*, vol. 240, no. 5, pp. R384–R392, May 1981.

[68] P. F. Migeotte, Q. Deliere, J. Tank, I. Funtova, R. Baevsky, et al., "3D-ballistocardiography in Microgravity: Comparison With Ground Based Recordings," *Engineering in Medicine and Biology Society, 2011. EMBS 2012. 35th Annual International Conference of the IEEE*. pp. 7012–7016, 2013.

[69] O. T. Inan, M. Etemadi, A. Paloma, L. Giovangrandi, and G. T. A. Kovacs, "Non-invasive Cardiac Output Trending During Exercise Recovery on a Bathroom-scale-based Ballistocardiograph," *Physiol. Meas.*, vol. 30, no. 3, p. 261, Feb. 2009.

[70] O. T. Inan, M. Etemadi, R. M. Wiard, G. T. A. Kovacs, and L. Giovangrandi, "Non-invasive Measurement of Valsalva-induced Hemodynamic Changes on a Bathroom Scale Ballistocardiograph," *Eng. Med. Biol. Soc. (EMBS), 2008. 30th Annu. Int. Conf. IEEE*, vol. 2008, pp. 674–7, Jan. 2008.

[71] M. Etemadi, O. T. Inan, R. M. Wiard, G. T. A. Kovacs, and L. Giovangrandi, "Non-invasive Assessment of Cardiac Contractility on a Weighing Scale," in *Engineering in Medicine and Biology Society (EMBS), 2009. 31th Annual International Conference of the IEEE*, 2009, pp. 6773–6776.

[72] J. Muehlsteff, X. L. Aubert, and M. Schuett, "Cuffless Estimation of Systolic Blood Pressure for Short Effort Bicycle Tests: the Prominent Role of the Pre-ejection Period," in *Engineering in Medicine and Biology Society (EMBS), 2006. 28th Annual International Conference of the IEEE*, 2006, pp. 5088–5092.

[73] I. Starr and A. Noordergraaf, *Ballistocardiography in Cardiovascular Research: Physical Aspects of the Circulation in Health and Disease*, 1st ed. Philadelphia: Lippincott, 1967.

[74] M. Etemadi, O. T. Inan, L. Giovangrandi, and G. T. A. Kovacs, "Rapid Assessment of Cardiac Contractility on a Home Bathroom Scale," *Inf. Technol. Biomed. IEEE Trans.*, vol. 15, no. 6, pp. 864–869, Nov. 2011.

[75] I. Starr, T. G. Schnabel, and R. L. Mayock, "Studies Made by Simulating Systole at Necropsy: II. Experiments on the Relation of Cardiac and Peripheral Factors to the Genesis of the Pulse Wave and the Ballistocardiogram," *Circulation*, vol. 8, no. 1, pp. 44–61, Jul. 1953.

[76] C. S. Kim, A. M. Carek, R. Mukkamala, O. T. Inan, and J. O. Hahn, "Ballistocardiogram as Proximal Timing Reference for Pulse Transit Time Measurement: Potential for Cuffless Blood Pressure Monitoring," *Biomed. Eng. IEEE Trans.*, vol. PP, no. 99, p. 1, 2015.

[77] A. D. Waller, "A Demonstration on Man of Electromotive Changes Accompanying the Heart's Beat," *J. Physiol.*, vol. 8, no. 5, pp. 229–234, 1887.

[78] M. Rivera-Ruiz, C. Cajavilca, and J. Varon, "Einthoven's String Galvanometer: the First Electrocardiograph.," *Tex. Heart Inst. J.*, vol. 35, no. 2, pp. 174–8, Jan. 2008.

[79] J. C. Huhta and J. G. Webster, "60-Hz Interference in Electrocardiography," *Biomed. Eng. IEEE Trans.*, vol. 20, no. 2, pp. 91–101, Mar. 1973.

[80] N. Meziane, J. G. Webster, M. Attari, and A. J. Nimunkar, "Dry Electrodes for Electrocardiography," *Physiol. Meas.*, vol. 34, no. 9, p. R47, 2013.

[81] M. R. Neuman, "Biopotential Electrodes," in *Medical Instrumentation Application and Design*, 4th ed., J. G. Webster, Ed. New York, USA: John Wiley & Sons, 2009, pp. 189–240.

[82] N. V Thakor and J. G. Webster, "Ground-Free ECG Recording with Two Electrodes," *Biomed. Eng. IEEE Trans.*, vol. BME-27, no. 12, pp. 699–704, 1980.

[83] "Patient Safety." Med. Electro. Div., Hewlett-Packard Co., Waltham, Mass., Appl. Note AN 718, 1971.

[84] D. Diaz, O. Casas, and R. Pallas-Areny, "Interference Reduction in ECG by Using a Dual Ground Electrode," in *19th IMEKO World Congress 2009*, 2009, pp. 1695–1700.

[85] J. Pan and W. J. Tompkins, "A Real-time QRS Detection Algorithm," *Biomed. Eng. IEEE Trans.*, vol. 32, no. 3, pp. 230–236, Mar. 1985.

[86] Joint Comitee for Guides in Metrology, "Evaluation of Measurement Data - Guide to the Expression of Uncertainty in Measurement (JCGM 100:2008)." JGCM, 2008.

[87] X. Zhou, R. Peng, H. Ding, N. Zhang, and P. Li, "Validation of New and Existing Decision Rules for the Estimation of Beat-to-Beat Pulse Transit Time," *Biomed Res. Int.*, vol. 2015, p. 306934, Mar. 2015.

[88] M. J. Drinnan, J. Allen, and A. Murray, "Relation Between Heart Rate and Pulse Transit Time During Paced Respiration," *Physiol. Meas.*, vol. 22, no. 3, pp. 425–432, 2001.

[89] E. M. Spinelli, R. Pallas-Areny, and M. A. Mayosky, "AC-Coupled Front-End for Biopotential Measurements," *Biomed. Eng. IEEE Trans.*, vol. 50, no. 3, pp. 391–5, Mar. 2003.

[90] C. Assambo and M. J. Burke, "Low-frequency Response and the Skin-electrode Interface in Dry-electrode Electrocardiography," in *Advances in Electrocardiograms - Methods and Analysis*, R. M. Millis, Ed. INTECH Open Access Publisher, 2012.

[91] D. Nunan, G. R. H. Sandercock, and D. A. Brodie, "A Quantitative Systematic Review of Normal Values for Short-Term Heart Rate Variability in Healthy Adults," *Pacing Clin. Electrophysiol.*, vol. 33, no. 11, pp. 1407–1417, Nov. 2010.

[92] C. Y. Liu, C. C. Wei, and P. C. Lo, "Variation Analysis of Sphygmogram to Assess Cardiovascular System under Meditation," *Evid. Based. Complement. Alternat. Med.*, vol. 6, no. 1, pp. 107–112, Mar. 2009.

[93] R. S. Vasan, "Pathogenesis of Elevated Peripheral Pulse Pressure: Some Reflections and Thinking Forward," *Hypertension*, vol. 51, no. 1, pp. 33–36, Jan. 2008.

[94] A. A. Alian and K. H. Shelley, "Photoplethysmography," *Best Pract. Res. Clin. Anaesthesiol.*, vol. 28, no. 4, pp. 395–406, Apr. 2015.

[95] R. A. Peura, "Blood Pressure and Sound," in *Medical Instrumentation Application and Design*, 4th ed., J. G. Webster, Ed. New York, USA: John Wiley & Sons, 2009, pp. 293–337.

[96] J. Allen and A. Murray, "Effects of Filtering on Multi-site Photoplethysmography Pulse Waveform Characteristics," in *Computers in Cardiology, 2004*, 2004, pp. 485–488.

[97] American National Standards Institute, "Safe Current Limits for Electromedical Apparatus (ANSI/AAMI ES1:1993)." Arlington, VA: Association for the Advancement of Medical Instrumentation, 1993.

[98] R. V Hill, J. C. Jansen, and J. L. Fling, "Electrical Impedance Plethysmography: A Critical Analysis," *J. Appl. Physiol.*, vol. 22, no. 1, pp. 161–168, 1967.

[99] B. H. Brown, A. J. Wilson, and P. Bertemes-Filho, "Bipolar and Tetrapolar Transfer Impedance Measurements from Volume Conductor," *Electron. Lett.*, vol. 36, no. 25, pp. 2060–2062, 2000.

[100] R. Pallas-Areny and J. G. Webster, "AC Instrumentation Amplifier for Bioimpedance Measurements," *Biomed. Eng. IEEE Trans.*, vol. 40, no. 8, pp. 830–833, 1993.

[101] R. S. Gubner, M. Rodstein, and H. E. Ungerleider, "Ballistocardiography: an Appraisal of Technic, Physiologic Principles, and Clinical Value," *Circulation*, vol. 7, no. 2, pp. 268–286, Feb. 1953.

[102] A. Noordergraaf, "Further Studies on a Theory of the Ballistocardiogram," *Circulation*, vol. 23, no. 3, pp. 413–425, Mar. 1961.

[103] J. R. Braunstein, C. E. Oelker, and R. C. Gowdy, "Design of a Two-dimensional Ballistocardiograph," *J. Clin. Invest.*, vol. 29, no. 9, pp. 1219–1226, Sep. 1950.

[104] M. B. Rappaport, H. B. Sprague, and W. B. Thompson, "Ballistocardiography - I. Physical Considerations," *Circulation*, vol. 7, no. 2, pp. 229–246, Feb. 1953.

[105] N. T. Smith, "Ballistocardiography," in *Noninvasive Cardiology*, A. M. Weissler, Ed. New York, USA: Grune & Stratton, 1974, pp. 39–148.

[106] O. T. Inan, M. Etemadi, R. M. Wiard, L. Giovangrandi, and G. T. A. Kovacs, "Robust Ballistocardiogram Acquisition for Home Monitoring," *Physiol. Meas.*, vol. 30, no. 2, p. 169, 2009.

[107] O. T. Inan, "Novel Technologies for Cardiovascular Monitoring Using Ballistocardiography and Electrocardiography," ProQuest LLC, 2009.

[108] O. T. Inan and G. T. A. Kovacs, "A Low-noise AC-bridge Amplifier for Ballistocardiogram Measurement on an Electronic Weighing Scale," *Physiol. Meas.*, vol. 31, no. 7, p. N51, 2010.

[109] J. H. Shin and K. S. Park, "HRV Analysis and Blood Pressure Monitoring on Weighing Scale Using BCG," in *Engineering in Medicine and Biology Society (EMBC), 2012 Annual International Conference of the IEEE*, 2012, pp. 3789–3792.

[110] C. Woody, "Characterization of an Adaptive Filter for the Analysis of Variable Latency Neuroelectric Signals," *Med. Biol. Eng.*, vol. 5, no. 6, pp. 539–554, 1967.

[111] S. Grimnes and O. G. Martinsen, *Bioimpedance and Bioelectricity Basics*, 2nd ed. Amsterdam, The Netherlands, 2008.

[112] L. Waite, "Anatomy and Physiology of Blood Vessels," in *Biofluid Mechanics in Cardiovascular Systems*, 1st ed., New York: Mc Graw Hill, 2006, pp. 89–104.

[113] M. N. Levy and A. J. Pappano, *Cardiovascular Physiology*, 9th ed. Philadelphia, USA: Mosby, Inc., 2007.

[114] J. J. Wang and K. H. Parker, "Wave Propagation in a Model of the Arterial Circulation," *J. Biomech.*, vol. 37, no. 4, pp. 457–470, Apr. 2004.

[115] P. Reymond, F. Merenda, F. Perren, D. Rüfenacht, and N. Stergiopulos, "Validation of a One-dimensional Model of the Systemic Arterial Tree," *Am. J. Physiol. - Hear. Circ. Physiol.*, vol. 297, no. 1, pp. H208–H222, Jun. 2009.

[116] J. C. Bramwell and A. V Hill, "The Velocity of the Pulse Wave in Man," *Proc. R. Soc. London. Ser. B, Contain. Pap. a Biol. Character*, vol. 93, no. 652, pp. 298–306, Apr. 1922.

[117] J. Sola, R. Vetter, P. Renevey, O. Chetelat, C. Sartori, et al., "Parametric Estimation of Pulse Arrival Time: A Robust Approach to Pulse Wave Velocity," *Physiol. Meas.*, vol. 30, no. 7, pp. 603–615, Jul. 2009.

[118] D. A. McDonald, W. W. Nichols, and M. F. O'Rourke, *McDonald's Blood Flow in Arteries. Theoretical, Experimental, and Clinical Principles*, 5th ed. London, UK: Arnold, 2005.

[119] D. H. Spodick and V. Q. Lance, "Noninvasive Stress Testing. Methodology for Elimination of the Phonocardiogram," *Circulation*, vol. 53, no. 4, pp. 673–676, 1976.

[120] D. B. Newlin, "Relationships of Pulse Transmission Times to Pre-ejection Period and Blood Pressure," *Psychophysiology*, vol. 18, no. 3, pp. 316–321, 1981.

[121] I. B. Wilkinson, S. S. Franklin, I. R. Hall, S. Tyrrell, and J. R. Cockcroft, "Pressure Amplification Explains Why Pulse Pressure Is Unrelated to Risk in Young Subjects," *Hypertension*, vol. 38, no. 6, pp. 1461–1466, Dec. 2001.

[122] F. Van de Werf, J. Piessens, H. Kesteloot, and H. De Geest, "A Comparison of Systolic Time Intervals Derived From the Central Aortic Pressure and From the External Carotid Pulse Tracing," *Circulation*, vol. 51, no. 2, pp. 310–316, Feb. 1975.

[123] D. Park, O. T. Inan, and L. Giovangrandi, "A Combined Heartbeat Detector Based on Individual BCG and IPG Heartbeat Detectors," in *Engineering in Medicine and Biology Society (EMBC), 2012 Annual International Conference of the IEEE*, 2012, pp. 3428–3431.

[124] O. T. Inan, D. Park, L. Giovangrandi, and G. T. A. Kovacs, "Noninvasive Measurement of Physiological Signals on a Modified Home Bathroom Scale," *Biomed. Eng. IEEE Trans.*, vol. 59, no. 8, pp. 2137–2143, Aug. 2012.

[125] S. Préau, F. Dewavrin, V. Soland, P. Bortolotti, D. Colling, et al., "Hemodynamic Changes During a Deep Inspiration Maneuver Predict Fluid Responsiveness in Spontaneously Breathing Patients," *Cardiol. Res. Pract.*, vol. 2012, no. 191807, pp. 1–8, Sep. 2011.

[126] J. Filipovsky, O. Mayer, M. Dolejsova, and J. Seidlerova, "The Assessment of Carotid–Femoral Distance for Aortic Pulse Wave Velocity: Should it Be Estimated from Body Height?," *Artery Res.*, vol. 4, no. 1, pp. 19–23, Feb. 2010.

Summary of research contributions

The novelties presented on this thesis have been disseminated through 2 journal papers, 1 patent, and 7 conference papers. The following summary relates the published results to the work described on each chapter.

Chapter 2: 2 journal papers and 4 conference papers.

[C1] J. Gomez-Clapers, E. Serrano-Finetti, R. Casanella, and R. Pallas-Areny, "Can Driven-Right-Leg Circuits Increase Interference in ECG Amplifiers?," in *Engineering in Medicine and Biology Society (EMBS), 2011. 33th Annual International Conference of the IEEE*, 2011, pp. 4780–4783.

[J1] J. Gomez-Clapers, and R. Casanella, "A Fast and Easy-to-Use ECG Acquisition and Heart Rate Monitoring System Using a Wireless Steering Wheel," *Sensors Journal, IEEE*, vol. 12, no. 3, pp. 610-616, Mar. 2012.

[C2] J. Gomez-Clapers, R. Casanella, and R. Pallas-Areny, "Multi-Signal Bathroom Scale to Assess Long-Term Trends in Cardiovascular Parameters," in *Engineering in Medicine and Biology Society (EMBS), 2012. 34th Annual International Conference of the IEEE*, 2012, pp. 550–553.

[C3] J. Gomez-Clapers, R. Casanella, and R. Pallas-Areny, "Obtención de parámetros cardiovasculares en una báscula electrónica doméstica," in *XXX Congreso Anual de la Sociedad Española de Ingeniería Biomédica CASEIB 2012*, 2012.

[C4] J. Gomez-Clapers, A. Serra-Rocamora, R. Casanella, and R. Pallas-Areny, "Uncertainty Factors in Time-Interval Measurements in Ballistocardiography," in *19th Symposium IMEKO TC 4 and 17th IWADC Workshop*, 2013.

[J2] J. Gomez-Clapers, A. Serra-Rocamora, R. Casanella, and R. Pallas-Areny, "Towards the Standardization of Ballistocardiography Systems for J-Peak Timing Measurement," *Measurement*, vol. 58, pp. 310–316, Dec. 2014.

Chapter 3: 1 conference paper and 1 patent.

[C5] J. Gomez-Clapers, R. Casanella, and R. Pallas-Areny, "Pulse Arrival Time Estimation from the Impedance Plethysmogram," in *Engineering in Medicine and Biology Society (EMBS), 2011. 33th Annual International Conference of the IEEE*, 2011, pp. 516–519.

[P1] R. Pallas-Areny, R. Casanella, and J. Gomez-Clapers, "Method and Apparatus for Obtaining Cardiovascular Information by Measuring Between Two Extremities," W.O. patent WO2013017718 A2, issued, Feb. 7th 2013.

Chapter 4: 2 conference papers.

[C6] J. Gomez-Clapers, R. Casanella, and R. Pallas-Areny, "Seguimiento de cambios hemodinámicos mediante la detección del intervalo RJ en tiempo real," in *XXVIII Congreso Anual de la Sociedad Española de Ingeniería Biomédica CASEIB 2010*, 2010.

[C7] R. Casanella, J. Gomez-Clapers, and R. Pallas-Areny, "On Time Interval Measurements Using BCG," in *Engineering in Medicine and Biology Society (EMBS), 2012. 34th Annual International Conference of the IEEE*, 2012, pp. 5034–5037.

During the development of this thesis the author the author has collaborated on the following publications:

[C8] J. Gomez-Clapers, and R. Casanella, "Wireless ECG and Heart Rate Monitoring Using Dual Ground Dry Electrodes," in *17th Symposium IMEKO TC 4*, 2010.

[C9] S. Gilaberte, J. Gomez-Clapers, R. Casanella, and R. Pallas-Areny, "Heart and Respiratory Rate Detection on a Bathroom Scale Based on the Ballistocardiogram and the Continuous Wavelet Transform," in *Engineering in Medicine and Biology Society (EMBS), 2010. 32th Annual International Conference of the IEEE*, 2010, pp. 2557–2560.

[P2] R. Pallas-Areny, O. Casas, R. Casanella, J. Gomez-Clapers, and D. Diaz, "Método y aparato para obtener el electrocardiograma mediante electrodos secos dobles," W.O. Patent WO2011104398, issued, Sep. 1st 2011.

The Shawshank Redemption (1994)